

FEB 8 1991

91N19042

NASA  
Technical  
Paper  
3032

C#2

November 1990

# Experimental Investigation of Porous-Floor Effects on Cavity Flow Fields at Supersonic Speeds

Floyd J. Wilcox, Jr.

TECHNICAL REPORTS  
FILE COPY

PROPERTY OF U.S. AIR FORCE  
AEDC TECHNICAL LIBRARY

NASA

**NASA  
Technical  
Paper  
3032**

1990

**Experimental Investigation  
of Porous-Floor Effects  
on Cavity Flow Fields  
at Supersonic Speeds**

Floyd J. Wilcox, Jr.  
*Langley Research Center*  
*Hampton, Virginia*



National Aeronautics and  
Space Administration  
Office of Management  
Scientific and Technical  
Information Division

## Summary

An experimental investigation was conducted to determine the effectiveness of a passive-venting system to modify the flow field over a rectangular-box cavity at supersonic speeds. The passive-venting system consisted of a cavity that had a porous floor with a vent chamber beneath the floor. The vent chamber allowed high pressure at the rear of the cavity to vent to the low-pressure region at the forward section of the cavity, thus modifying the cavity flow field. Two wind-tunnel tests (one drag and one pressure test) were conducted to determine the effectiveness of this passive-venting system.

The wind-tunnel model consisted of a rectangular-box cavity mounted in a flat plate. For the drag test, the cavity was mounted on a one-component balance such that only the drag of the cavity was measured. The cavity height remained constant throughout the entire test, and the cavity length was varied with block inserts. Solid-, porous-, and a combination of solid- and porous-floor configurations were tested for comparison. The tests were conducted at Mach numbers of 1.60, 1.90, 2.16, and 2.86 and at a constant Reynolds number of  $2 \times 10^6$  per foot. The results showed that the porous floor was very effective in modifying the cavity flow field as evidenced by a large reduction in the cavity drag. The data also showed that the porosity near the cavity midlength did not significantly affect the venting process; this result suggested that other methods (e.g., an array of tubes) could be used to modify the cavity flow field. In order to define completely the cavity flow field, a second test was conducted to measure pressures in the cavity. The same flat-plate model (except with a new cavity that had pressure orifices located along the cavity floor, on the forward- and rear-cavity faces, and on the vent chamber floor) was used. The results showed that the porous floor modified the cavity flow field to an intermediate type flow field. The results also showed that stores mounted in the cavity did not diminish significantly the effectiveness of the porous-floor venting system.

## Introduction

One of the most important mission goals for military fighter aircraft is to carry and launch weapons successfully. For supersonic cruise fighter aircraft, internal store carriage has received considerable interest because of the reduced aircraft radar cross section and reduced store carriage drag compared to external store carriage arrangements. The successful launch of weapons from internal weapons bays (cavities) requires a knowledge of the cavity flow field to prevent store separation problems. This paper examines a

method for modifying the flow field of certain cavities which typically causes adverse store separation characteristics and thus possibly improves the separation characteristics of stores from these cavities. Although this paper focuses primarily on cavities used for weapons bays, other uses for cavities include observation ports on aircraft and recessed areas for fins before deployment on wraparound fin missiles.

Existing data available in the literature (refs. 1 to 4) show that three basic types of cavity flow fields exist at supersonic speeds. These flow fields are commonly referred to as closed-, transitional-, and open-cavity flows. The type flow field which exists for a given cavity depends primarily on the cavity length-to-height  $L/h$  ratio. Cavity flow fields with  $L/h \gtrsim 13$  are generally referred to as closed-cavity flows and are characterized by a flow that separates at the cavity leading edge, expands into the cavity, attaches to the cavity floor, and then separates and exits ahead of the cavity rear face (fig. 1). The corresponding pressure distribution shows a low-pressure region at the forward section of the cavity as the flow separates and expands into the cavity, an increase in pressure as the flow impinges on the cavity floor, a pressure plateau as the flow passes along the cavity floor, and an increase in pressure as the flow compresses as it turns to exit the cavity ahead of the rear face. Keeping the cavity height constant and decreasing the cavity length will shorten the pressure plateau region on the cavity floor. When the pressure plateau region is eliminated and the pressure increases steadily from the forward section of the cavity to the rear of the cavity, the flow field generally is referred to as a transitional-cavity flow, and the cavity  $L/h$  is generally between 10 and 13. If the cavity length is decreased more so that  $L/h \lesssim 10$ , the flow field switches to what generally is known as open-cavity flow and is characterized by a flow field that passes over the cavity without any appreciable expansion into the cavity. The corresponding pressure distribution shows a slight positive pressure coefficient over most of the cavity length and an increase in pressure at the rear of the cavity caused by a slight flow impingement at the top of the cavity rear face.

A recent experimental investigation (ref. 5) has shown that the drag of a cavity with closed flow was substantially higher than that of a cavity with open flow. A typical distribution of cavity drag measured while varying the cavity length and holding the height constant is shown in figure 2. For  $L/h \lesssim 10$ , the cavity has open flow and a relatively small drag. This drag is primarily a result of the small pressure difference between the forward and rear faces of the cavity (fig. 1). A substantial increase

in drag is obtained when the flow field switches from open- to closed-cavity flow. For  $L/h \gtrsim 13$ , the cavity has closed flow and a relatively large drag, which is primarily caused by the large pressure difference between the forward and rear faces of the cavity (fig. 1).

A number of experimental investigations (refs. 6 to 8) have shown that adverse store separation can occur when stores are launched from a cavity with closed flow. This adverse effect is a result of the store nose being in the upwash region at the forward section of the cavity and the tail being in the downwash region at the rear section of the cavity (fig. 3(a)). This flow field situation causes a large pitching moment and normal force on the store which tend to force the store back into the cavity. For cavities with open flow, the store generally has favorable separation characteristics because of the relatively benign flow field that causes a small pitching moment and normal force (fig. 3(b)).

Because of the large drag and adverse store separation characteristics associated with a closed-cavity flow, a system that causes the flow field to switch to an open-cavity flow would be beneficial. A passive system that modifies the cavity flow field would be preferred because typically a passive system would be less complex than an active system. Although a deeper cavity would reduce the cavity drag and improve the store separation characteristics, the additional aircraft volume would be detrimental to the overall aircraft performance, i.e., increased wave drag and reduced range.

The idea for a passive-venting system was spurred by research (refs. 9 to 12) associated with airfoil drag reduction at transonic speeds. Airfoil drag in transonic flow increases dramatically as the airflow over the wing reaches a Mach number  $M_\infty = 1$ . This increase in drag is primarily a result of the formation of a shock wave on the top surface of the airfoil (fig. 4(a)); this shock wave causes wave drag and boundary-layer separation, thus increasing the total airfoil drag. Bahi, Ross, and Nagamatsu (ref. 9) have used a passive system to reduce the airfoil drag in transonic flow. As shown in figure 4(b), this system used a porous plate for part of the airfoil upper surface and a vent chamber beneath the porous surface. This arrangement allowed the high-pressure air downstream of the shock wave to vent to the upstream side of the shock. The additional air entering the flow field ahead of the shock caused an oblique shock to form and resulted in a lambda shock-wave system. The oblique shock reduced the local Mach number of the flow ahead of the normal shock, thus decreasing the strength of the shock and reducing the wave drag of the airfoil. Another benefit of the passive system was that part of the separated

boundary layer was removed downstream of the normal shock which helped to reduce the drag due to boundary-layer separation. Additional experimental investigations using this type system have been conducted (refs. 10 to 12); these investigations studied the effects of various airfoil shapes and porous-surface porosities.

By adapting the porous-surface concept used on airfoils, a cavity model was designed which housed a porous floor with a vent chamber beneath the floor. The expectation was that for closed-cavity flow the high-pressure air at the rear of the cavity would vent to the low-pressure region at the front of the cavity and would cause the flow field to switch to an open-cavity flow (fig. 5). Wind-tunnel tests were conducted in two phases to determine the effectiveness of this passive-venting system. The first test measured the cavity drag with both solid and porous floors. The cavity length was varied while the cavity height remained constant. The results of the force test showed that the passive-venting system did modify the closed-cavity flow field. To define better the porous-floor cavity flow field, a second test was conducted to measure pressures along the cavity floor centerline, on the forward- and rear-cavity faces, and along the vent chamber floor. Again, both solid- and porous-floor configurations were tested for comparison. Both wind-tunnel tests were conducted at Mach numbers of 1.60, 1.90, 2.16, and 2.86.

## Symbols

$A$	cavity rear-face area, $0.005889 \text{ ft}^2$
$C_D$	drag coefficient, $\frac{\text{cavity drag}}{q_\infty A}$
$C_p$	pressure coefficient, $\frac{p - p_\infty}{q_\infty}$
$d$	vent chamber height, in.
$h$	cavity height, 0.40 in.
$L$	cavity length, in.
$M_\infty$	free-stream Mach number
$p$	measured surface pressure, $\text{lb}/\text{ft}^2$
$p_\infty$	free-stream static pressure, $\text{lb}/\text{ft}^2$
$q_\infty$	free-stream dynamic pressure, $\text{lb}/\text{ft}^2$
$x_1$	axial surface distance on cavity floor as defined in figure 14
$x_2$	axial surface distance on vent chamber floor as defined in figure 14
$y_1$	surface distance on cavity forward face as defined in figure 14

$y_2$  surface distance on cavity rear face as defined in figure 14  
 $z_1$  lateral surface distance on cavity forward face as defined in figure 14  
 $z_2$  lateral surface distance on cavity rear face as defined in figure 14

Abbreviations:

FF	forward face
CFL	cavity floor
LOC	location
ORF	orifice
RF	rear face
VCF	vent chamber floor

## Apparatus and Experimental Methods

### Model Description

**Drag model.** A photograph and a drawing of the cavity drag model are shown in figure 6. The model consisted of a flat plate, a cavity pallet, and a balance. The flat plate was approximately 30 in. long with a maximum span of 34 in. The leading edge of the plate directly ahead of the cavity had a sweep of  $0^\circ$ , which provided a two-dimensional boundary layer approaching the cavity. The outboard leading edges were swept  $30^\circ$  to decrease the plate planform area and thus reduce the tunnel starting loads on the support strut and to position the tip vortices downstream as far as possible to minimize their effect on the flat-plate flow field. Also, the swept outboard leading edges ensured that the Mach lines produced by the tips would propagate downstream of the cavity. The lower surface leading-edge wedge angle of  $5^\circ$  was sufficiently small to allow a supersonic attached flow to be maintained at the leading edge throughout the Mach number range.

A recessed area that housed test instrumentation was located on the centerline of the flat plate and was covered with a filler plate (figs. 6 and 7). The cavity pallet was located within a cutout in the filler plate as shown in the photograph of the cavity filler plate area. The cavity pallet was isolated from the filler plate by an air gap of 0.015 in. and was mounted on a one-component (axial force) balance such that only the drag of the cavity pallet was measured. Figure 8 is a photograph of the recessed instrumentation area with the filler plate removed to expose the cavity pallet, balance, and pressure tubing. A foam rubber seal was attached to the filler plate as shown in

figure 8(a) to prevent flow through the cavity pallet and filler plate gap. Four static-pressure orifices were located in the recessed instrumentation area to verify negligible flow through the gap. Five static-pressure orifices, which were located on the forward and rear lips of the cavity pallet in the pallet and filler plate gap, were used for correcting axial pressure forces on the outside of the cavity pallet (fig. 8). The tare due to the foam rubber seal and pressure tubes is discussed in the "Measurements and Corrections" section of this paper. The recessed instrumentation area was vented to the flat-plate surface through four multihole vent plates to reduce the starting load normal force on the balance (fig. 6).

Details of the cavity drag pallet are shown in figure 9. Approximately 3340 holes with a diameter of 0.021 in. were drilled in the porous floor in rows 0.065 in. apart with alternating rows containing 31 and 32 holes each. This configuration resulted in a porosity of 7.9 percent based on the total floor area. The solid floor was simulated by placing adhesive tape over the porous floor. The cavity height  $h$  of 0.40 in. and the width of 2.12 in. were held constant throughout the entire test; the cavity length was varied by using rectangular-block inserts at the rear of the cavity so that the distance from the leading edge of the plate to the leading edge of the cavity remained constant. A photograph and a sketch of the various block inserts are shown in figure 10. Estimates of the skin friction drag for the top surface of the block inserts and pallet were calculated and subtracted from the cavity drag measurements. The method used to estimate the skin friction drag of the blocks is discussed in the "Measurements and Corrections" section of this report. The vent chamber height could be varied from 0.30 in. to 0.15 in. by installing a spacer onto the vent chamber floor and replacing the porous-floor supports to keep the cavity height constant.

**Pressure model.** The cavity pressure model used the same flat plate as that used in the drag tests; the only difference was that a different cavity pallet was used. A photograph of the cavity pressure model is shown in figure 11. The cavity pallet was located within the filler plate and was mounted on a dummy balance similar to the drag test setup. Figure 12 shows the cavity pallet with the filler plate removed. Again, a foam rubber seal attached to the filler plate prevented the flow from entering the recessed instrumentation area.

Details of the cavity pressure pallet are shown in figure 13. The holes in the porous floor followed the same pattern as those in the drag model except that the hole diameter was 0.025 in. This configuration

resulted in a porosity of 11.2 percent based on the total floor area. The reason for the change in the hole diameter between the two models was an error in the construction of the drag model. No direct comparison of the effect of hole size was conducted during these tests. As discussed in the "Pressure Tests" section of this paper, both porosities affected the cavity flow fields; therefore, the small change in hole diameter probably had a minimal effect on the porous-floor passive-venting system. The solid-floor configuration again was simulated by placing adhesive tape over the holes.

Pressure orifices were located on the forward and rear faces of the cavity, along the centerline of the porous floor, and along each side of the centerline of the vent chamber floor. Because the pressures on each side of the vent chamber centerline were similar, only pressures measured along one side of the vent chamber floor are presented in this report. Figure 14 shows the location and numbering system for the orifices. The orifices on the rear face of the cavity were mounted in a movable block as shown in figures 13 and 15. The cavity length was varied by placing rectangular-block inserts behind the rear-face block to obtain the same cavity lengths as were tested in the drag study. The cavity height of 0.40 in. and the width of 2.12 in. also remained constant and were the same as those used in the drag study. The vent chamber height was held constant at 0.15 in. for the pressure test.

Pressure data also were obtained with stores mounted in the cavity. Two configurations were tested which consisted of two and three stores each, as shown in figure 16. The stores were cylinders with an ogive nose and without fins as shown in figure 17. The relative location of the stores mounted in the cavity is shown in figure 18. The offset position of the three-store arrangement accounts for the interference between fins that would be on an actual missile. Both the store configurations were tested in a cavity with  $L/h = 17.500$  for a solid floor, a porous floor, and a porous floor with adhesive tape covering the floor symmetrically about the cavity midlength.

### Wind-Tunnel Tests

The wind-tunnel tests were conducted in the low Mach number test section of the Langley Unitary Plan Wind Tunnel (UPWT), which is a continuous-flow, variable-pressure supersonic wind tunnel. The test section is approximately 4 ft square and 7 ft long. The nozzle ahead of the test section consists of an asymmetric sliding block that allows continuous Mach number variation from 1.5 to 2.9 during tunnel operation. A complete description of the facility

along with test section calibration information is contained in reference 13.

The tests were conducted at the following conditions:

Mach number	Reynolds number, per foot	Stagnation pressure, lb/ft <sup>2</sup>	Stagnation temperature, °F	Dynamic pressure, lb/ft <sup>2</sup>
1.60	$2 \times 10^6$	1079	125	455
1.90	$2 \times 10^6$	1154	125	435
2.16	$2 \times 10^6$	1349	125	439
2.86	$2 \times 10^6$	1934	125	372

The tunnel air dewpoint was maintained below  $-20^{\circ}\text{F}$  to prevent water vapor condensation effects. The angle of attack of the flat plate was held constant at  $0^{\circ}$  throughout the entire test based on estimated tunnel flow angularity.

A grit-type boundary-layer transition strip was applied to the plate leading edge to ensure a fully turbulent boundary layer on the flat plate. The transition strip consisted of number 35 sand grit (0.0215 in. nominal height) individually spaced along a line 0.4 in. aft of the plate leading edge measured streamwise. The distance between the sand grit particles was approximately 0.09 in. measured parallel to the plate leading edge. The grit size and location were selected based on unpublished data (Floyd J. Wilcox, Jr.) from a similar flat-plate experiment conducted in the UPWT.

During a previous experiment that used the same flat plate, the boundary-layer thickness on the plate was measured (using an 18-probe stagnation pressure rake) at a location 13.6 in. aft of the plate leading edge. Because the boundary-layer thickness measurements were made at a location slightly aft of the cavity leading edge, the boundary-layer thickness at the cavity leading edge was estimated to be approximately 0.24 in. The effect of varying the boundary-layer height on the cavity flow field was not investigated during this test.

### Measurements and Corrections

**Drag tests.** The cavity drag was measured with a one-component (axial force) electrical strain-gage balance (fig. 19). All the drag data were corrected for the foam rubber seal and pressure tubes tare, the cavity pallet lip pressures, and the skin friction drag of the rectangular-block inserts.

The tare resulting from the foam rubber seal and pressure tubes was determined through two balance

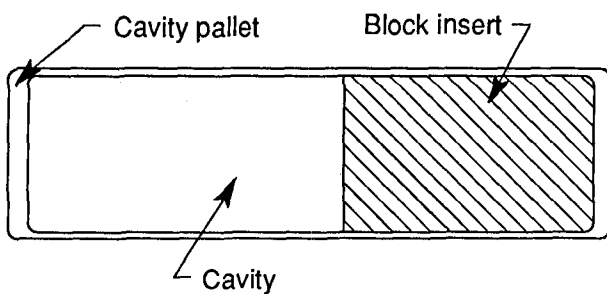
calibrations. The first balance calibration was conducted with the filler plate removed from the plate and the pressure tubes disconnected from the cavity pallet. This calibration resulted in a balance sensitivity that did not contain any tares due to the foam rubber seal or pressure tubes. A second balance calibration was conducted to obtain the balance sensitivity with the cavity pallet, filler plate, and pressure tubes installed in the test configuration. The balance sensitivity obtained during this calibration was both linear and repeatable. The difference between the two sensitivities, which indicates the tare of the foam rubber seal and pressure tubes, was 1.65 percent, and all drag data were corrected for this tare.

The drag force on the cavity pallet resulting from the cavity pallet lip pressures was calculated for each data point and subtracted from the measured cavity drag. An average pressure was calculated from the five static-pressure orifices on the cavity pallet forward and rear lips (fig. 8) and used to calculate the drag force on the pallet.

Estimates of the skin friction drag for the top surface of the rectangular-block inserts and pallet were calculated using the following procedure. The drag of a block insert, which completely filled the cavity (fig. 20), was measured, and the results were as follows:

$M_\infty$	$C_D$
1.60	0.0494
1.90	.0496
2.16	.0469
2.86	.0438

The estimate of skin friction drag for a given block insert was determined by multiplying the previously mentioned drag by the percentage of exposed pallet planform area as shown below.



$$\text{Factor} = \frac{\text{Total pallet planform area} - \text{Cavity planform area}}{\text{Total pallet planform area}}$$

Skin friction drag = (factor) (Drag of solid-block insert from above)

The estimated skin friction of the block inserts was determined for each data point and subtracted from the measured cavity drag.

The pallet lip pressures were measured with electronic pressure scanners, and the tunnel stagnation pressure was measured with a mercury manometer.

The drag data are contained in table I. The uncertainties of the drag measurements were calculated with the method discussed in appendix A (ref. 14 is found in this appendix) and are approximately as follows (in terms of drag coefficient):

$M_\infty$	Uncertainty in $C_D$
1.60	$\pm 0.017$
1.90	$\pm .019$
2.16	$\pm .019$
2.86	$\pm .023$

**Pressure tests.** All the static-pressure orifices on the cavity pallet were measured with 15 lb/in<sup>2</sup> full-scale electronic pressure transducers. This arrangement allowed all the pressures to be measured at the same time. As in the drag tests, the tunnel stagnation pressure was measured with a mercury manometer.

The pressure data are contained in tables II to IV. The uncertainties of the pressure measurements, which were calculated with the method discussed in appendix B, are approximately as follows (in terms of pressure coefficient):

$M_\infty$	Uncertainty in $C_p$
1.60	$\pm 0.023$
1.90	$\pm .022$
2.16	$\pm .021$
2.86	$\pm .024$

## Results and Discussion

### Drag Tests

Figure 21 shows the effect of porosity on the cavity drag. The solid-floor data show the typical large drag increase at  $L/h \approx 12$  as the flow field switches from open- to closed-cavity flow. In comparison, the porous floor eliminated the large drag increase, which suggests that the flow field is probably typical of open-cavity flow. At the smaller values of  $L/h$ , the

difference between the solid- and porous-floor cavity drag is minimal; this result indicates that only a small amount of venting occurs. Varying the height of the vent chamber from 0.30 in. to 0.15 in. has no effect on the cavity drag for  $L/h \lesssim 12$  and has a minimal effect for  $L/h \gtrsim 12$ , although the effect becomes greater as  $L/h$  increases. This result suggests that as the amount of venting increases, the height of the vent chamber restricts the vent chamber flow.

A comparison of schlieren photographs for both the solid- and porous-floor cavities ( $L/h = 17.500$ ) is shown in figure 22. This comparison illustrates the effect of the porous floor on the cavity flow field. In the solid-floor photographs, the impingement shock that forms as the flow expands into the cavity and attaches to the cavity floor and the shock that is formed as the flow exits the cavity are clearly visible. The porous-floor photographs show a complete elimination of this entire shock-wave system; this elimination again suggests that the flow field is probably typical of open-cavity flow (fig. 1).

Data also were obtained with adhesive tape partially covering the porous floor. The tape was arranged symmetrically about the cavity midlength (fig. 23) to determine if the porosity near the cavity midlength had a significant effect on the cavity flow field. Figure 24 shows data for a cavity with  $L/h = 17.500$  and a vent chamber height of 0.30 in. The results show a steady decrease in the cavity drag as the percentage of floor area with porosity increases. The solid-floor cavity drag was reduced by one-half when approximately 35 percent of the floor area was porous. When more than 50 percent of the floor area was porous, the additional drag reduction obtained was small. Therefore, the porosity near the cavity midlength does not significantly affect the cavity flow field (i.e., the porosity on the forward and rear sections of the cavity floor has the largest effect). This result suggests the possibility that other methods (e.g., an array of tubes) could be used to directly transport the high-pressure air at the rear of the cavity to the low-pressure region at the forward part of the cavity and still obtain the same results as for the porous floor.

The results of the drag test showed that the passive-venting system was effective in modifying the cavity flow field and thus reduced the cavity drag. Because the results of the drag study could not define completely the porous-floor cavity flow field, a second wind-tunnel test was conducted to measure the pressures inside the cavity and thus define the flow field of the porous-floor cavity.

## Pressure Tests

Because the drag results of the porous-floor cavity showed very little effect of vent chamber height, all the pressure data were obtained with a vent chamber height of 0.15 in. (i.e., the smallest vent chamber height studied during the drag tests). As discussed in the "Model Description" section of this report, the floor porosity was 11.2 percent during the pressure tests instead of 7.9 percent used during the drag tests. Both floor porosities modified the cavity flow field, although no direct comparison of the effect of porosity was conducted during this investigation.

**Solid-floor results.** Figure 25 shows the centerline pressure distributions on the cavity forward face, floor, and rear face along with the forward- and rear-face lateral distributions for the solid-floor cavity. Data are presented for selected cavity  $L/h$  ratios to illustrate closed flow, transitional flow just before switching (transitional-closed flow), transitional flow just after switching (transitional-open flow), and open flow. Note that transitional-cavity flow has been divided into two types of flow: transitional-closed and transitional-open flow. Transitional-closed flow is the same flow field that is referred to as transitional flow in the "Introduction" section of this paper. Transitional-open flow occurs as the cavity  $L/h$  is decreased slightly from that required for transitional-closed cavity flow. For this type flow field, the flow separates and expands into the cavity, is turned through a series of compression waves (but does not attach to the cavity floor), and then exits at the rear of the cavity. Sketches of the flow fields and the terms used to describe the various types of flow fields discussed in the remainder of this paper are shown in figure 26. For Mach numbers of 1.60, 1.90, and 2.16, each of the previously discussed flow types occurs at the same  $L/h$  at each Mach number. At a Mach number of 2.86, transitional-closed and transitional-open flows occur at  $L/h$  ratios slightly smaller than those for the other Mach numbers. The centerline pressure distributions agree with the results discussed in the "Introduction" and therefore give credence to this experimental setup.

All the lateral pressure distributions on the forward and rear faces of the cavity are symmetrical about the cavity centerline. The rear-face data show that a large increase in pressure occurs at the outside edges of the cavity for the closed- and transitional-closed-flow cases. This pressure increase is caused by the impingement of vortices, which are formed along the cavity side edges as the flow expands into the cavity. This flow phenomenon has been documented in references 1 and 5. The pressure distributions for

transitional-open flow (except at  $M_\infty = 2.86$ ) show a slight pressure increase at the cavity edges; this pressure increase is probably the result of the impingement of a weak vortex that formed from the relatively smaller expansion (as compared to the expansion for the closed- and transitional-closed-flow cases) at the cavity leading edge. In contrast, the pressure distributions for the open-flow case show a slight pressure decrease at the cavity edges. The pressure magnitudes on the rear face decrease with decreasing  $L/h$ , and the largest decrease occurs when the flow switches from transitional-closed to transitional-open flow. The forward-face distributions for closed and transitional-closed flows show a slight increase in pressure at the cavity centerline for  $M_\infty = 1.60, 1.90$ , and  $2.16$ , although the magnitude of the pressure increase is reduced as  $M_\infty$  is increased. The pressure distributions for open and transitional-open flows are nearly constant across the cavity width. The magnitude of the pressures increases as  $L/h$  decreases; the largest increase occurs when the flow switches from transitional-closed to transitional-open flow.

The pressure difference on the forward and rear faces gives an approximation of the cavity drag for a given  $L/h$ . The closed-flow and transitional-closed-flow cases have the largest pressure differences and consequently the largest drag. A large decrease in the pressure difference, which is due to the decrease in pressure on the rear face and an increase in pressure on the forward face, occurs as the flow switches from transitional-closed to transitional-open flow. These effects also were seen in the drag data discussed previously.

**Solid- and porous-floor comparisons.** Comparisons of the solid- (closed-) and porous- (transitional-open) floor cavity pressure distributions for  $L/h = 17.500$  and the pressure distributions for a solid-floor cavity with transitional-open flow are shown in figure 27. The centerline pressure distributions show the typical closed-cavity flow field for the solid-floor cavity with  $L/h = 17.500$ . The porous-floor data show that the flow field has switched from closed flow to a flow field that is similar to the one found for a solid floor with transitional-open flow; however, the magnitudes of the pressures on the floor are slightly different. On the forward and rear faces of the cavity, the magnitudes and trends of the centerline and lateral pressure distributions are nearly the same for the porous floor and the solid floor with transitional-open flow. Hence, the porous-floor cavity with  $L/h = 17.500$  has a flow field that is similar to transitional-open flow.

Figure 28 shows a comparison of the cavity floor and vent chamber floor (figs. 5 and 13) pressure distributions for a porous-floor cavity with  $L/h = 17.500$ . The pressure difference between the cavity floor and the vent chamber floor indicates that at the rear of the cavity, air passes from the cavity to the vent chamber; near the cavity midlength, little or no air passes between the cavity and the vent chamber; and at the forward section of the cavity, air passes from the vent chamber to the cavity. The pressure distribution on the vent chamber floor shows a decrease in pressure from the rear of the cavity toward the cavity midlength where the pressure reaches a minimum before increasing at the forward section of the cavity. This distribution suggests that the flow velocity at the rear and forward sections of the vent chamber (where the air enters and exits the vent chamber) is slower than that near the cavity midlength (where the flow velocity reaches a maximum).

These results (figs. 27 and 28) indicate that the porous-floor flow field is similar to the hypothetical description discussed in the Introduction except that the flow changes to transitional-open flow rather than open flow. This change suggests that the porous-floor flow field has reached an equilibrium state such that a large enough pressure differential exists between the forward and rear sections of the cavity to allow the venting process to continue. If the porous-floor flow field switched to completely open flow, essentially no pressure differential would exist to maintain the venting process. This change to open flow would result in the flow field switching back to closed flow and thus starting an oscillating behavior. If this oscillating behavior were present, data points would not repeat readily, and schlieren photographs of the porous-floor cases would show an unsteady shock-wave system. Analysis of repeat data points and schlieren photographs indicates that this oscillating behavior did not occur.

A comparison between the pressure distribution for the solid-floor cavity with transitional-closed flow and the porous floor is shown in figure 29. This figure shows that the porous floor has caused the flow field to switch from transitional-closed to transitional-open flow similar to the closed-flow case presented in figure 27. Figure 30 shows a comparison of the cavity and the vent chamber floor pressure distributions for the porous-floor configuration. These data show the same general trend as the case in which  $L/h$  is 17.500 (fig. 28), thus indicating that the venting process still is performing in the same manner.

Figure 31 shows the pressure distributions for the solid floor with transitional-open flow and for the porous floor. These data (except  $M_\infty = 2.86$ )

show that the porous floor has modified the pressure distribution along the cavity floor such that it is approaching an open-flow distribution, although it has not yet reached that point. Note that in the figure the porous-floor distributions are labeled as open flow (except for  $M_\infty = 2.86$ ) because they have a distribution closer to open flow than to transitional-open flow. (Open-cavity flow has a slight positive pressure coefficient along the cavity floor.) At  $M_\infty = 2.86$ , the porous-floor pressure distribution on the cavity floor still is similar to the solid-floor distribution except at the rear of the cavity where the pressures are slightly lower. A comparison between the pressure distributions on the vent chamber floor and the porous floor is shown in figure 32. These data show the same general trend as the case in which  $L/h = 17.500$ ; however, the magnitudes of the pressure differences are much smaller thus indicating that the amount of venting is smaller.

The pressure distributions for the solid-floor cavity with open flow and for the porous floor are shown in figure 33. Little difference exists between the two pressure distributions on the cavity floor, although at the rear of the cavity, the magnitude of the porous-floor distributions is slightly lower than that seen for the solid floor. The distributions on the forward face show no effect of the porous floor, whereas the distribution on the rear face shows a slight reduction in the magnitude of the pressures similar to the pressures on the cavity floor. A comparison of the vent chamber floor pressures and the porous-floor pressures is shown in figure 34. The vent chamber floor pressures are essentially constant and equal in magnitude to the porous-floor pressures except at the rear of the cavity, which indicates that virtually no venting is occurring through the vent chamber as would be expected based on the drag test data. These data show that the porous floor has little effect on the cavity flow field when the cavity  $L/h$  is in the region where open-cavity flow would normally exist for a solid-floor cavity.

**Varying percent of floor area with porosity.** Shown in figure 35 are the pressure distributions for a solid-floor cavity and for the cavities with adhesive tape symmetrically covering the porous floor about the cavity midlength. All cavities had an  $L/h = 17.500$ . The solid-floor data (0 percent of the floor area with porosity) show the typical closed-flow pressure distributions. All the remaining configurations cause the flow field to switch to transitional-open flow. The distributions for the porous floor (100 percent of the floor area with porosity) and the 57.1-percent porous floor (57.1 percent of the floor area with porosity) are nearly identical; these dis-

tributions indicate that the porosity near the cavity midlength has a small effect on the venting process, thus confirming the drag test results. The distribution for the 28.6-percent porous floor (28.6 percent of the floor area with porosity) shows that the full benefit of the porous-floor venting process has not yet been attained although a large improvement exists over the solid-floor case.

The vent chamber floor pressure distributions for the porous-floor and partial-porous-floor configurations are shown in figure 36. The magnitude of the pressures is approximately the same near the rear of the vent chamber. The 28.6-percent porous-floor distribution is nearly constant, although the pressures at the rear of the cavity are slightly higher than the forward section of the vent chamber. The 57.1-percent porous floor and the porous-floor distributions have the same general trends except near the vent chamber midlength. In this region, the 57.1-percent porous-floor distribution remains approximately constant, and the porous-floor distribution decreases and reaches a minimum level. The regions where the pressure distributions remain nearly constant for the 28.6-percent and 57.1-percent porous-floor configurations are approximately where the porous floor was covered with adhesive tape, thus indicating the velocities in the vent chamber were essentially constant through these regions. The 57.1- and 100-percent porous-floor cavities have a larger pressure drop from the rear to the forward section of the cavity compared to the 28.6-percent porous floor. This fact, coupled with a larger porous-floor area at the forward and rear sections of the cavity for air to pass through, suggests that the 57.1- and 100-percent porous-floor configurations are passing a larger mass flow through the vent chamber than those for the 28.6-percent porous floor. This result implies that for the 28.6-percent porous-floor configuration (as compared to the 57.1- and 100-percent porous-floor cavities), insufficient mass flow is passing through the vent chamber to the forward section of the cavity to prevent as much of the free-stream flow from expanding into the cavity.

**Effect of stores.** The preceding data have shown that a porous floor can modify the flow field of an empty cavity. In the practical application of a cavity on an aircraft (such as a weapons bay), stores would be carried in the cavity until they were launched. Because these stores could affect the cavity flow field, data were obtained with two and three stores mounted in the cavity to determine their effect on the flow field for cavities with a solid floor, a porous floor, and a porous floor with adhesive tape symmetrically covering the floor about the cavity

midlength. A discussion of the store installation details is contained in the "Model Description" section of this report.

The effect of stores on the pressure distributions for a solid-floor cavity is shown in figure 37. The pressure distributions on the cavity floor show that closed flow still exists for the cavities with stores although as the number of stores increases, the magnitude of the pressure on the forward section of the floor increases while it decreases at the rear of the cavity. The distributions on the forward face (both lateral and centerline distributions) have the same general magnitude as the pressures on the forward-cavity floor. The centerline distribution on the cavity rear face shows that a large increase in pressure at the upper edge of the cavity exists for the two-store case compared to the no-store case, except at  $M_\infty = 2.86$ . The three-store case shows a reduced pressure level compared to the no-store case. The lateral distribution on the rear face shows a large effect due to the stores. The general trend for the no-store case shows a convex-shaped distribution (a result of vortex impingement as described previously), whereas the two- and three-store cases show a concave-shaped distribution. These data indicate that the stores mounted in the cavity hinder the expansion of the flow into the cavity and thus affect the vortices that impinge on the cavity rear face.

The effect of stores on the pressure distributions for the porous floor is shown in figure 38. The stores have virtually no effect on the pressure distributions on the forward face and the forward section of the cavity floor. At the rear of the cavity floor, a slight decrease in pressure exists due to the presence of the stores. The rear-face pressure distributions for the two- and three-store cases show virtually no differences, and their magnitude is slightly less than in the no-store case. These results show that stores have a small effect on the porous-floor cavity flow field.

Figures 39 and 40 show, respectively, the pressure distributions for the 28.6- and 57.1-percent porous-floor cavities. The 28.6-percent porous-floor cavity shows a small variation in the magnitude of the pressures on the forward face and in the forward and rear sections of the cavity floor as the number of stores is increased. On the rear face, the pressure distributions for the two- and three-store cases show little difference although their magnitude is slightly less than that in the no-store case. The results for the 57.1-percent porous-floor cavity are very similar to the porous-floor cavity results; these results are expected because of the similarity of these two cavity configurations with no stores (fig. 38).

In general, stores have a larger effect on the solid-floor cavity flow field than on the porous-floor or partial-porous-floor cavity flow fields. The disturbances caused by the stores appear to diminish as more of the floor area becomes porous. Although the stores have a small effect on the porous-floor flow field, the effect of a store separating from a porous-floor cavity (e.g., how the store shock-wave system affects the venting process) is unknown. However, reference 15 contains data for stores separating from a cavity with a passive-venting system; this system uses pipes to transport the high-pressure air at the rear of the cavity to the forward section of the cavity. The results showed that the passive-venting system did improve the separation characteristics of the stores. These data suggest that the porous-floor system could be effective in improving the separation characteristics of stores.

## Conclusions

An experimental investigation was conducted to determine the effectiveness of a passive-venting system to modify cavity flow fields at supersonic speeds. The passive-venting system consisted of a porous floor with a vent chamber beneath the floor. This arrangement allows high-pressure air from the rear of the cavity to vent to the forward part of the cavity, thereby modifying the cavity flow field. Tests were conducted to measure the drag of the cavity and to measure the pressure distributions inside the cavity for both solid- and porous-floor configurations. Pressure data were also obtained with stores mounted in the cavity. These tests were conducted with the cavity mounted in a flat plate at Mach numbers of 1.60, 1.90, 2.16, and 2.86.

The following is a summary of the significant findings:

1. The passive-venting system was extremely effective in modifying the flow field over a cavity with closed flow at supersonic speeds. The flow field over the cavity maintained a steady-state equilibrium position with no apparent oscillation between closed and open flows.
2. The passive-venting system reduced the drag of cavities with closed flow by a factor of approximately 3 and had little effect on the drag of cavities with open flow.
3. Reducing the vent chamber height by 50 percent did not significantly diminish the effectiveness of the passive-venting system as evidenced from the cavity drag measurements.
4. Porosity near the cavity midlength did not significantly affect the cavity flow field; this result suggests that other methods (e.g., an

array of tubes) could be used as a passive-venting system.

5. Pressure distributions inside a cavity which had closed or transitional-closed flow with a solid floor indicated that the passive-venting system modified the flow field to a transitional-open-type flow.
6. Stores mounted in the porous-floor cavity did not modify significantly the cavity pressure distributions, thus indicating that the passive-venting system effectiveness was not diminished significantly by the stores.

7. Cavity-floor porosities of 7.1 and 11.2 percent based on the total floor area were effective in modifying the cavity flow fields.

These results suggest that the passive-venting system would be extremely useful in an aircraft weapons bay for reducing the drag of the weapons bay and probably improving the separation characteristics of stores.

NASA Langley Research Center  
Hampton, VA 23665-5225  
August 16, 1990

## Appendix A

### Experimental Drag Data Uncertainty Analysis

The uncertainty in the drag measurements was calculated with the method discussed in reference 14. For this investigation, the experimental drag coefficient was calculated from six variables as shown below.

$$C_D = C_D (p_t, D, p_{fl}, p_{al}, M_\infty, SF)$$

$$= \frac{D + (p_{al} - p_{fl}) A_l - SF}{1/2\gamma M_\infty^2 p_t (1 + 0.2M_\infty^2)^{-3.5} A} \quad (A1)$$

where

- $A$  cavity rear-face area, 0.005889 ft<sup>2</sup>
- $A_l$  cavity pallet lip area, 0.004934 ft<sup>2</sup>
- $D$  measured drag force, lb
- $M_\infty$  free-stream Mach number
- $p_{al}$  measured static pressure on pallet rear lip, lb/ft<sup>2</sup>
- $p_{fl}$  measured static pressure on pallet forward lip, lb/ft<sup>2</sup>
- $p_t$  measured free-stream stagnation pressure, lb/ft<sup>2</sup>
- $SF$  calculated skin friction correction, lb
- $\gamma$  ratio of specific heats, 1.4

The uncertainty in  $C_D$ , because of the uncertainty in each of the six variables used to calculate  $C_D$ , is

$$\omega_{C_D} = \left[ \left( \frac{\partial C_D}{\partial p_t} \omega_{p_t} \right)^2 + \left( \frac{\partial C_D}{\partial D} \omega_D \right)^2 + \left( \frac{\partial C_D}{\partial p_{fl}} \omega_{p_{fl}} \right)^2 + \left( \frac{\partial C_D}{\partial p_{al}} \omega_{p_{al}} \right)^2 + \left( \frac{\partial C_D}{\partial M_\infty} \omega_{M_\infty} \right)^2 + \left( \frac{\partial C_D}{\partial SF} \omega_{SF} \right)^2 \right]^{1/2} \quad (A2)$$

where

- $\omega_{C_D}$  uncertainty in  $C_D$
- $\omega_{p_t}$  uncertainty in measured  $p_t$ ,  $\pm 1.0$  lb/ft<sup>2</sup>
- $\omega_D$  uncertainty in measured  $D$ ,  $\pm 0.0125$  lb
- $\omega_{p_{al}}$  uncertainty in measured  $p_{al}$ ,  $\pm 5.8$  lb/ft<sup>2</sup>
- $\omega_{p_{fl}}$  uncertainty in measured  $p_{fl}$ ,  $\pm 5.8$  lb/ft<sup>2</sup>
- $\omega_{M_\infty}$  uncertainty in  $M_\infty$  (from ref. 13),  $\pm 0.02$
- $\omega_{SF}$  uncertainty in calculated  $SF$ ,
  - $\pm 0.0158$  lb at  $M_\infty = 1.60$
  - $\pm 0.0165$  lb at  $M_\infty = 1.90$
  - $\pm 0.0164$  lb at  $M_\infty = 2.16$
  - $\pm 0.0193$  lb at  $M_\infty = 2.86$

The uncertainty in  $C_D$  was calculated for each data point with equation (A2), and the largest uncertainty in  $C_D$  at each Mach number is as follows:

$M_\infty$	Uncertainty in $C_D$
1.60	$\pm 0.017$
1.90	$\pm 0.019$
2.16	$\pm 0.019$
2.86	$\pm 0.023$

## Appendix B

### Experimental Pressure Data Uncertainty Analysis

The uncertainty of the static-pressure measurements was calculated with the method discussed in reference 14. For this investigation, the experimental pressure coefficient was calculated from three variables as shown below.

$$\begin{aligned}
 C_p &= C_p(p, p_t, M_\infty) \\
 &= \frac{p - p_\infty}{1/2 \gamma p_\infty M_\infty^2} \\
 &= \frac{2p(1 + 0.2M_\infty^2)^{3.5}}{\gamma p_t M_\infty^2} - \frac{2}{\gamma M_\infty^2} \quad (B1)
 \end{aligned}$$

where

$M_\infty$  free-stream Mach number  
 $p$  measured static pressure, lb/ft<sup>2</sup>  
 $p_\infty$  free-stream static pressure, lb/ft<sup>2</sup>  
 $p_t$  measured free-stream stagnation pressure, lb/ft<sup>2</sup>  
 $\gamma$  ratio of specific heats, 1.4

The uncertainty in  $C_p$ , because of the uncertainty in each of the three variables used to calculate  $C_p$ , is

$$\omega_{C_p} = \left[ \left( \frac{\partial C_p}{\partial p} \omega_p \right)^2 + \left( \frac{\partial C_p}{\partial p_t} \omega_{p_t} \right)^2 + \left( \frac{\partial C_p}{\partial M_\infty} \omega_{M_\infty} \right)^2 \right]^{1/2} \quad (B2)$$

where

$\omega_{C_p}$  uncertainty in  $C_p$

$\omega_p$  uncertainty in measured  $p$ ,  $\pm 5.8$  lb/ft<sup>2</sup>

$\omega_{p_t}$  uncertainty in measured  $p_t$ ,  $\pm 1.0$  lb/ft<sup>2</sup>

$\omega_{M_\infty}$  uncertainty in  $M_\infty$  (from ref. 14),  $\pm 0.02$

The uncertainty in  $C_p$  was calculated for each orifice for each data point with equation (B2), and the largest uncertainty in  $C_p$  at each Mach number is as follows:

$M_\infty$	Uncertainty in $C_p$
1.60	$\pm 0.023$
1.90	$\pm 0.022$
2.16	$\pm 0.021$
2.86	$\pm 0.024$

## References

1. Stallings, Robert L., Jr.; and Wilcox, Floyd J., Jr.: *Experimental Cavity Pressure Distributions at Supersonic Speeds*. NASA TP-2683, 1987.
2. Kaufman, Louis G., II; Maciulaitis, Algirdas; and Clark, Rodney L.: *Mach 0.6 to 3.0 Flows Over Rectangular Cavities*. AFWAL-TR-82-3112, U.S. Air Force, May 1983. (Available from DTIC as AD A134 579.)
3. Charwat, A. F.; Roos, J. N.; Dewey, F. C., Jr.; and Hitz, J. A.: An Investigation of Separated Flows—Part I: The Pressure Field. *J. Aerosp. Sci.*, vol. 28, no. 6, June 1961, pp. 457-470.
4. McDearmon, Russell W.: *Investigation of the Flow in a Rectangular Cavity in a Flat Plate at a Mach Number of 3.55*. NASA TN D-523, 1960.
5. Blair, A. B., Jr.; and Stallings, Robert L., Jr.: *Supersonic Axial-Force Characteristics of a Rectangular-Box Cavity With Various Length-to-Depth Ratios in a Flat Plate*. NASA TM-87659, 1986.
6. Stallings, Robert L., Jr.: Store Separation From Cavities at Supersonic Flight Speeds. *J. Spacecr. & Rockets*, vol. 20, no. 2, Mar.-Apr. 1983, pp. 129-132.
7. Blair, A. B., Jr.; and Stallings, R. L., Jr.: Cavity Door Effects on Aerodynamic Loadings of Compressed-Carriage Store Configurations Separating From Cavities at Supersonic Speeds. AIAA-88-0333, Jan. 1988.
8. Rainey, Robert W.: *A Wind-Tunnel Investigation of Bomb Release at a Mach Number of 1.62*. NACA RM L53L29, 1954.
9. Bahi, L.; Ross, J. M.; and Nagamatsu, H. T.: Passive Shock Wave/Boundary Layer Control for Transonic Airfoil Drag Reduction. AIAA-83-0137, Jan. 1983.
10. Orozco, Robert D.: *Porosity Effects on Supercritical Airfoil Drag Reduction by Shock Wave/Boundary Layer Control*. M.E. Thesis, Rensselaer Polytechnic Inst., 1983.
11. Nagamatsu, H. T.; Orozco, R. D.; and Ling, D. C.: Porosity Effect on Supercritical Airfoil Drag Reduction by Shock Wave/Boundary Layer Control. AIAA-84-1682, June 1984.
12. Nagamatsu, H. T.; Trilling, T. W.; and Bossard, J. A.: Passive Drag Reduction on a Complete NACA 0012 Airfoil at Transonic Mach Numbers. AIAA-87-1263, June 1987.
13. Jackson, Charlie M., Jr.; Corlett, William A.; and Monta, William J.: *Description and Calibration of the Langley Unitary Plan Wind Tunnel*. NASA TP-1905, 1981.
14. Holman, J. P.: *Experimental Methods for Engineers*, Second ed. McGraw-Hill, Inc., c.1971.
15. Stallings, Robert L., Jr.; and Forrest, Dana K.: *Separation Characteristics of Internally Carried Stores at Supersonic Speeds*. NASA TP-2993, 1990.

Table I. Cavity Drag Data

(a) Solid-floor data

$L/h$	$C_D$ at $M_\infty$ of—			
	1.60	1.90	2.16	2.86
4.120	0.063	0.048	0.040	0.027
6.070	.080	.066	.057	.044
8.020	.099	.084	.074	.055
8.995	.112	.095	.085	.066
9.970	.139	.116	.105	.081
10.945	.173	.146	.132	.100
11.920	.224	.191	.175	.135
12.895	.321	.296	.281	.485
14.845	.613	.572	.548	.545
17.500	.707	.663	.617	.591

(b) Porous-floor data ( $d = 0.30$  in.)

$L/h$	$C_D$ at $M_\infty$ of—			
	1.60	1.90	2.16	2.86
4.120	0.050	0.040	0.036	0.028
6.070	.069	.060	.054	.042
8.020	.085	.075	.067	.053
8.995	.095	.083	.073	.060
9.970	.108	.095	.085	.071
10.945	.123	.107	.097	.082
11.920	.139	.122	.111	.093
12.895	.157	.137	.126	.107
14.845	.204	.182	.171	.147
17.500	.273	.253	.239	.209

(c) Porous-floor data ( $d = 0.15$  in.)

$L/h$	$C_D$ at $M_\infty$ of—			
	1.60	1.90	2.16	2.86
4.120	0.056	0.041	0.037	0.028
8.020	.087	.076	.068	.054
9.970	.108	.096	.087	.072
11.920	.140	.122	.112	.095
14.845	.209	.188	.177	.153
17.500	.297	.277	.263	.232

(d) Partial-porous-floor data  
( $L/h = 17.500$ ,  $d = 0.30$  in.)

Percent of floor area with porosity	$C_D$ at $M_\infty$ of—			
	1.60	1.90	2.16	2.86
0	0.707	0.663	0.617	0.591
28.6	.392	.372	.352	.320
57.1	.297	.276	.265	.235
100.0	.273	.253	.239	.209

Table II. Solid-Floor Pressure Data

(a)  $M_\infty = 1.60$

ORF	LOC	$C_p$ at $L/h$ of							
		17.500	14.845	12.895	11.920	10.945	9.970	8.020	4.120
1	FF	-.1559	-.1411	-.0371	.0013	.0131	.0167	.0315	.0527
2	FF	-.1583	-.1437	-.0391	-.0008	.0115	.0147	.0300	.0533
3	FF	-.1524	-.1385	-.0377	.0014	.0131	.0160	.0316	.0540
4	FF	-.1585	-.1445	-.0451	-.0041	.0074	.0110	.0255	.0456
5	FF	-.1616	-.1488	-.0419	-.0003	.0112	.0145	.0301	.0486
38	FF	-.1878	-.1816	-.0454	-.0150	.0067	.0068	.0222	.0399
39	FF	-.1818	-.1743	-.0391	-.0101	.0113	.0102	.0186	.0387
40	FF	-.1812	-.1747	-.0383	-.0092	.0124	.0119	.0206	.0448
41	FF	-.1915	-.1863	-.0463	-.0145	.0057	.0079	.0224	.0402
33	RF	.5082	.4584	.2629	.2172	.1994	.1733	.1599	.1343
34	RF	.4789	.4327	.2388	.1904	.1741	.1470	.1314	.1013
35	RF	.4763	.4307	.2427	.1936	.1726	.1451	.1249	.0841
36	RF	.4803	.4305	.2673	.2186	.2017	.1739	.1572	.1137
37	RF	.4559	.4069	.3034	.2635	.2522	.2324	.2282	.1963
42	RF	.5948	.5429	.2772	.2057	.1808	.1439	.1008	.0689
43	RF	.5526	.4834	.2444	.1914	.1703	.1429	.1243	.0924
44	RF	.5442	.4804	.2353	.1815	.1598	.1348	.1197	.0869
45	RF	.5966	.5492	.2648	.1948	.1665	.1354	.0998	.0672
74	VCF	.0273	.0238	.0260	.0296	.0336	.0274	.0307	.0299
76	VCF	.0304	.0271	.0280	.0319	.0357	.0293	.0325	.0310
78	VCF	.0302	.0265	.0266	.0313	.0348	.0281	.0321	.0313
80	VCF	.0297	.0268	.0263	.0315	.0335	.0285	.0311	
82	VCF	.0280	.0239	.0232	.0291	.0317	.0252	.0294	
84	VCF	.0310	.0270	.0262	.0328	.0347	.0288	.0323	
86	VCF	.0310	.0260	.0253	.0322	.0327	.0270		
88	VCF	.0319	.0273	.0258	.0339	.0346			
90	VCF	.0299	.0246	.0226	.0316				
92	VCF	.0330	.0270	.0253					
94	VCF	.0321	.0266						
96	VCF	.0330							
98	VCF	.0269							
6	CFL	-.1715	-.1594	-.0461	-.0040	.0086	.0111	.0267	.0404
7	CFL	-.1763	-.1655	-.0460	-.0031	.0103	.0133	.0282	.0377
8	CFL	-.1957	-.1849	-.0573	-.0138	.0012	.0035	.0202	.0262
9	CFL	-.1891	-.1793	-.0564	-.0116	.0026	.0074	.0233	.0225
10	CFL	-.1664	-.1587	-.0615	-.0179	-.0017	.0014	.0185	.0164
11	CFL	-.1176	-.1122	-.0535	-.0142	.0009	.0032	.0194	.0368
12	CFL	-.0761	-.0708	-.0460	-.0123	.0008	.0017	.0163	.1382
13	CFL	-.0275	-.0217	-.0231	-.0034	.0150	.0128	.0256	
14	CFL	.0071	.0144	-.0032	.0167	.0261	.0215	.0309	
15	CFL	.0383	.0507	.0228	.0364	.0443	.0366	.0417	
16	CFL	.0495	.0692	.0369	.0438	.0516	.0390	.0386	
17	CFL	.0737	.1040	.0682	.0692	.0720	.0595	.0649	
18	CFL	.0803	.1273	.0887	.0845	.0832	.0677		
19	CFL	.0862	.1558	.1109	.1006	.0976	.0753		
20	CFL	.0871	.1820	.1292	.1121	.1031	.0812		
21	CFL	.0957	.2156	.1531	.1292	.1112	.1766		
22	CFL	.0994	.2411	.1687	.1341	.1328			
23	CFL	.1218	.2706	.1852	.1393				
24	CFL	.1548	.2909	.1842	.2092				
25	CFL	.2173	.3275	.1993					
26	CFL	.2654	.3514						
27	CFL	.3063	.3758						
28	CFL	.3343	.3936						
29	CFL	.3666							
30	CFL	.3894							
31	CFL	.4110							
32	CFL	.4270							

Table II. Continued

(b)  $M_\infty = 1.90$ 

ORF	LOC	$C_p$ at $L/h$ of							
		17.500	14.845	12.895	11.920	10.945	9.970	8.020	4.120
1	FF	-.1571	-.1520	-.0385	-.0050	.0108	.0097	.0217	.0423
2	FF	-.1598	-.1545	-.0399	-.0073	.0084	.0080	.0207	.0426
3	FF	-.1549	-.1512	-.0385	-.0049	.0110	.0094	.0223	.0441
4	FF	-.1618	-.1580	-.0445	-.0099	.0046	.0042	.0160	.0362
5	FF	-.1615	-.1598	-.0407	-.0060	.0088	.0078	.0214	.0400
38	FF	-.1708	-.1671	-.0447	-.0111	.0081	.0033	.0172	.0350
39	FF	-.1668	-.1622	-.0410	-.0075	.0115	.0048	.0128	.0336
40	FF	-.1673	-.1622	-.0393	-.0069	.0132	.0063	.0160	.0397
41	FF	-.1750	-.1711	-.0466	-.0122	.0059	.0017	.0166	.0345
33	RF	.4557	.4111	.2263	.1870	.1708	.1429	.1322	.1037
34	RF	.4306	.3892	.2057	.1649	.1495	.1216	.1098	.0809
35	RF	.4242	.3845	.2079	.1674	.1480	.1188	.1031	.0664
36	RF	.4222	.3801	.2292	.1905	.1738	.1445	.1307	.0885
37	RF	.4038	.3639	.2680	.2378	.2262	.2020	.1999	.1613
42	RF	.5673	.5055	.2372	.1706	.1500	.1128	.0792	.0547
43	RF	.4675	.4139	.2059	.1622	.1457	.1158	.1029	.0744
44	RF	.4681	.4123	.2006	.1558	.1375	.1072	.0979	.0684
45	RF	.5748	.5241	.2362	.1705	.1465	.1103	.0797	.0527
74	VCF	.0287	.0239	.0197	.0273	.0262	.0169	.0222	.0263
76	VCF	.0311	.0264	.0215	.0300	.0276	.0193	.0243	.0277
78	VCF	.0311	.0254	.0201	.0288	.0266	.0183	.0236	.0271
80	VCF	.0313	.0263	.0203	.0286	.0250	.0192	.0233	
82	VCF	.0289	.0229	.0169	.0259	.0231	.0157	.0211	
84	VCF	.0318	.0258	.0202	.0301	.0261	.0191	.0251	
86	VCF	.0313	.0249	.0188	.0289	.0237	.0181		
88	VCF	.0329	.0254	.0191	.0304	.0253			
90	VCF	.0305	.0229	.0163	.0284				
92	VCF	.0338	.0253	.0189					
94	VCF	.0335	.0240						
96	VCF	.0338							
98	VCF	.0278							
6	CFL	-.1684	-.1667	-.0438	-.0087	.0053	.0045	.0181	.0325
7	CFL	-.1697	-.1701	-.0435	-.0075	.0076	.0061	.0194	.0310
8	CFL	-.1856	-.1858	-.0532	-.0173	-.0017	-.0020	.0124	.0204
9	CFL	-.1710	-.1720	-.0514	-.0152	-.0005	.0010	.0151	.0178
10	CFL	-.1357	-.1385	-.0559	-.0207	-.0047	-.0041	.0106	.0126
11	CFL	-.0875	-.0904	-.0453	-.0155	-.0009	-.0009	.0120	.0288
12	CFL	-.0526	-.0549	-.0375	-.0132	-.0013	-.0027	.0083	.1082
13	CFL	-.0142	-.0150	-.0156	-.0010	-.0010	.0120	.0076	.0168
14	CFL	.0097	.0119	.0019	.0127	.0208	.0147	.0210	
15	CFL	.0333	.0398	.0251	.0302	.0365	.0283	.0301	
16	CFL	.0382	.0524	.0342	.0346	.0397	.0285	.0254	
17	CFL	.0579	.0830	.0632	.0582	.0587	.0471	.0489	
18	CFL	.0623	.1052	.0794	.0700	.0681	.0531		
19	CFL	.0674	.1318	.0985	.0843	.0792	.0591		
20	CFL	.0676	.1552	.1139	.0931	.0831	.0650		
21	CFL	.0755	.1842	.1350	.1075	.0906	.1490		
22	CFL	.0782	.2041	.1488	.1113	.1099			
23	CFL	.1009	.2282	.1640	.1171				
24	CFL	.1363	.2422	.1617	.1786				
25	CFL	.1977	.2747	.1760					
26	CFL	.2357	.2982						
27	CFL	.2646	.3266						
28	CFL	.2830	.3470						
29	CFL	.3099							
30	CFL	.3305							
31	CFL	.3594							
32	CFL	.3809							

Table II. Continued

(c)  $M_\infty = 2.16$ 

ORF	LOC	$C_p$ at $L/h$ of							
		17.500	14.845	12.895	11.920	10.945	9.970	8.020	4.120
1	FF	-.1501	-.1525	-.0493	-.0092	.0060	.0055	.0198	.0346
2	FF	-.1528	-.1556	-.0510	-.0123	.0042	.0037	.0189	.0349
3	FF	-.1494	-.1536	-.0492	-.0096	.0058	.0045	.0200	.0366
4	FF	-.1553	-.1604	-.0558	-.0147	.0001	-.0008	.0143	.0279
5	FF	-.1526	-.1590	-.0518	-.0104	.0044	.0024	.0196	.0316
38	FF	-.1647	-.1623	-.0523	-.0165	.0020	-.0010	.0173	.0342
39	FF	-.1658	-.1625	-.0498	-.0133	.0050	.0000	.0137	.0330
40	FF	-.1660	-.1620	-.0497	-.0144	.0041	.0001	.0162	.0362
41	FF	-.1704	-.1669	-.0565	-.0190	-.0018	-.0037	.0163	.0326
33	RF	.4072	.3753	.2167	.1625	.1457	.1199	.1171	.0869
34	RF	.3824	.3559	.1999	.1435	.1296	.1026	.0984	.0712
35	RF	.3746	.3492	.2005	.1461	.1274	.1005	.0918	.0580
36	RF	.3682	.3390	.2165	.1674	.1508	.1233	.1179	.0749
37	RF	.3489	.3187	.2496	.2150	.2029	.1807	.1868	.1402
42	RF	.5385	.4842	.2337	.1451	.1231	.0918	.0695	.0483
43	RF	.4079	.3660	.1981	.1392	.1230	.0985	.0935	.0647
44	RF	.3986	.3662	.1991	.1369	.1203	.0946	.0877	.0656
45	RF	.5467	.5033	.2482	.1513	.1304	.1035	.0740	.0545
74	VCF	.0280	.0283	.0174	.0251	.0238	.0227	.0246	.0273
76	VCF	.0309	.0306	.0196	.0274	.0258	.0249	.0263	.0276
78	VCF	.0307	.0302	.0178	.0260	.0251	.0238	.0264	.0270
80	VCF	.0307	.0308	.0177	.0259	.0233	.0242	.0253	
82	VCF	.0291	.0274	.0144	.0235	.0215	.0201	.0220	
84	VCF	.0323	.0306	.0180	.0280	.0255	.0245	.0263	
86	VCF	.0323	.0302	.0164	.0273	.0235	.0232		
88	VCF	.0341	.0309	.0168	.0283	.0255			
90	VCF	.0311	.0277	.0141	.0257				
92	VCF	.0343	.0300	.0172					
94	VCF	.0341	.0291						
96	VCF	.0346							
98	VCF	.0286							
6	CFL	-.1574	-.1633	-.0556	-.0133	.0017	-.0005	.0168	.0252
7	CFL	-.1571	-.1644	-.0548	-.0114	.0037	.0017	.0188	.0236
8	CFL	-.1699	-.1762	-.0655	-.0217	-.0060	-.0069	.0114	.0140
9	CFL	-.1430	-.1488	-.0641	-.0185	-.0043	-.0040	.0145	.0122
10	CFL	-.1015	-.1071	-.0649	-.0248	-.0079	-.0084	.0100	.0071
11	CFL	-.0573	-.0621	-.0486	-.0182	-.0038	-.0048	.0119	.0205
12	CFL	-.0300	-.0335	-.0369	-.0150	-.0027	-.0066	.0080	.0879
13	CFL	-.0006	-.0025	-.0135	.0005	.0104	.0041	.0161	
14	CFL	.0163	.0156	.0041	.0108	.0191	.0111	.0192	
15	CFL	.0334	.0351	.0265	.0271	.0341	.0235	.0276	
16	CFL	.0334	.0412	.0350	.0301	.0353	.0224	.0212	
17	CFL	.0503	.0672	.0624	.0519	.0544	.0402	.0434	
18	CFL	.0521	.0889	.0768	.0619	.0620	.0442		
19	CFL	.0535	.1184	.0945	.0737	.0714	.0499		
20	CFL	.0530	.1454	.1097	.0814	.0745	.0531		
21	CFL	.0592	.1741	.1314	.0956	.0811	.1285		
22	CFL	.0574	.1906	.1448	.0982	.0976			
23	CFL	.0719	.2090	.1603	.1031				
24	CFL	.1041	.2167	.1595	.1556				
25	CFL	.1704	.2453	.1735					
26	CFL	.2098	.2671						
27	CFL	.2360	.2957						
28	CFL	.2486	.3173						
29	CFL	.2698							
30	CFL	.2894							
31	CFL	.3188							
32	CFL	.3363							

Table II. Concluded

(d)  $M_\infty = 2.86$ 

ORF	LOC	$C_p$ at $L/h$ of							
		17.500	14.845	12.895	11.920	10.945	9.970	8.020	4.120
1	FF	-.1082	-.1090	-.1121	-.0068	.0051	.0068	.0205	.0261
2	FF	-.1139	-.1142	-.1173	-.0090	.0009	.0042	.0190	.0274
3	FF	-.1104	-.1133	-.1146	-.0067	.0027	.0059	.0211	.0285
4	FF	-.1163	-.1204	-.1211	-.0121	-.0037	-.0006	.0133	.0190
5	FF	-.1107	-.1156	-.1146	-.0065	.0004	.0036	.0200	.0248
38	FF	-.1010	-.0995	-.0992	-.0104	-.0003	.0093	.0152	.0308
39	FF	-.1177	-.1159	-.1184	-.0156	-.0026	.0051	.0075	.0250
40	FF	-.1169	-.1157	-.1174	-.0156	-.0028	.0084	.0111	.0320
41	FF	-.1109	-.1096	-.1125	-.0161	-.0037	.0046	.0114	.0270
33	RF	.3684	.3450	.3139	.1352	.1148	.1053	.0885	.0668
34	RF	.3432	.3221	.2920	.1220	.1023	.0942	.0765	.0574
35	RF	.3319	.3126	.2825	.1232	.1031	.0915	.0712	.0473
36	RF	.3168	.2958	.2697	.1407	.1241	.1129	.0928	.0607
37	RF	.2932	.2760	.2556	.1864	.1759	.1684	.1531	.1173
42	RF	.7153	.6419	.5557	.1087	.0906	.0782	.0543	.0390
43	RF	.3321	.3075	.2786	.1140	.1012	.0898	.0745	.0547
44	RF	.3278	.3089	.2748	.1080	.0953	.0843	.0697	.0485
45	RF	.7489	.6955	.5680	.1089	.0917	.0781	.0566	.0411
74	VCF	.0455	.0325	.0278	.0265	.0239	.0261	.0270	.0225
76	VCF	.0490	.0352	.0310	.0299	.0274	.0285	.0294	.0241
78	VCF	.0482	.0343	.0294	.0286	.0269	.0269	.0286	.0223
80	VCF	.0474	.0340	.0280	.0278	.0275	.0261	.0264	
82	VCF	.0453	.0306	.0253	.0248	.0238	.0229	.0245	
84	VCF	.0501	.0351	.0285	.0300	.0285	.0271	.0286	
86	VCF	.0493	.0338	.0274	.0300	.0267	.0256		
88	VCF	.0515	.0341	.0277	.0315	.0282			
90	VCF	.0480	.0304	.0248	.0278				
92	VCF	.0520	.0335	.0275					
94	VCF	.0517	.0319						
96	VCF	.0525							
98	VCF	.0453							
6	CFL	-.1120	-.1174	-.1165	-.0078	-.0034	.0012	.0161	.0183
7	CFL	-.1088	-.1167	-.1128	-.0055	-.0020	.0038	.0188	.0185
8	CFL	-.1160	-.1221	-.1185	-.0144	-.0118	-.0055	.0110	.0099
9	CFL	-.0916	-.0970	-.0915	-.0100	-.0073	-.0008	.0132	.0095
10	CFL	-.0585	-.0637	-.0577	-.0162	-.0131	-.0054	.0087	.0034
11	CFL	-.0265	-.0308	-.0243	-.0064	-.0067	.0006	.0122	.0144
12	CFL	-.0144	-.0187	-.0118	-.0028	-.0052	.0008	.0088	.0662
13	CFL	.0049	.0018	.0079	.0128	.0072	.0125	.0176	
14	CFL	.0141	.0101	.0182	.0213	.0159	.0180	.0193	
15	CFL	.0251	.0229	.0408	.0351	.0283	.0306	.0269	
16	CFL	.0181	.0154	.0680	.0346	.0255	.0245	.0170	
17	CFL	.0321	.0319	.1301	.0528	.0452	.0423	.0354	
18	CFL	.0324	.0337	.1593	.0598	.0506	.0438		
19	CFL	.0343	.0578	.1771	.0684	.0609	.0479		
20	CFL	.0343	.1131	.1830	.0731	.0587	.0499		
21	CFL	.0421	.1658	.1985	.0854	.0664	.1151		
22	CFL	.0396	.1859	.2104	.0847	.0795			
23	CFL	.0480	.1999	.2290	.0902				
24	CFL	.0751	.1993	.2324	.1322				
25	CFL	.1515	.2225	.2721					
26	CFL	.1905	.2362						
27	CFL	.2120	.2586						
28	CFL	.2171	.2924						
29	CFL	.2354							
30	CFL	.2450							
31	CFL	.2719							
32	CFL	.3053							

Table III. Porous-Floor Pressure Data

(a)  $M_\infty = 1.60$

ORF	LOC	$C_p$ at $L/h$ of							
		17.500	14.845	12.895	11.920	10.945	9.970	8.020	4.120
1	FF	-.0186	-.0157	.0029	.0106	.0105	.0152	.0249	.0550
2	FF	-.0169	-.0187	.0003	.0074	.0080	.0122	.0223	.0524
3	FF	-.0170	-.0177	.0019	.0083	.0096	.0135	.0239	.0522
4	FF	-.0263	-.0232	-.0034	.0022	.0035	.0073	.0188	.0433
5	FF	-.0203	-.0198	.0004	.0058	.0071	.0116	.0230	.0467
38	FF	-.0313	-.0104	-.0075	.0022	.0069	.0109	.0183	.0384
39	FF	-.0335	-.0104	-.0077	.0012	.0067	.0104	.0174	.0377
40	FF	-.0246	-.0105	-.0075	.0034	.0103	.0110	.0178	.0413
41	FF	-.0321	-.0111	-.0074	.0029	.0083	.0110	.0186	.0404
33	RF	.2673	.2226	.1815	.1709	.1560	.1482	.1365	.1157
34	RF	.2486	.2034	.1591	.1464	.1330	.1237	.1085	.0828
35	RF	.2475	.2084	.1618	.1479	.1340	.1252	.1061	.0711
36	RF	.2696	.2318	.1893	.1780	.1667	.1574	.1415	.1024
37	RF	.2880	.2674	.2350	.2309	.2265	.2228	.2194	.1944
42	RF	.2533	.1885	.1469	.1363	.1247	.1073	.0813	.0649
43	RF	.2663	.2117	.1636	.1511	.1372	.1223	.1056	.0780
44	RF	.2565	.2061	.1587	.1457	.1306	.1159	.1016	.0690
45	RF	.2411	.1800	.1384	.1286	.1181	.1011	.0816	.0602
74	VCF	.0456	.0358	.0251	.0266	.0265	.0164	.0175	.0331
76	VCF	.0378	.0331	.0256	.0275	.0274	.0186	.0205	.0354
78	VCF	.0285	.0241	.0210	.0239	.0252	.0168	.0199	.0396
80	VCF	.0109	.0133	.0155	.0196	.0216	.0153	.0199	
82	VCF	-.0030	-.0001	.0083	.0146	.0199	.0125	.0184	
84	VCF	-.0077	.0040	.0172	.0234	.0280	.0201	.0269	
86	VCF	.0017	.0162	.0285	.0323	.0343	.0247		
88	VCF	.0235	.0379	.0453	.0446	.0439			
90	VCF	.0441	.0566	.0548	.0507				
92	VCF	.0738	.0789	.0706					
94	VCF	.1003	.0922						
96	VCF	.1252							
98	VCF	.1380							
6	CFL	-.0255	-.0220	-.0020	.0031	.0044	.0094	.0213	.0392
7	CFL	-.0230	-.0188	.0012	.0056	.0062	.0119	.0231	.0388
8	CFL	-.0274	-.0265	-.0063	-.0021	-.0008	.0046	.0148	.0284
9	CFL	-.0251	-.0191	-.0003	.0043	.0049	.0113	.0201	.0333
10	CFL	-.0255	-.0201	-.0026	.0016	.0015	.0080	.0158	.0199
11	CFL	-.0200	-.0154	.0017	.0070	.0077	.0117	.0172	.0224
12	CFL	-.0236	-.0178	-.0009	.0042	.0041	.0078	.0110	.0129
13	CFL	-.0198	-.0106	.0046	.0100	.0099	.0138	.0160	
14	CFL	-.0219	-.0104	.0041	.0101	.0107	.0140	.0148	
15	CFL	-.0141	-.0052	.0094	.0162	.0182	.0208	.0200	
16	CFL	-.0242	-.0093	.0037	.0131	.0137	.0162	.0144	
17	CFL	-.0125	.0042	.0196	.0287	.0293	.0316	.0426	
18	CFL	-.0076	.0107	.0271	.0357	.0356	.0362		
19	CFL	.0036	.0242	.0395	.0461	.0446	.0433		
20	CFL	.0140	.0336	.0488	.0533	.0505	.0563		
21	CFL	.0322	.0518	.0650	.0673	.0645	.1537		
22	CFL	.0424	.0647	.0741	.0731	.0919			
23	CFL	.0586	.0821	.0852	.0894				
24	CFL	.0663	.0888	.0861	.1621				
25	CFL	.0893	.1091	.1217					
26	CFL	.1059	.1194						
27	CFL	.1262	.1322						
28	CFL	.1414	.1532						
29	CFL	.1617							
30	CFL	.1728							
31	CFL	.1810							
32	CFL	.2049							

Table III. Continued

(b)  $M_\infty = 1.90$ 

ORF	LOC	$C_p$ at $L/h$ of							
		17.500	14.845	12.895	11.920	10.945	9.970	8.020	4.120
1	FF	-.0228	-.0165	.0011	.0030	.0087	.0121	.0198	.0363
2	FF	-.0218	-.0200	-.0015	-.0011	.0055	.0083	.0173	.0330
3	FF	-.0212	-.0179	.0002	.0004	.0069	.0100	.0194	.0336
4	FF	-.0293	-.0225	-.0039	-.0054	.0012	.0039	.0140	.0266
5	FF	-.0234	-.0191	-.0012	-.0030	.0041	.0083	.0177	.0306
38	FF	-.0266	-.0103	-.0042	.0021	.0092	.0082	.0119	.0344
39	FF	-.0295	-.0120	-.0056	.0006	.0077	.0073	.0104	.0338
40	FF	-.0214	-.0117	-.0050	.0023	.0122	.0083	.0112	.0346
41	FF	-.0281	-.0122	-.0049	.0018	.0096	.0077	.0114	.0339
33	RF	.2392	.1941	.1597	.1460	.1368	.1262	.1110	.0789
34	RF	.2234	.1779	.1402	.1256	.1171	.1059	.0885	.0569
35	RF	.2206	.1807	.1416	.1257	.1162	.1062	.0852	.0465
36	RF	.2379	.2009	.1680	.1527	.1466	.1348	.1153	.0724
37	RF	.2569	.2379	.2155	.2044	.2047	.1999	.1893	.1590
42	RF	.2296	.1588	.1229	.1127	.1055	.0869	.0631	.0351
43	RF	.2399	.1833	.1431	.1290	.1216	.1041	.0850	.0468
44	RF	.2305	.1752	.1384	.1238	.1166	.0984	.0811	.0435
45	RF	.2271	.1533	.1200	.1089	.1050	.0852	.0643	.0344
74	VCF	.0362	.0257	.0187	.0180	.0236	.0129	.0089	.0238
76	VCF	.0294	.0238	.0195	.0191	.0241	.0145	.0127	.0271
78	VCF	.0211	.0164	.0159	.0161	.0218	.0136	.0115	.0277
80	VCF	.0055	.0084	.0118	.0126	.0190	.0128	.0122	
82	VCF	-.0050	-.0031	.0059	.0082	.0172	.0100	.0102	
84	VCF	-.0086	.0013	.0132	.0166	.0242	.0164	.0177	
86	VCF	-.0023	.0112	.0228	.0231	.0281	.0193		
88	VCF	.0161	.0292	.0367	.0324				
90	VCF	.0331	.0437	.0440	.0362				
92	VCF	.0585	.0648	.0576					
94	VCF	.0814	.0742						
96	VCF	.1036							
98	VCF	.1145							
6	CFL	-.0285	-.0215	-.0027	-.0043	.0021	.0058	.0159	.0272
7	CFL	-.0262	-.0185	-.0005	-.0019	.0045	.0089	.0170	.0295
8	CFL	-.0310	-.0256	-.0078	-.0101	-.0025	.0016	.0095	.0212
9	CFL	-.0283	-.0177	-.0019	-.0035	.0023	.0080	.0144	.0245
10	CFL	-.0291	-.0190	-.0033	-.0063	-.0007	.0050	.0104	.0167
11	CFL	-.0229	-.0141	.0012	-.0010	.0049	.0090	.0117	.0086
12	CFL	-.0264	-.0166	-.0019	-.0044	.0021	.0044	.0062	.0841
13	CFL	-.0229	-.0088	.0041	.0015	.0072	.0110	.0110	
14	CFL	-.0243	-.0087	.0036	.0016	.0085	.0114	.0098	
15	CFL	-.0165	-.0023	.0089	.0085	.0156	.0179	.0137	
16	CFL	-.0258	-.0083	.0049	.0036	.0112	.0129	.0089	
17	CFL	-.0145	.0058	.0184	.0187	.0252	.0267	.0320	
18	CFL	-.0100	.0117	.0240	.0246	.0303	.0301		
19	CFL	-.0003	.0234	.0350	.0335	.0372	.0359		
20	CFL	.0082	.0309	.0413	.0395	.0411	.0471		
21	CFL	.0241	.0477	.0561	.0506	.0535	.1351		
22	CFL	.0330	.0584	.0632	.0545	.0791			
23	CFL	.0475	.0733	.0723	.0696				
24	CFL	.0538	.0779	.0713	.1358				
25	CFL	.0743	.0963	.1051					
26	CFL	.0898	.1048						
27	CFL	.1072	.1154						
28	CFL	.1201	.1346						
29	CFL	.1419							
30	CFL	.1527							
31	CFL	.1627							
32	CFL	.1852							

Table III. Continued

(c)  $M_\infty = 2.16$ 

ORF	LOC	$C_p$ at $L/h$ of							
		17.500	14.845	12.895	11.920	10.945	9.970	8.020	4.120
1	FF	-.0287	-.0170	-.0057	.0018	.0019	.0108	.0218	.0314
2	FF	-.0276	-.0203	-.0084	-.0015	-.0014	.0070	.0197	.0273
3	FF	-.0268	-.0183	-.0057	.0000	.0001	.0087	.0211	.0272
4	FF	-.0351	-.0239	-.0106	-.0059	-.0059	.0029	.0161	.0201
5	FF	-.0291	-.0212	-.0067	-.0030	-.0022	.0066	.0199	.0239
38	FF	-.0240	-.0173	-.0102	-.0005	.0017	.0066	.0112	.0250
39	FF	-.0275	-.0196	-.0123	-.0026	-.0004	.0052	.0084	.0232
40	FF	-.0193	-.0197	-.0117	-.0015	.0029	.0051	.0102	.0239
41	FF	-.0267	-.0199	-.0115	-.0025	.0011	.0061	.0105	.0242
33	RF	.2185	.1695	.1379	.1331	.1158	.1118	.0966	.0581
34	RF	.2053	.1553	.1215	.1138	.0993	.0948	.0785	.0427
35	RF	.2002	.1567	.1223	.1128	.0985	.0940	.0748	.0330
36	RF	.2141	.1750	.1456	.1376	.1253	.1198	.1028	.0538
37	RF	.2315	.2117	.1927	.1891	.1832	.1831	.1736	.1316
42	RF	.2122	.1354	.1007	.0929	.0839	.0736	.0552	.0253
43	RF	.2143	.1586	.1223	.1126	.1019	.0931	.0768	.0357
44	RF	.2147	.1567	.1203	.1102	.0990	.0892	.0734	.0351
45	RF	.2226	.1380	.1028	.0968	.0890	.0776	.0604	.0286
74	VCF	.0273	.0202	.0104	.0132	.0147	.0096	.0092	.0178
76	VCF	.0219	.0190	.0115	.0145	.0152	.0115	.0117	.0207
78	VCF	.0140	.0123	.0069	.0122	.0137	.0100	.0114	.0212
80	VCF	-.0001	.0051	.0042	.0096	.0118	.0088	.0110	
82	VCF	-.0081	-.0044	-.0013	.0053	.0089	.0062	.0092	
84	VCF	-.0102	-.0005	.0064	.0133	.0169	.0128	.0163	
86	VCF	-.0053	.0090	.0155	.0200	.0207	.0149		
88	VCF	.0103	.0255	.0278	.0283	.0269			
90	VCF	.0246	.0386	.0334	.0310				
92	VCF	.0480	.0575	.0454					
94	VCF	.0690	.0665						
96	VCF	.0875							
98	VCF	.0983							
6	CFL	-.0331	-.0226	-.0083	-.0039	-.0046	.0050	.0184	.0202
7	CFL	-.0301	-.0202	-.0053	-.0020	-.0019	.0075	.0204	.0226
8	CFL	-.0353	-.0280	-.0123	-.0095	-.0087	-.0004	.0114	.0132
9	CFL	-.0328	-.0202	-.0059	-.0029	-.0036	.0065	.0169	.0167
10	CFL	-.0328	-.0221	-.0079	-.0057	-.0063	.0037	.0122	.0097
11	CFL	-.0275	-.0166	-.0029	-.0003	-.0009	.0076	.0142	.0037
12	CFL	-.0297	-.0200	-.0054	-.0026	-.0040	.0034	.0074	.0678
13	CFL	-.0253	-.0118	.0001	.0036	.0023	.0105	.0131	
14	CFL	-.0265	-.0114	.0007	.0038	.0032	.0111	.0120	
15	CFL	-.0174	-.0055	.0059	.0103	.0111	.0172	.0152	
16	CFL	-.0272	-.0112	.0009	.0062	.0056	.0118	.0092	
17	CFL	-.0152	.0030	.0158	.0217	.0203	.0265	.0306	
18	CFL	-.0124	.0080	.0206	.0265	.0238	.0288		
19	CFL	-.0034	.0184	.0300	.0349	.0306	.0339		
20	CFL	.0046	.0241	.0358	.0389	.0325	.0428		
21	CFL	.0196	.0394	.0496	.0496	.0439	.1253		
22	CFL	.0280	.0481	.0547	.0520	.0667			
23	CFL	.0413	.0620	.0639	.0660				
24	CFL	.0459	.0654	.0610	.1261				
25	CFL	.0655	.0827	.0914					
26	CFL	.0786	.0906						
27	CFL	.0952	.1002						
28	CFL	.1068	.1161						
29	CFL	.1277							
30	CFL	.1376							
31	CFL	.1468							
32	CFL	.1711							

Table III. Concluded

(d)  $M_\infty = 2.86$ 

ORF	LOC	$C_p$ at $L/h$ of							
		17.500	14.845	12.895	11.920	10.945	9.970	8.020	4.120
1	FF	-.0217	-.0180	-.0101	-.0061	.0002	.0067	.0102	.0293
2	FF	-.0203	-.0220	-.0138	-.0105	-.0031	.0027	.0071	.0257
3	FF	-.0187	-.0201	-.0115	-.0072	-.0007	.0052	.0094	.0262
4	FF	-.0270	-.0255	-.0165	-.0145	-.0081	-.0024	.0033	.0185
5	FF	-.0199	-.0210	-.0127	-.0096	-.0041	.0025	.0095	.0232
38	FF	-.0195	-.0106	-.0034	.0047	.0077	.0074	.0121	.0206
39	FF	-.0292	-.0169	-.0096	-.0025	.0005	.0012	.0058	.0154
40	FF	-.0207	-.0166	-.0084	-.0002	.0045	.0016	.0075	.0178
41	FF	-.0260	-.0152	-.0084	-.0006	.0032	.0035	.0086	.0191
33	RF	.1709	.1331	.1133	.1111	.0978	.0893	.0795	.0413
34	RF	.1615	.1243	.1033	.0983	.0876	.0786	.0681	.0332
35	RF	.1541	.1253	.1034	.0964	.0861	.0781	.0650	.0251
36	RF	.1649	.1385	.1227	.1184	.1080	.0988	.0847	.0433
37	RF	.1781	.1724	.1643	.1644	.1608	.1561	.1458	.1143
42	RF	.1735	.1123	.0841	.0779	.0710	.0581	.0457	.0214
43	RF	.1668	.1245	.1022	.0962	.0893	.0780	.0650	.0345
44	RF	.1717	.1234	.1001	.0945	.0859	.0734	.0601	.0287
45	RF	.1886	.1151	.0878	.0790	.0729	.0594	.0481	.0236
74	VCF	.0191	.0123	.0072	.0077	.0115	.0048	.0011	.0156
76	VCF	.0157	.0121	.0089	.0104	.0142	.0081	.0042	.0186
78	VCF	.0087	.0080	.0076	.0095	.0133	.0076	.0033	.0185
80	VCF	.0006	.0055	.0043	.0066	.0105	.0053	.0028	
82	VCF	-.0021	-.0031	.0006	.0033	.0087	.0034	.0021	
84	VCF	-.0023	.0027	.0077	.0115	.0161	.0091	.0084	
86	VCF	.0005	.0084	.0145	.0163	.0192	.0110		
88	VCF	.0118	.0205	.0252	.0229	.0234			
90	VCF	.0207	.0279	.0271	.0222				
92	VCF	.0392	.0430	.0374					
94	VCF	.0540	.0487						
96	VCF	.0673							
98	VCF	.0718							
6	CFL	-.0253	-.0230	-.0142	-.0116	-.0061	.0004	.0077	.0198
7	CFL	-.0231	-.0206	-.0104	-.0078	-.0032	.0029	.0099	.0213
8	CFL	-.0269	-.0285	-.0193	-.0159	-.0105	-.0048	.0017	.0119
9	CFL	-.0259	-.0207	-.0124	-.0089	-.0051	.0017	.0088	.0153
10	CFL	-.0271	-.0221	-.0156	-.0128	-.0091	-.0024	.0026	.0069
11	CFL	-.0207	-.0165	-.0084	-.0059	-.0021	.0038	.0069	.0055
12	CFL	-.0230	-.0193	-.0117	-.0075	-.0045	-.0009	.0008	.0574
13	CFL	-.0171	-.0097	-.0051	-.0009	-.0039	.0086	.0094	
14	CFL	-.0176	-.0080	-.0029	.0024	.0053	.0091	.0085	
15	CFL	-.0079	-.0001	.0044	.0115	.0145	.0171	.0136	
16	CFL	-.0196	-.0069	-.0039	.0066	.0071	.0100	.0065	
17	CFL	-.0066	.0095	.0127	.0225	.0238	.0260	.0260	
18	CFL	-.0054	.0116	.0167	.0263	.0260	.0267		
19	CFL	.0012	.0210	.0235	.0330	.0309	.0306		
20	CFL	.0074	.0236	.0285	.0352	.0315	.0353		
21	CFL	.0211	.0372	.0411	.0457	.0420	.1052		
22	CFL	.0259	.0425	.0448	.0469	.0590			
23	CFL	.0359	.0537	.0522	.0584				
24	CFL	.0361	.0525	.0470	.1052				
25	CFL	.0530	.0689	.0731					
26	CFL	.0619	.0744						
27	CFL	.0745	.0828						
28	CFL	.0811	.0926						
29	CFL	.0990							
30	CFL	.1040							
31	CFL	.1099							
32	CFL	.1355							

Table IV. Solid-/Porous-Floor Combination Pressure Data

 (a)  $C_p$  at  $L/h = 17.500$  at  $M_\infty = 1.60$ 

ORF	LOC	Percent of floor area with porosity									
		0		28.6			57.1			100	
		2 stores	3 stores	0 stores	2 stores	3 stores	0 stores	2 stores	3 stores	2 stores	3 stores
1	FF	-.1242	-.1163	-.0517	-.0442	-.0302	-.0242	-.0203	-.0168	-.0178	-.0212
2	FF	-.1264	-.1192	-.0558	-.0473	-.0334	-.0266	-.0234	-.0182	-.0181	-.0231
3	FF	-.1250	-.1146	-.0566	-.0476	-.0348	-.0260	-.0226	-.0180	-.0167	-.0216
4	FF	-.1330	-.1168	-.0675	-.0558	-.0441	-.0343	-.0281	-.0257	-.0239	-.0274
5	FF	-.1331	-.1153	-.0644	-.0518	-.0404	-.0312	-.0255	-.0213	-.0187	-.0235
38	FF	-.1498	-.1239	-.0578	-.0453	-.0401	-.0321	-.0165	-.0228	-.0282	-.0303
39	FF	-.1463	-.1219	-.0610	-.0479	-.0416	-.0331	-.0170	-.0230	-.0290	-.0310
40	FF	-.1472	-.1189	-.0605	-.0446	-.0376	-.0302	-.0165	-.0183	-.0215	-.0284
41	FF	-.1527	-.1310	-.0580	-.0454	-.0386	-.0315	-.0152	-.0221	-.0278	-.0312
33	RF	.5383	.3836	.3286	.2828	.2831	.2668	.2411	.2497	.2317	.2344
34	RF	.4747	.3460	.3137	.2593	.2600	.2508	.2205	.2285	.2090	.2150
35	RF	.4988	.3562	.3157	.2616	.2660	.2540	.2250	.2305	.2085	.2154
36	RF	.5788	.3857	.3152	.2785	.2831	.2677	.2414	.2463	.2327	.2285
37	RF	.6215	.3809	.3085	.2911	.2930	.2808	.2644	.2564	.2581	.2408
42	RF	.3147	.3072	.3474	.2365	.2234	.2661	.2227	.2042	.2023	.1894
43	RF	.5212	.3871	.3535	.3043	.2904	.2734	.2428	.2534	.2260	.2392
44	RF	.5197	.3824	.3308	.2719	.2895	.2656	.2336	.2501	.2166	.2288
45	RF	.3203	.3039	.3350	.2346	.2262	.2540	.2171	.2049	.2008	.1898
74	VCF	.0136	.0101	.0957	.0668	.0684	.0534	.0439	.0443	.0327	.0217
76	VCF	.0159	.0122	.0869	.0611	.0638	.0464	.0392	.0386	.0270	.0195
78	VCF	.0152	.0118	.0860	.0594	.0630	.0334	.0282	.0277	.0191	.0122
80	VCF	.0156	.0102	.0898	.0615	.0642	.0164	.0169	.0151	.0040	.0026
82	VCF	.0124	.0092	.0863	.0611	.0640	.0181	.0162	.0170	-.0029	-.0075
84	VCF	.0155	.0128	.0915	.0664	.0688	.0256	.0226	.0234	-.0055	-.0095
86	VCF	.0145	.0120	.0934	.0674	.0702	.0282	.0259	.0265	-.0002	-.0075
88	VCF	.0154	.0137	.0961	.0717	.0726	.0329	.0300	.0312	.0184	.0060
90	VCF	.0127	.0101	.0962	.0707	.0724	.0341	.0310	.0316	.0336	.0192
92	VCF	.0145	.0124	.1015	.0758	.0758	.0455	.0407	.0413	.0582	.0428
94	VCF	.0136	.0116	.1034	.0774	.0778	.0852	.0706	.0684	.0812	.0660
96	VCF	.0142	.0118	.1108	.0840	.0837	.1169	.0963	.0936	.1018	.0901
98	VCF	.0076	.0050	.1451	.1094	.1052	.1331	.1098	.1080	.1132	.1030
6	CFL	-.1412	-.1238	-.0672	-.0551	-.0441	-.0346	-.0279	-.0241	-.0229	-.0256
7	CFL	-.1450	-.1253	-.0648	-.0533	-.0431	-.0329	-.0250	-.0225	-.0208	-.0242
8	CFL	-.1593	-.1387	-.0680	-.0569	-.0504	-.0383	-.0330	-.0300	-.0274	-.0314
9	CFL	-.1560	-.1383	-.0619	-.0517	-.0451	-.0325	-.0263	-.0246	-.0253	-.0260
10	CFL	-.1463	-.1234	-.0700	-.0568	-.0461	-.0342	-.0295	-.0263	-.0274	-.0287
11	CFL	-.1091	-.0938	-.0689	-.0537	-.0472	-.0305	-.0243	-.0207	-.0211	-.0239
12	CFL	-.0706	-.0245	-.0718	-.0565	-.0418	-.0346	-.0281	-.0243	-.0252	-.0266
13	CFL	-.0213	-.0011	-.0585	-.0457	-.0363	-.0315	-.0219	-.0182	-.0192	-.0199
14	CFL	.0097	.0239	-.0467	-.0378	-.0310	-.0355	-.0245	-.0217	-.0206	-.0213
15	CFL	.0308	.0418	-.0290	-.0223	-.0172	-.0299	-.0199	-.0175	-.0133	-.0167
16	CFL	.0325	.0388	-.0190	-.0209	-.0180	-.0313	-.0211	-.0249	-.0245	-.0252
17	CFL	.0552	.0551	.0045	.0009	.0004	-.0107	-.0053	-.0109	-.0123	-.0158
18	CFL	.0636	.0602	.0181	.0112	.0084	-.0010	.0016	-.0065	-.0123	-.0164
19	CFL	.0742	.0693	.0354	.0252	.0200	.0136	.0120	.0003	-.0048	-.0124
20	CFL	.0765	.0735	.0457	.0346	.0272	.0222	.0183	.0055	.0037	-.0095
21	CFL	.0859	.0864	.0649	.0522	.0425	.0394	.0334	.0177	.0201	.0029
22	CFL	.0889	.0957	.0787	.0630	.0512	.0496	.0414	.0246	.0296	.0100
23	CFL	.1017	.1138	.0977	.0792	.0657	.0643	.0551	.0365	.0445	.0228
24	CFL	.1143	.1288	.1054	.0857	.0712	.0681	.0577	.0386	.0504	.0261
25	CFL	.1602	.1776	.1302	.1085	.0986	.0863	.0753	.0595	.0698	.0498
26	CFL	.2054	.1687	.1460	.1217	.1030	.0996	.0859	.0702	.0861	.0652
27	CFL	.2527	.2050	.1660	.1413	.1204	.1207	.1041	.0852	.1048	.0820
28	CFL	.2843	.2302	.1784	.1521	.1299	.1352	.1174	.1007	.1165	.0967
29	CFL	.3231	.2481	.1966	.1675	.1368	.1575	.1376	.1198	.1339	.1150
30	CFL	.3665	.2648	.2121	.1772	.1437	.1742	.1496	.1314	.1425	.1255
31	CFL	.4074	.2871	.2371	.1905	.1748	.1888	.1653	.1545	.1469	.1476
32	CFL	.3440	.2828	.2609	.2063	.1951	.2064	.1754	.1750	.1669	.1634

Table IV. Continued

(b)  $C_p$  at  $L/h = 17.500$  at  $M_\infty = 1.90$ 

ORF	LOC	Percent of floor area with porosity									
		0		28.6			57.1			100	
		2 stores	3 stores	0 stores	2 stores	3 stores	0 stores	2 stores	3 stores	2 stores	3 stores
1	FF	-.1123	-.1082	-.0478	-.0404	-.0319	-.0260	-.0153	-.0164	-.0180	-.0224
2	FF	-.1153	-.1115	-.0516	-.0441	-.0350	-.0291	-.0189	-.0179	-.0183	-.0249
3	FF	-.1122	-.1068	-.0535	-.0442	-.0360	-.0295	-.0183	-.0174	-.0169	-.0228
4	FF	-.1197	-.1098	-.0632	-.0522	-.0434	-.0367	-.0235	-.0234	-.0229	-.0281
5	FF	-.1217	-.1068	-.0589	-.0477	-.0392	-.0329	-.0204	-.0200	-.0181	-.0239
38	FF	-.1371	-.1105	-.0538	-.0464	-.0348	-.0312	-.0211	-.0218	-.0246	-.0269
39	FF	-.1333	-.1143	-.0559	-.0480	-.0360	-.0320	-.0220	-.0224	-.0257	-.0273
40	FF	-.1343	-.1109	-.0558	-.0444	-.0328	-.0305	-.0223	-.0174	-.0182	-.0240
41	FF	-.1398	-.1148	-.0540	-.0467	-.0337	-.0316	-.0202	-.0219	-.0245	-.0269
33	RF	.5086	.3386	.2995	.2304	.2396	.2386	.2017	.2147	.1965	.2022
34	RF	.4459	.3011	.2862	.2129	.2197	.2250	.1836	.1953	.1774	.1830
35	RF	.4560	.3022	.2858	.2117	.2216	.2258	.1848	.1943	.1736	.1829
36	RF	.5270	.3294	.2819	.2196	.2323	.2369	.1963	.2062	.1932	.1927
37	RF	.5716	.3323	.2741	.2283	.2400	.2513	.2188	.2144	.2190	.2041
42	RF	.2784	.2673	.3216	.2101	.1997	.2375	.1843	.1762	.1733	.1648
43	RF	.5062	.3382	.3132	.2546	.2532	.2426	.2027	.2234	.1957	.2105
44	RF	.5595	.3327	.3002	.2319	.2539	.2371	.1993	.2216	.1886	.2052
45	RF	.2953	.2694	.3233	.2208	.2113	.2375	.1941	.1854	.1843	.1749
74	VCF	.0134	.0074	.0881	.0576	.0600	.0434	.0358	.0356	.0265	.0193
76	VCF	.0159	.0099	.0833	.0570	.0590	.0371	.0319	.0316	.0224	.0180
78	VCF	.0151	.0099	.0832	.0552	.0581	.0254	.0220	.0219	.0149	.0118
80	VCF	.0153	.0084	.0866	.0561	.0591	.0127	.0147	.0129	.0024	.0042
82	VCF	.0114	.0074	.0829	.0562	.0577	.0134	.0127	.0139	-.0023	-.0040
84	VCF	.0150	.0115	.0884	.0612	.0629	.0206	.0195	.0199	-.0038	-.0041
86	VCF	.0140	.0109	.0893	.0623	.0631	.0235	.0217	.0225	.0004	-.0033
88	VCF	.0141	.0126	.0910	.0655	.0652	.0279	.0261	.0275	.0155	.0077
90	VCF	.0118	.0101	.0918	.0641	.0647	.0295	.0276	.0275	.0277	.0171
92	VCF	.0135	.0126	.0969	.0688	.0679	.0401	.0360	.0355	.0489	.0373
94	VCF	.0126	.0118	.0980	.0704	.0686	.0711	.0597	.0565	.0679	.0565
96	VCF	.0136	.0119	.1045	.0760	.0736	.0978	.0812	.0773	.0850	.0764
98	VCF	.0068	.0060	.1305	.0958	.0904	.1113	.0905	.0882	.0928	.0856
6	CFL	-.1298	-.1138	-.0611	-.0506	-.0422	-.0356	-.0228	-.0229	-.0216	-.0267
7	CFL	-.1332	-.1138	-.0590	-.0496	-.0401	-.0333	-.0195	-.0208	-.0198	-.0248
8	CFL	-.1485	-.1245	-.0630	-.0546	-.0474	-.0401	-.0275	-.0276	-.0264	-.0314
9	CFL	-.1427	-.1204	-.0556	-.0488	-.0414	-.0337	-.0214	-.0231	-.0243	-.0260
10	CFL	-.1250	-.1030	-.0635	-.0538	-.0429	-.0359	-.0245	-.0245	-.0263	-.0286
11	CFL	-.0866	-.0655	-.0613	-.0509	-.0423	-.0312	-.0188	-.0177	-.0190	-.0242
12	CFL	-.0549	-.0175	-.0641	-.0535	-.0382	-.0366	-.0225	-.0212	-.0229	-.0260
13	CFL	-.0163	.0034	-.0511	-.0429	-.0315	-.0317	-.0159	-.0160	-.0179	-.0196
14	CFL	.0060	.0204	-.0403	-.0349	-.0263	-.0350	-.0186	-.0182	-.0186	-.0202
15	CFL	.0211	.0327	-.0241	-.0216	-.0142	-.0292	-.0136	-.0141	-.0111	-.0162
16	CFL	.0170	.0287	-.0200	-.0213	-.0155	-.0304	-.0174	-.0207	-.0216	-.0238
17	CFL	.0385	.0424	.0040	-.0025	.0014	-.0121	-.0009	-.0081	-.0109	-.0139
18	CFL	.0453	.0460	.0157	.0054	.0074	-.0037	.0053	.0042	-.0101	-.0145
19	CFL	.0526	.0526	.0304	.0167	.0170	.0083	.0143	.0027	-.0040	-.0113
20	CFL	.0543	.0568	.0400	.0242	.0228	.0163	.0193	.0060	.0030	-.0098
21	CFL	.0617	.0690	.0578	.0402	.0367	.0321	.0327	.0180	.0173	.0018
22	CFL	.0617	.0766	.0701	.0498	.0433	.0408	.0393	.0227	.0253	.0074
23	CFL	.0676	.0934	.0881	.0640	.0560	.0543	.0512	.0334	.0384	.0176
24	CFL	.0696	.1059	.0937	.0685	.0594	.0574	.0522	.0333	.0422	.0195
25	CFL	.1074	.1439	.1167	.0892	.0822	.0738	.0675	.0510	.0600	.0395
26	CFL	.1574	.1481	.1298	.1017	.0916	.0851	.0754	.0618	.0744	.0559
27	CFL	.2118	.1746	.1478	.1190	.1047	.1040	.0913	.0738	.0909	.0691
28	CFL	.2475	.1996	.1585	.1281	.1144	.1161	.1015	.0861	.1009	.0813
29	CFL	.2927	.2187	.1753	.1415	.1240	.1370	.1175	.1041	.1168	.0997
30	CFL	.3418	.2272	.1876	.1476	.1257	.1520	.1258	.1111	.1224	.1063
31	CFL	.3685	.2423	.2136	.1588	.1481	.1697	.1377	.1296	.1241	.1223
32	CFL	.3165	.2400	.2374	.1700	.1643	.1860	.1462	.1414	.1375	

Table IV. Continued

(c)  $C_p$  at  $L/h = 17.500$  at  $M_\infty = 2.16$ 

ORF	LOC	Percent of floor area with porosity									
		0		28.6			57.1			100	
		2 stores	3 stores	0 stores	2 stores	3 stores	0 stores	2 stores	3 stores	2 stores	3 stores
1	FF	-.1101	-.1043	-.0507	-.0388	-.0318	-.0285	-.0206		-.0249	-.0241
2	FF	-.1136	-.1072	-.0552	-.0424	-.0348	-.0324	-.0251		-.0251	-.0258
3	FF	-.1097	-.1030	-.0578	-.0426	-.0351	-.0328	-.0237		-.0236	-.0235
4	FF	-.1160	-.1066	-.0664	-.0502	-.0420	-.0394	-.0290		-.0296	-.0288
5	FF	-.1171	-.1028	-.0614	-.0460	-.0381	-.0357	-.0261		-.0250	-.0242
38	FF	-.1257	-.1032	-.0529	-.0450	-.0361	-.0310	-.0209		-.0267	-.0288
39	FF	-.1250	-.1111	-.0576	-.0484	-.0386	-.0338	-.0223		-.0290	-.0304
40	FF	-.1260	-.1071	-.0596	-.0460	-.0375	-.0321	-.0226		-.0213	-.0291
41	FF	-.1302	-.1095	-.0553	-.0460	-.0367	-.0317	-.0203		-.0270	-.0305
33	RF	.4599	.3132	.2652	.2001	.1980	.2160	.1738		.1669	.1712
34	RF	.4092	.2763	.2556	.1861	.1816	.2046	.1597		.1510	.1546
35	RF	.4095	.2742	.2546	.1826	.1794	.2046	.1595		.1453	.1519
36	RF	.4587	.3009	.2473	.1853	.1840	.2107	.1674		.1616	.1581
37	RF	.4915	.3060	.2395	.1889	.1858	.2224	.1875		.1866	.1673
42	RF	.2479	.2271	.2929	.1920	.1747	.2182	.1667		.1496	.1399
43	RF	.4865	.3200	.2661	.2152	.2156	.2170	.1794		.1684	.1814
44	RF	.5955	.3074	.2714	.2040	.2138	.2207	.1759		.1655	.1790
45	RF	.2664	.2277	.3028	.2022	.1844	.2309	.1732		.1624	.1525
74	VCF	.0071	.0028	.0732	.0450	.0428	.0371	.0259		.0168	.0083
76	VCF	.0099	.0049	.0720	.0466	.0448	.0321	.0228		.0135	.0065
78	VCF	.0091	.0048	.0726	.0462	.0445	.0209	.0139		.0064	.0007
80	VCF	.0084	.0034	.0751	.0468	.0453	.0116	.0084		-.0038	-.0066
82	VCF	.0045	.0016	.0711	.0467	.0429	.0111	.0057		-.0078	-.0113
84	VCF	.0089	.0060	.0768	.0517	.0483	.0192	.0128		-.0079	-.0099
86	VCF	.0070	.0053	.0771	.0527	.0490	.0221	.0150		-.0058	-.0099
88	VCF	.0079	.0079	.0801	.0559	.0516	.0261	.0188		.0079	-.0013
90	VCF	.0049	.0041	.0798	.0552	.0500	.0273	.0191		.0165	.0059
92	VCF	.0069	.0071	.0849	.0601	.0539	.0369	.0264		.0363	.0232
94	VCF	.0061	.0063	.0857	.0618	.0549	.0634	.0468		.0524	.0375
96	VCF	.0067	.0075	.0912	.0671	.0597	.0863	.0651		.0683	.0556
98	VCF	.0007	.0009	.1119	.0828	.0726	.0978	.0722		.0739	.0627
6	CFL	-.1242	-.1087	-.0619	-.0478	-.0400	-.0373	-.0280		-.0288	-.0259
7	CFL	-.1264	-.1082	-.0597	-.0461	-.0378	-.0349	-.0253		-.0277	-.0241
8	CFL	-.1413	-.1191	-.0657	-.0511	-.0451	-.0423	-.0338		-.0340	-.0319
9	CFL	-.1295	-.1125	-.0590	-.0459	-.0390	-.0359	-.0265		-.0316	-.0258
10	CFL	-.1051	-.0899	-.0657	-.0510	-.0404	-.0380	-.0309		-.0341	-.0284
11	CFL	-.0670	-.0494	-.0628	-.0472	-.0399	-.0334	-.0246		-.0278	-.0234
12	CFL	-.0410	-.0160	-.0652	-.0486	-.0343	-.0377	-.0284		-.0311	-.0253
13	CFL	-.0091	.0049	-.0510	-.0362	-.0274	-.0331	-.0214		-.0258	-.0186
14	CFL	.0063	.0163	-.0411	-.0286	-.0219	-.0357	-.0238		-.0254	-.0198
15	CFL	.0168	.0244	-.0266	-.0160	-.0100	-.0291	-.0175		-.0186	-.0142
16	CFL	.0111	.0161	-.0212	-.0168	-.0125	-.0313	-.0209		-.0282	-.0239
17	CFL	.0298	.0302	-.0024	.0012	.0034	-.0127	-.0050		-.0176	-.0125
18	CFL	.0345	.0317	.0072	.0075	.0078	-.0051	-.0004		-.0171	-.0135
19	CFL	.0408	.0358	.0205	.0175	.0165	.0062	.0085		-.0120	-.0105
20	CFL	.0405	.0379	.0284	.0224	.0212	.0124	.0137		-.0063	-.0098
21	CFL	.0475	.0485	.0454	.0375	.0341	.0280	.0253		.0079	.0008
22	CFL	.0461	.0539	.0567	.0450	.0387	.0362	.0315		.0147	.0057
23	CFL	.0499	.0688	.0736	.0589	.0502	.0486	.0428		.0265	.0146
24	CFL	.0438	.0792	.0782	.0621	.0510	.0498	.0419		.0292	.0139
25	CFL	.0671	.1151	.0987	.0820	.0702	.0658	.0567		.0466	.0317
26	CFL	.1127	.1213	.1113	.0940	.0826	.0745	.0641		.0600	.0471
27	CFL	.1741	.1430	.1272	.1090	.0926	.0912	.0776		.0750	.0572
28	CFL	.2172	.1680	.1359	.1165	.1008	.1020	.0870		.0843	.0666
29	CFL	.2684	.1916	.1521	.1284	.1106	.1213	.1034		.0999	.0848
30	CFL	.3096	.1974	.1623	.1319	.1074	.1341	.1093		.1037	.0875
31	CFL	.3199	.2088	.1891	.1415	.1236	.1505	.1197		.1033	.1005
32	CFL	.2968	.2079	.2120	.1515	.1357	.1692	.1267		.1187	.1138

Table IV. Concluded

(d)  $C_p$  at  $L/h = 17.500$  at  $M_\infty = 2.86$ 

ORF	LOC	Percent of floor area with porosity									
		0		28.6			57.1			100	
		2 stores	3 stores	0 stores	2 stores	3 stores	0 stores	2 stores	3 stores	2 stores	3 stores
1	FF	-.0952	-.0436	-.0443	-.0336	-.0258	-.0244	-.0167	-.0175	-.0185	-.0238
2	FF	-.1002	-.0717	-.0501	-.0379	-.0293	-.0280	-.0212	-.0204	-.0195	-.0250
3	FF	-.0989	-.0684	-.0519	-.0379	-.0293	-.0272	-.0208	-.0188	-.0162	-.0225
4	FF	-.1067	-.0719	-.0590	-.0466	-.0377	-.0353	-.0249	-.0268	-.0236	-.0281
5	FF	-.1013	-.0664	-.0539	-.0416	-.0321	-.0298	-.0221	-.0219	-.0183	-.0228
38	FF	-.0850	-.0686	-.0331	-.0332	-.0232	-.0229	-.0160	-.0138	-.0182	-.0226
39	FF	-.0991	-.0809	-.0430	-.0425	-.0315	-.0308	-.0223	-.0221	-.0263	-.0299
40	FF	-.0970	-.0805	-.0442	-.0386	-.0294	-.0296	-.0226	-.0165	-.0163	-.0259
41	FF	-.0924	-.0732	-.0369	-.0372	-.0270	-.0267	-.0184	-.0178	-.0225	-.0269
33	RF	.3314	.2824	.2331	.1626	.1477	.1738	.1336	.1316	.1274	.1243
34	RF	.3040	.2489	.2256	.1534	.1368	.1659	.1251	.1203	.1165	.1119
35	RF	.2999	.2454	.2257	.1512	.1339	.1648	.1240	.1162	.1088	.1083
36	RF	.3218	.2710	.2161	.1505	.1356	.1659	.1240	.1210	.1188	.1131
37	RF	.3540	.2785	.2070	.1526	.1431	.1743	.1392	.1336	.1390	.1278
42	RF	.2025	.1483	.2630	.1636	.1340	.1873	.1306	.1179	.1180	.1068
43	RF	.4309	.2779	.2432	.1828	.1587	.1760	.1390	.1370	.1322	.1275
44	RF	.3756	.2862	.2425	.1759	.1723	.1818	.1413	.1513	.1351	.1387
45	RF	.2129	.1649	.2618	.1788	.1487	.1963	.1451	.1362	.1371	.1256
74	VCF	.0113	-.0036	.0649	.0454	.0338	.0249	.0175	.0139	.0131	.0002
76	VCF	.0141	.0007	.0678	.0477	.0366	.0218	.0184	.0146	.0104	.0001
78	VCF	.0134	-.0010	.0670	.0465	.0353	.0180	.0154	.0122	.0053	-.0035
80	VCF	.0131	.0006	.0693	.0465	.0358	.0132	.0121	.0071	-.0009	-.0072
82	VCF	.0095	-.0054	.0660	.0466	.0332	.0124	.0099	.0077	.0003	-.0090
84	VCF	.0137	.0002	.0706	.0512	.0383	.0198	.0165	.0128	.0017	-.0052
86	VCF	.0123	-.0013	.0714	.0516	.0385	.0219	.0183	.0151	.0028	-.0041
88	VCF	.0128	.0014	.0730	.0544	.0405	.0250	.0222	.0186	.0128	.0033
90	VCF	.0097	-.0020	.0724	.0513	.0382	.0252	.0220	.0155	.0165	.0053
92	VCF	.0116	.0035	.0774	.0561	.0408	.0334	.0287	.0227	.0327	.0186
94	VCF	.0111	.0014	.0783	.0571	.0422	.0492	.0413	.0312	.0447	.0275
96	VCF	.0123	.0048	.0828	.0611	.0458	.0650	.0543	.0428	.0565	.0394
98	VCF	.0047	-.0036	.0928	.0686	.0502	.0702	.0557	.0440	.0570	.0400
6	CFL	-.1039	-.0692	-.0545	-.0438	-.0343	-.0318	-.0233	-.0251	-.0227	-.0263
7	CFL	-.1022	-.0653	-.0525	-.0415	-.0314	-.0293	-.0192	-.0229	-.0211	-.0248
8	CFL	-.1109	-.0804	-.0610	-.0486	-.0404	-.0376	-.0285	-.0303	-.0281	-.0316
9	CFL	-.0975	-.0653	-.0549	-.0435	-.0342	-.0320	-.0209	-.0256	-.0270	-.0273
10	CFL	-.0724	-.0539	-.0607	-.0489	-.0378	-.0346	-.0265	-.0280	-.0296	-.0307
11	CFL	-.0377	-.0228	-.0559	-.0439	-.0344	-.0289	-.0186	-.0197	-.0218	-.0247
12	CFL	-.0190	-.0051	-.0568	-.0452	-.0301	-.0337	-.0227	-.0221	-.0254	-.0256
13	CFL	.0032	.0143	-.0420	-.0323	-.0195	-.0275	-.0146	-.0145	-.0183	-.0177
14	CFL	.0084	.0175	-.0354	-.0263	-.0152	-.0296	-.0155	-.0155	-.0176	-.0187
15	CFL	.0130	.0187	-.0240	-.0147	-.0046	-.0201	-.0080	-.0078	-.0088	-.0116
16	CFL	-.0002	.0066	-.0251	-.0214	-.0093	-.0237	-.0146	-.0179	-.0195	-.0223
17	CFL	.0158	.0194	-.0061	-.0041	.0056	-.0062	.0038	-.0022	-.0090	-.0101
18	CFL	.0181	.0190	.0000	-.0001	.0072	-.0012	.0063	-.0008	-.0096	-.0115
19	CFL	.0252	.0239	.0107	.0076	.0142	.0083	.0127	.0053	-.0068	-.0088
20	CFL	.0232	.0192	.0166	.0101	.0163	.0131	.0154	.0069	-.0027	-.0081
21	CFL	.0313	.0274	.0339	.0242	.0278	.0278	.0278	.0177	.0111	.0032
22	CFL	.0292	.0280	.0431	.0309	.0316	.0339	.0316	.0197	.0147	.0045
23	CFL	.0335	.0385	.0589	.0445	.0409	.0444	.0424	.0274	.0245	.0125
24	CFL	.0262	.0434	.0594	.0457	.0385	.0422	.0386	.0221	.0233	.0081
25	CFL	.0505	.0826	.0767	.0648	.0530	.0556	.0515	.0339	.0371	.0215
26	CFL	.0933	.0834	.0866	.0757	.0660	.0610	.0571	.0437	.0482	.0358
27	CFL	.1408	.1008	.1011	.0887	.0707	.0744	.0676	.0476	.0613	.0423
28	CFL	.1653	.1210	.1075	.0937	.0731	.0792	.0720	.0504	.0666	.0461
29	CFL	.1920	.1547	.1273	.1053	.0870	.0952	.0841	.0689	.0810	.0661
30	CFL	.2005	.1574	.1350	.1083	.0780	.1040	.0872	.0652	.0809	.0630
31	CFL	.2157	.1661	.1606	.1169	.0861	.1184	.0955	.0741	.0761	.0664
32	CFL	.2299	.1718	.1821	.1238	.0967	.1369	.0984	.0867	.0917	.0811

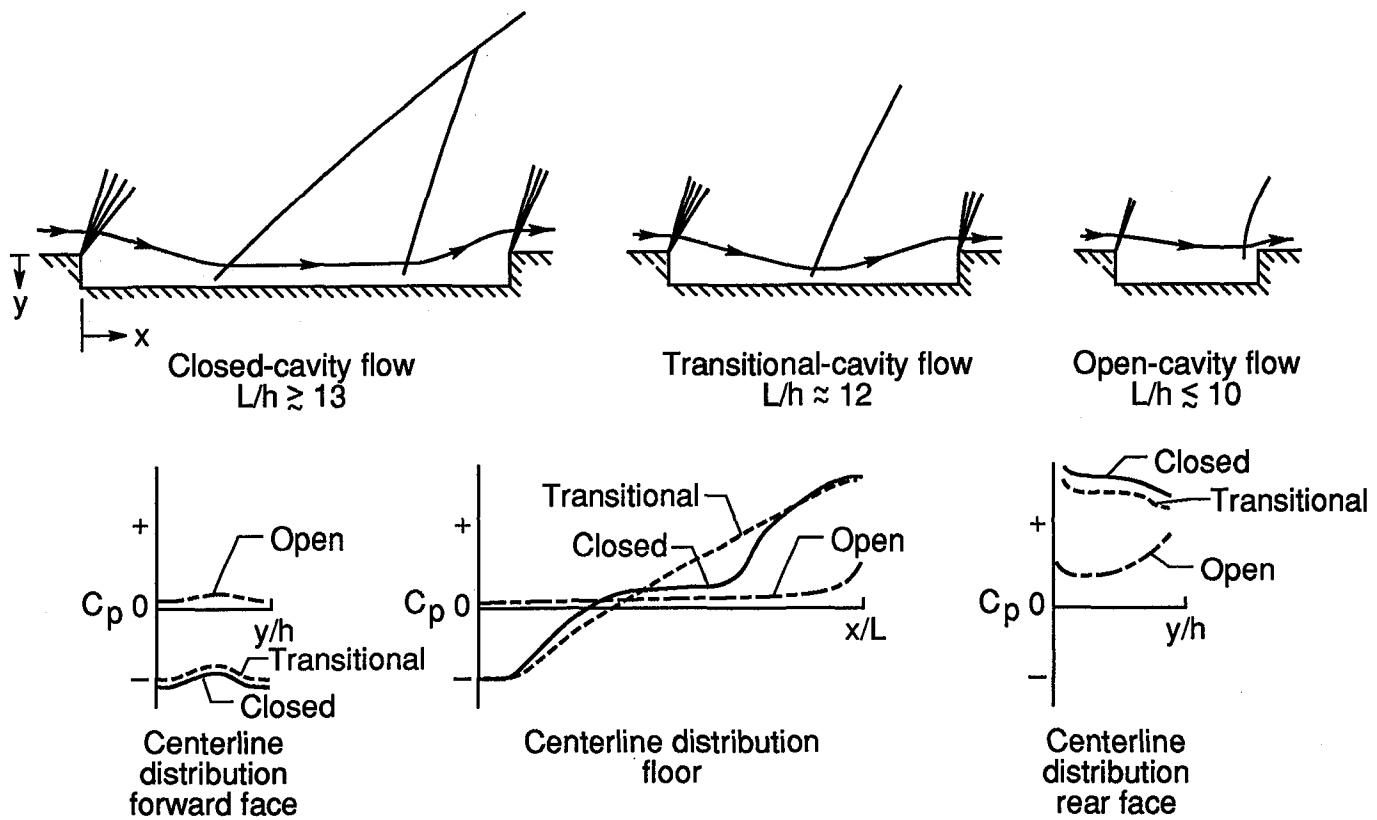


Figure 1. Cavity flow field sketches and typical pressure distributions.

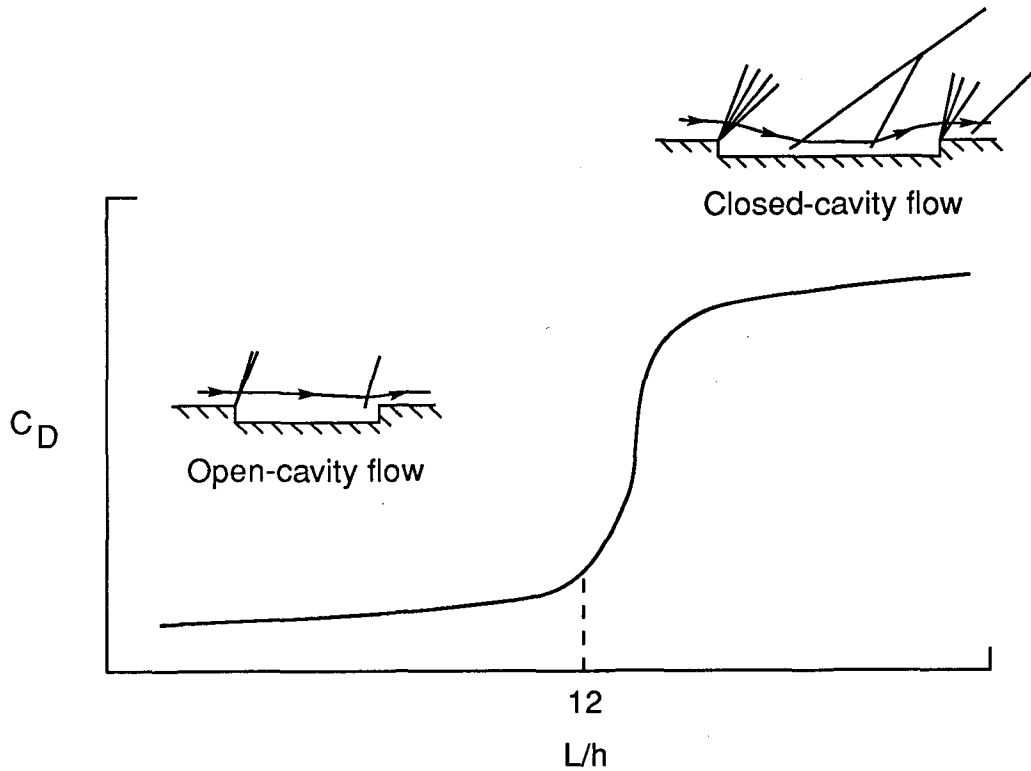
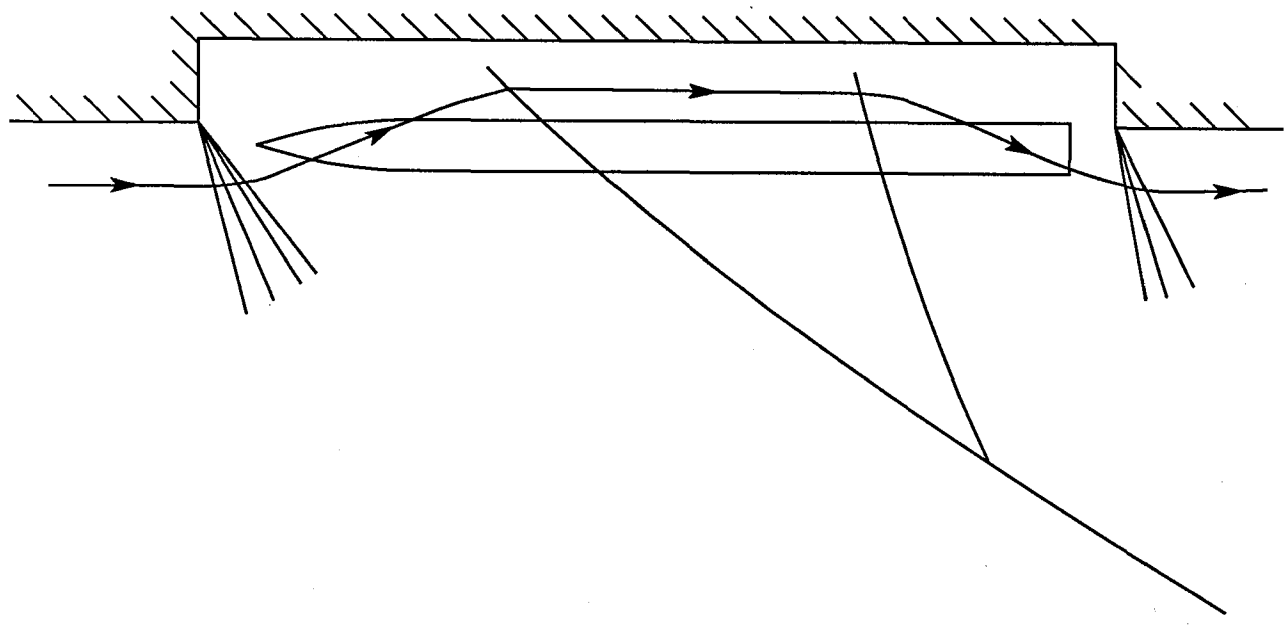
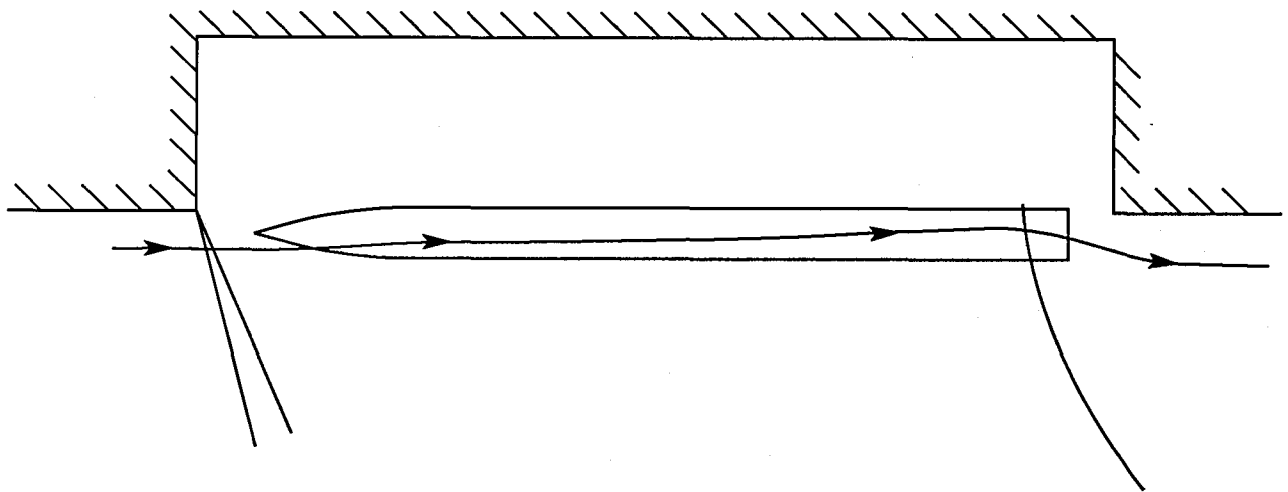


Figure 2. Typical cavity drag characteristics with cavity height  $h$  held constant.

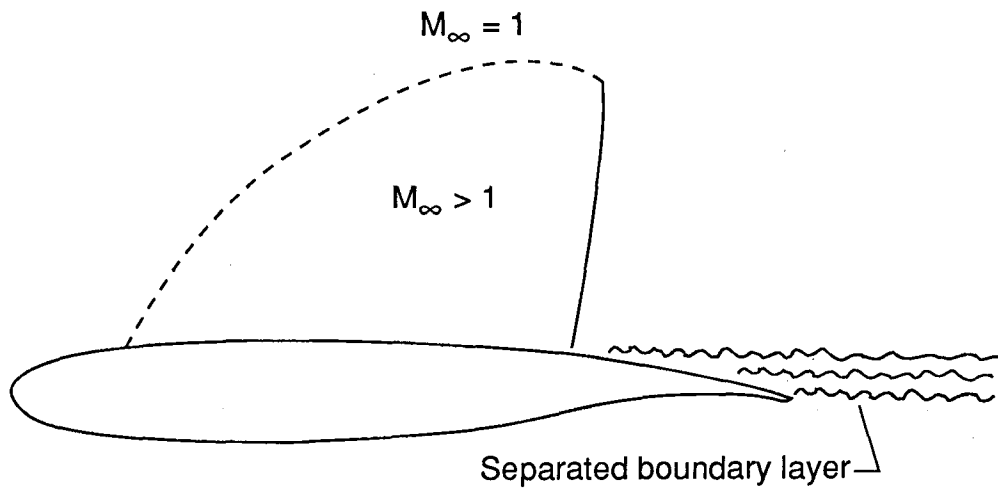


(a) Closed-cavity flow.

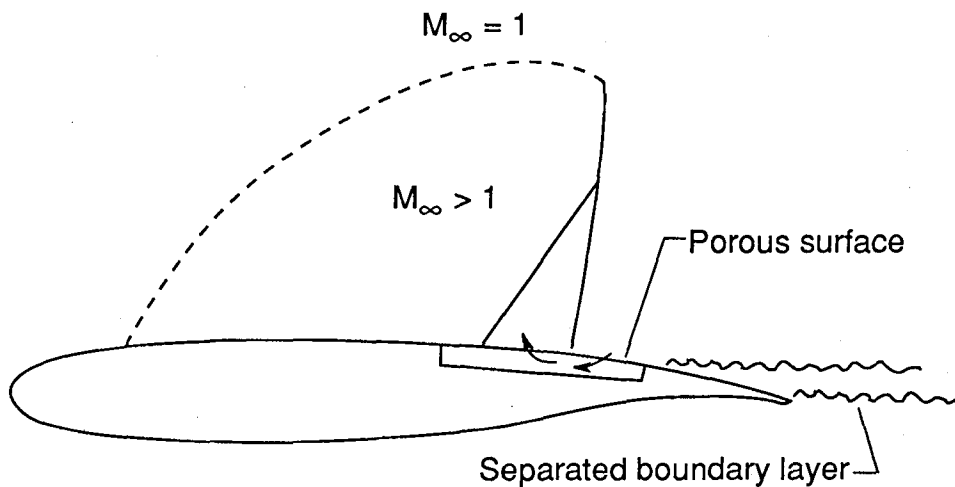


(b) Open-cavity flow.

Figure 3. Cavity flow field sketches during store separation.



(a) Without passive-venting system.



(b) With passive-venting system.

Figure 4. Flow over airfoil at transonic speeds.

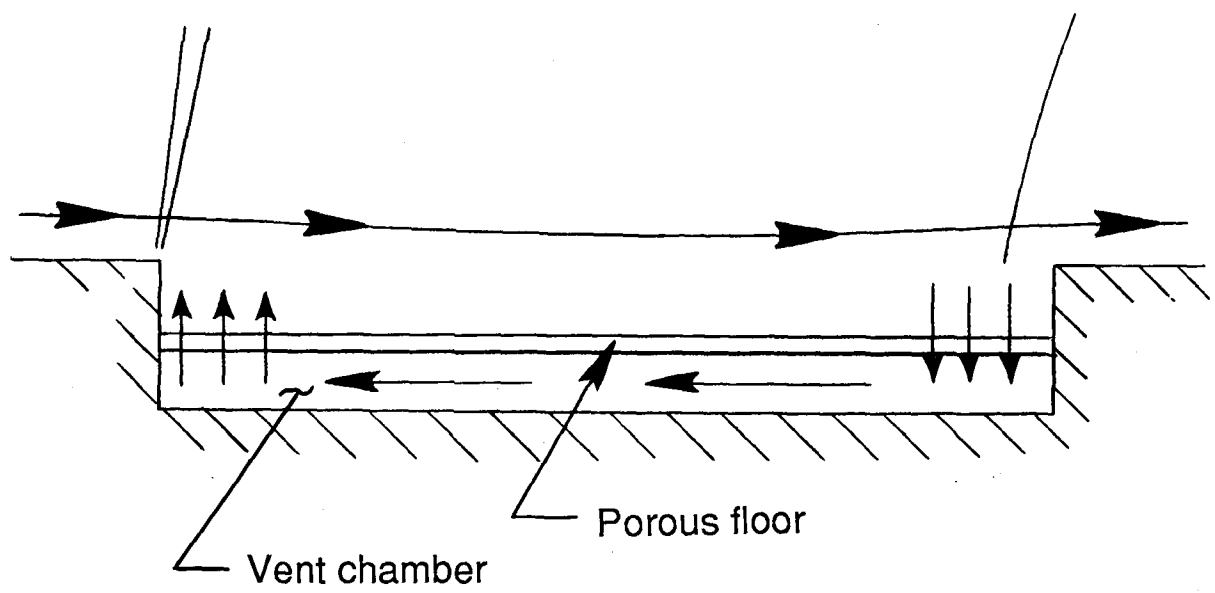
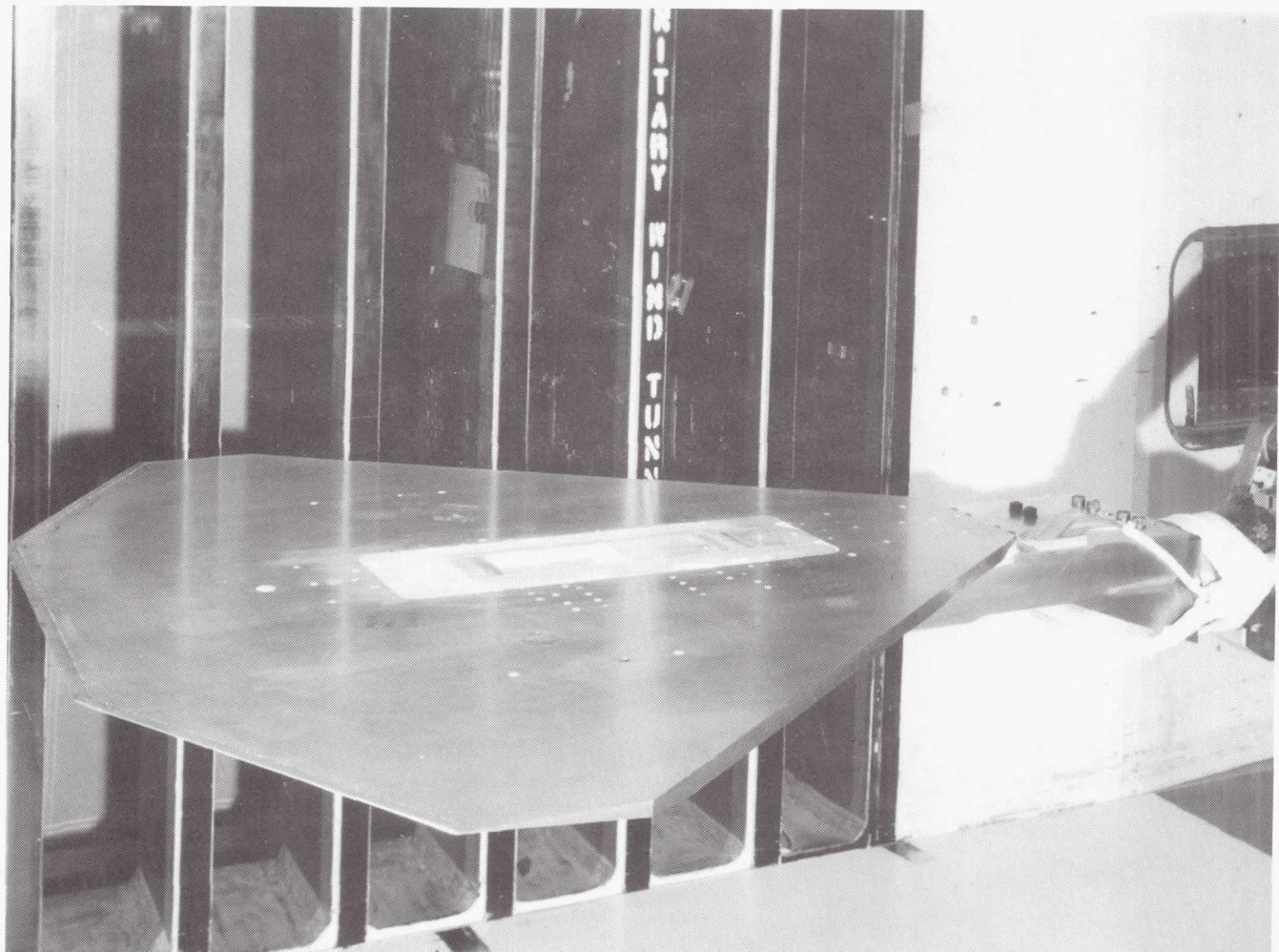


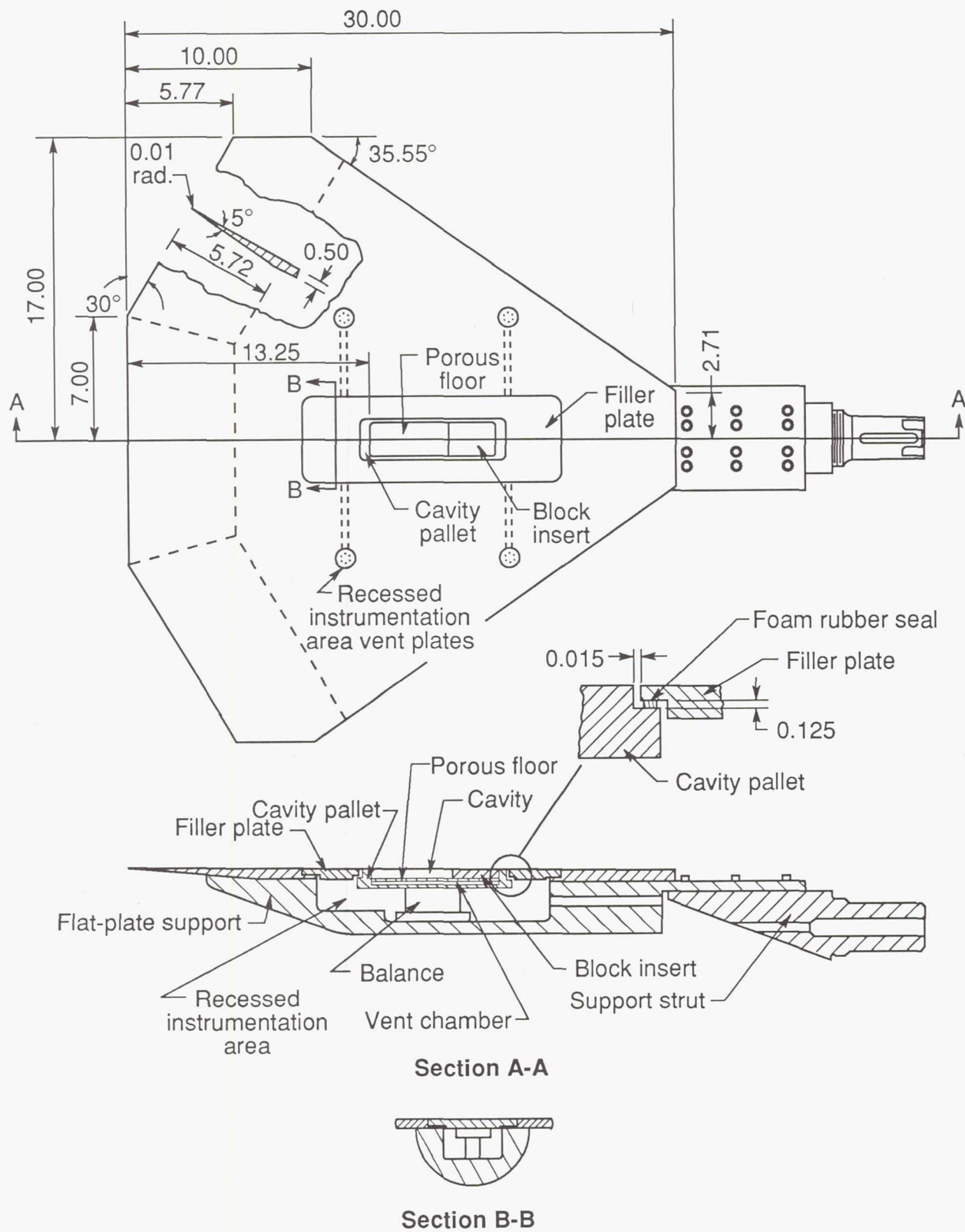
Figure 5. Porous-floor cavity flow field sketch.



L-87-3157

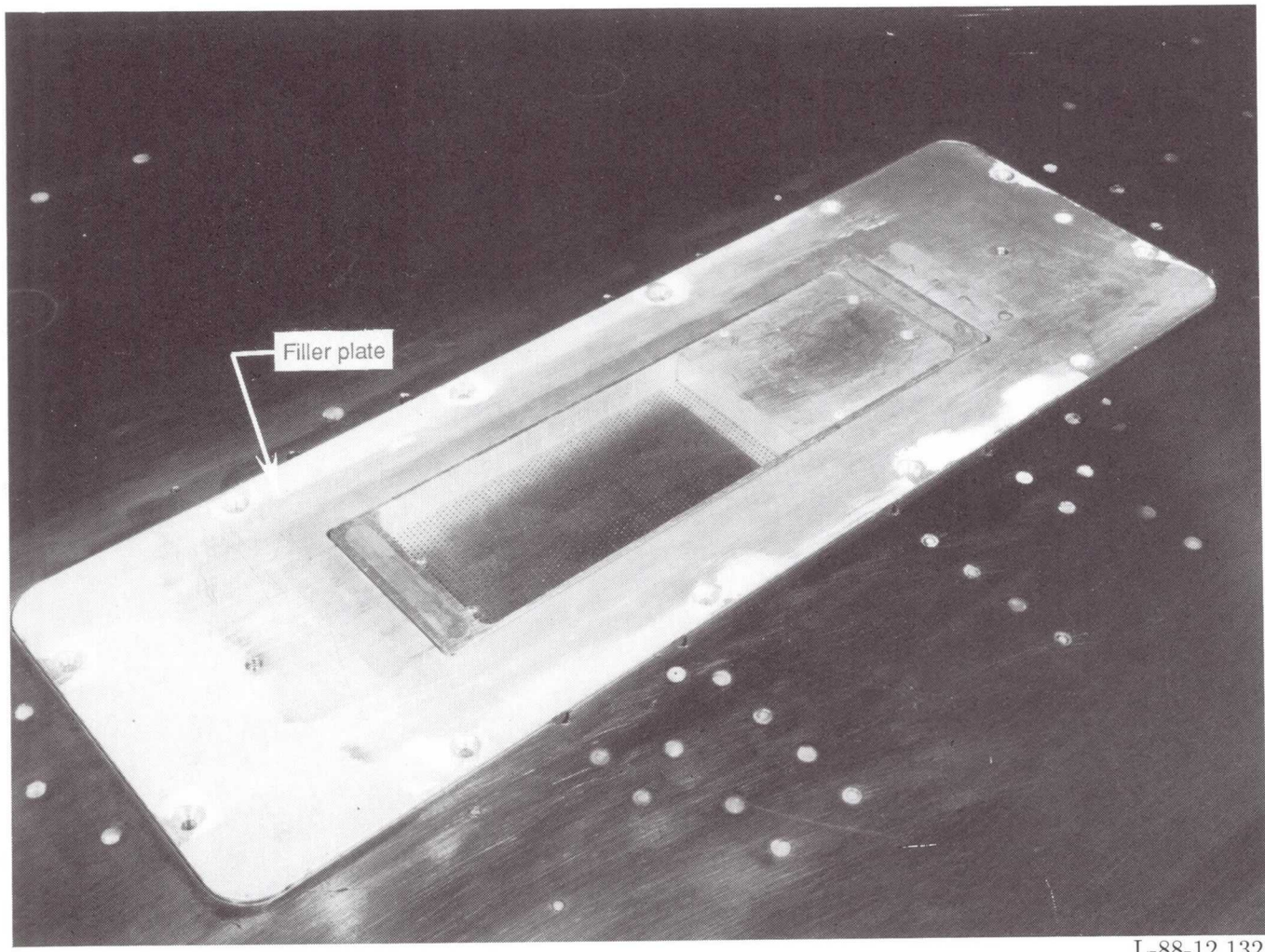
(a) Photograph of model mounted in wind tunnel.

Figure 6. Flat-plate model description.



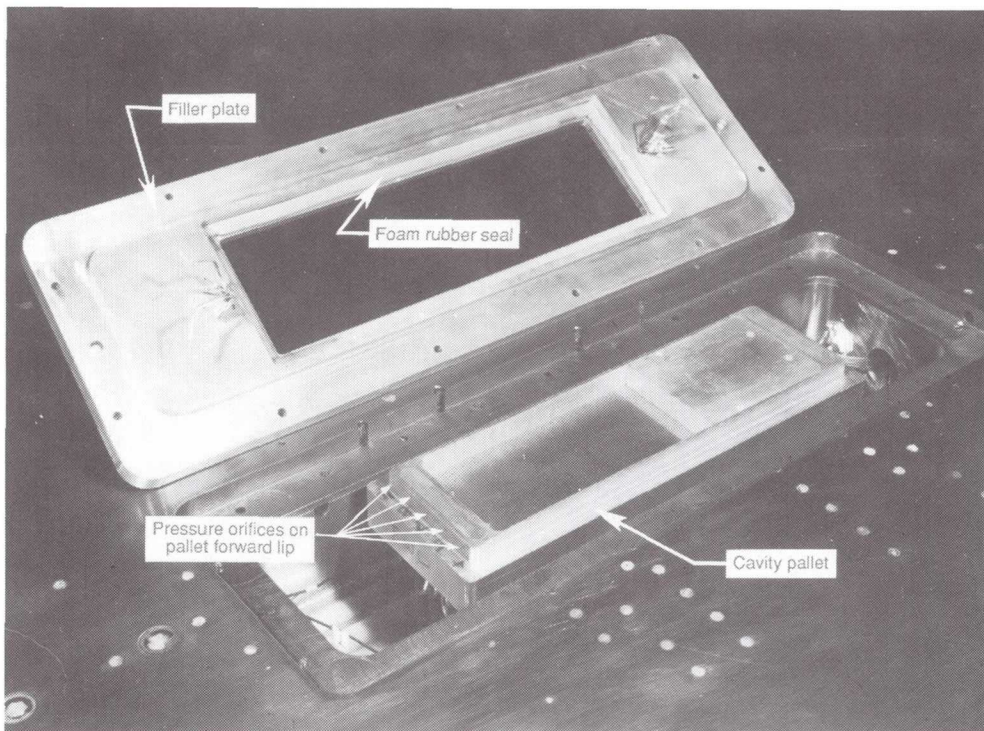
(b) Flat-plate drawing. All linear dimensions are in inches.

Figure 6. Concluded.



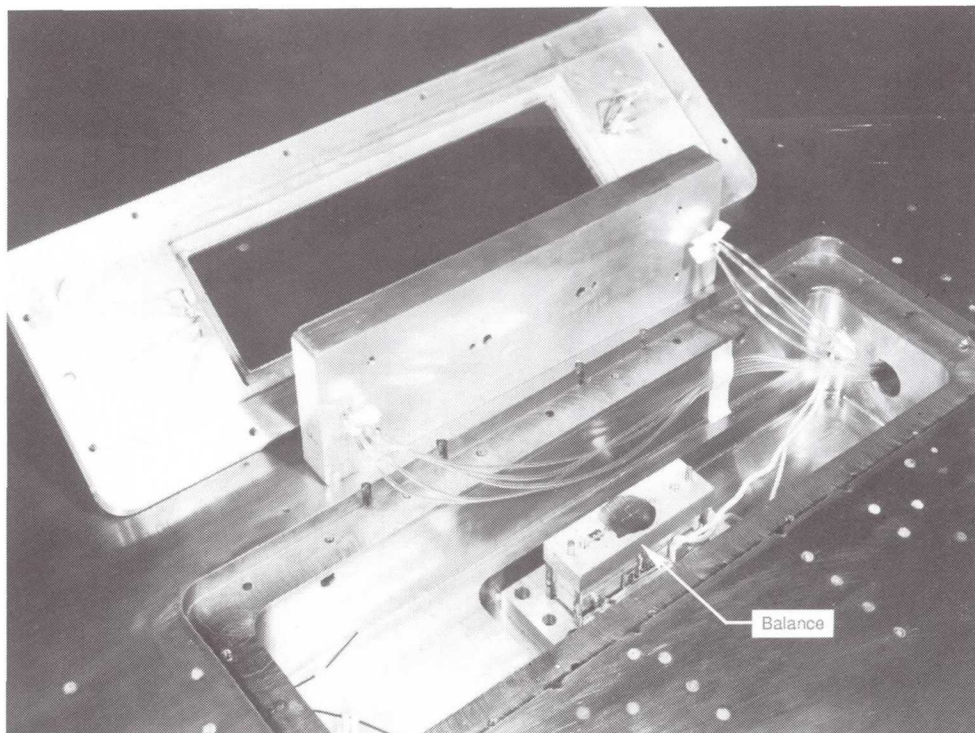
L-88-12,132

Figure 7. Photograph of cavity filler plate area.



L-88-12,131

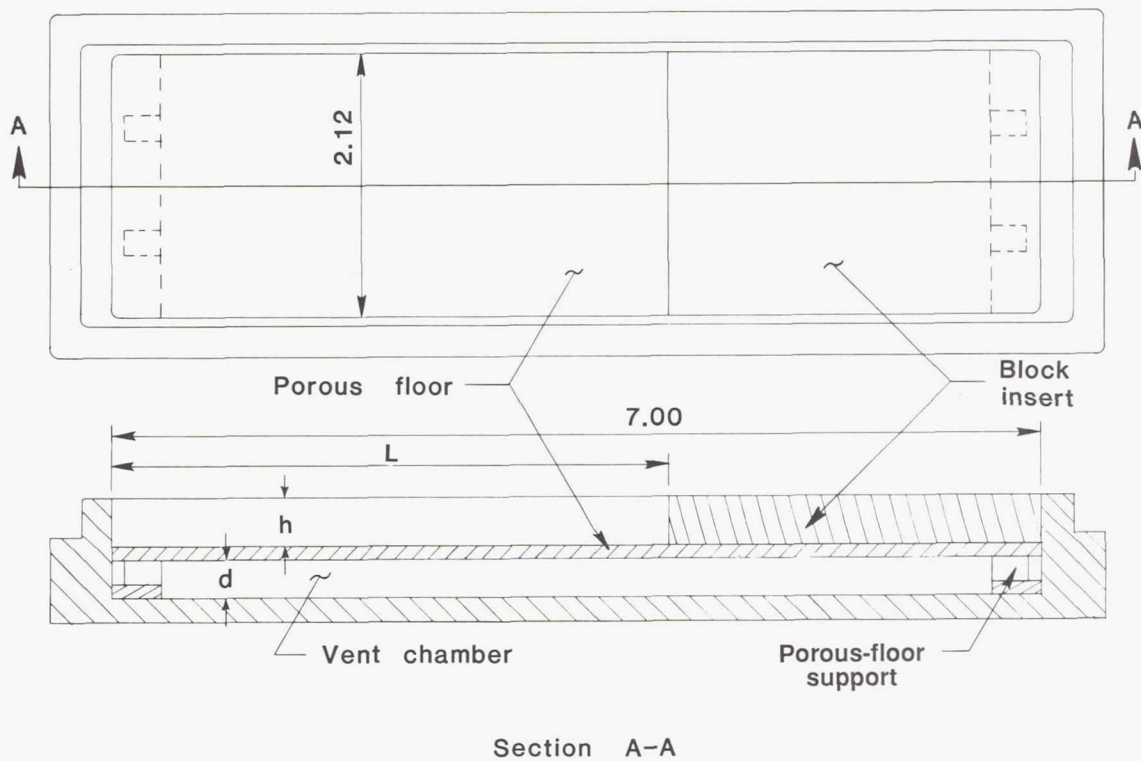
(a) Filler plate removed.



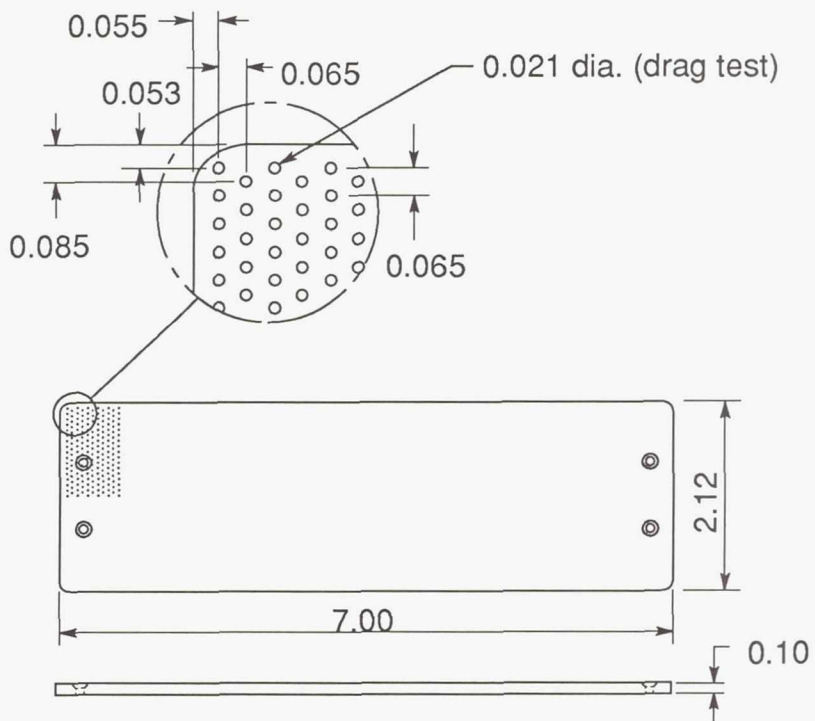
L-88-12,129

(b) Cavity drag pallet removed.

Figure 8. Photograph of recessed instrumentation area.

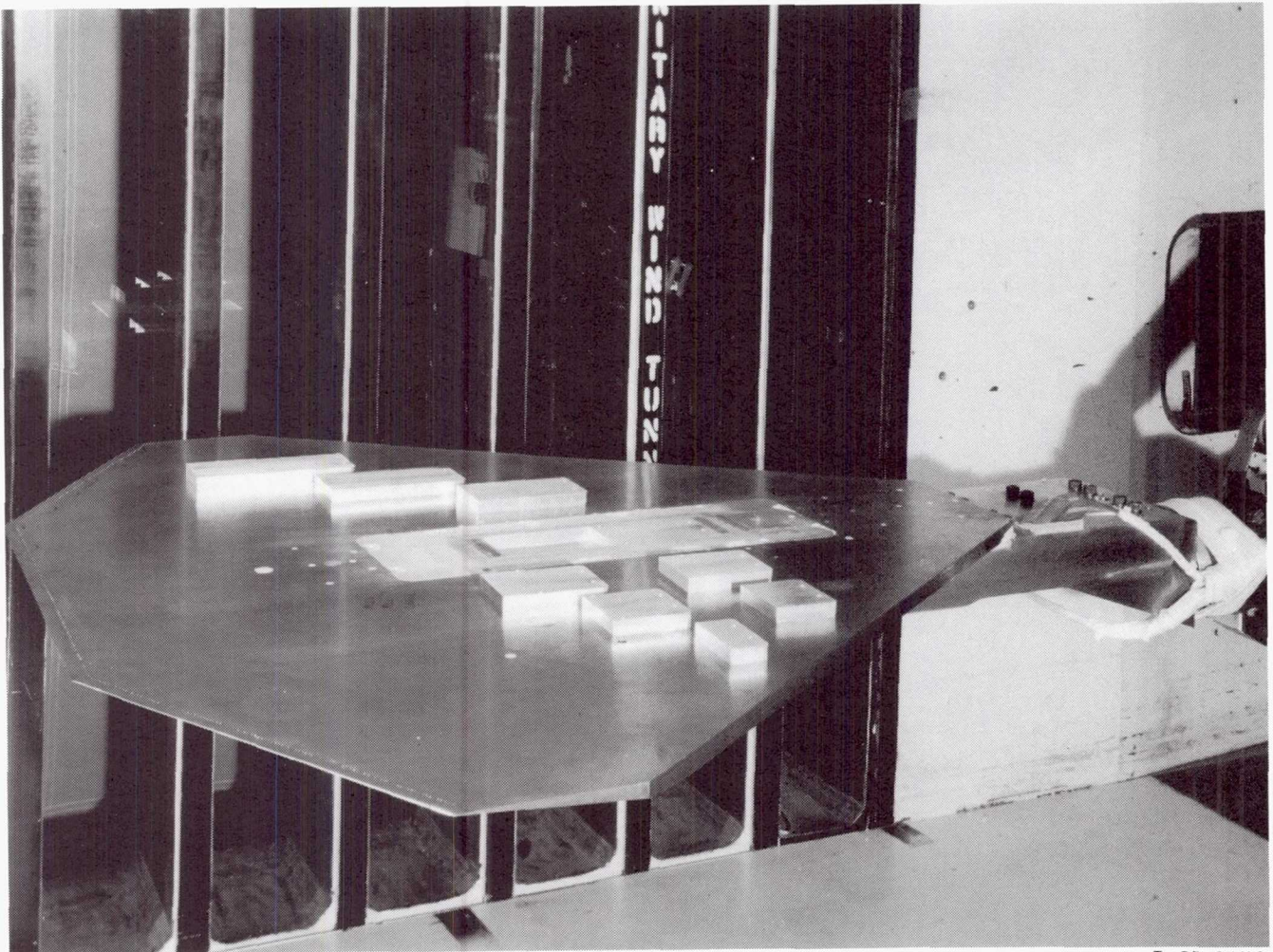


(a) Cavity pallet.



(b) Porous-floor details.

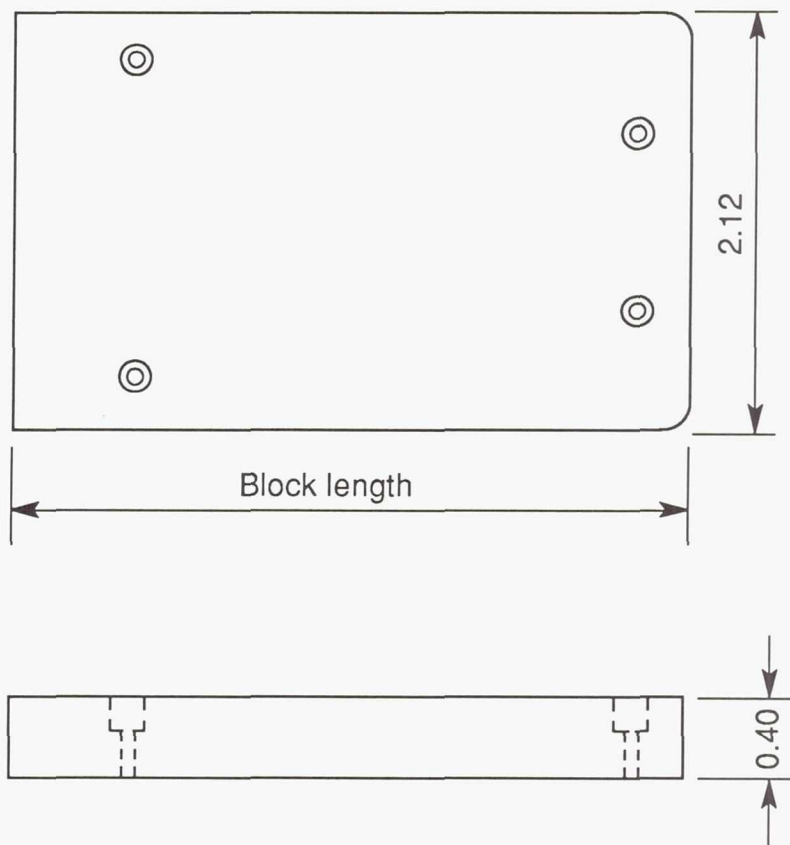
Figure 9. Cavity drag pallet details. All dimensions are in inches.



L-87-3156

(a) Photograph of inserts.

Figure 10. Details of rectangular-block inserts.

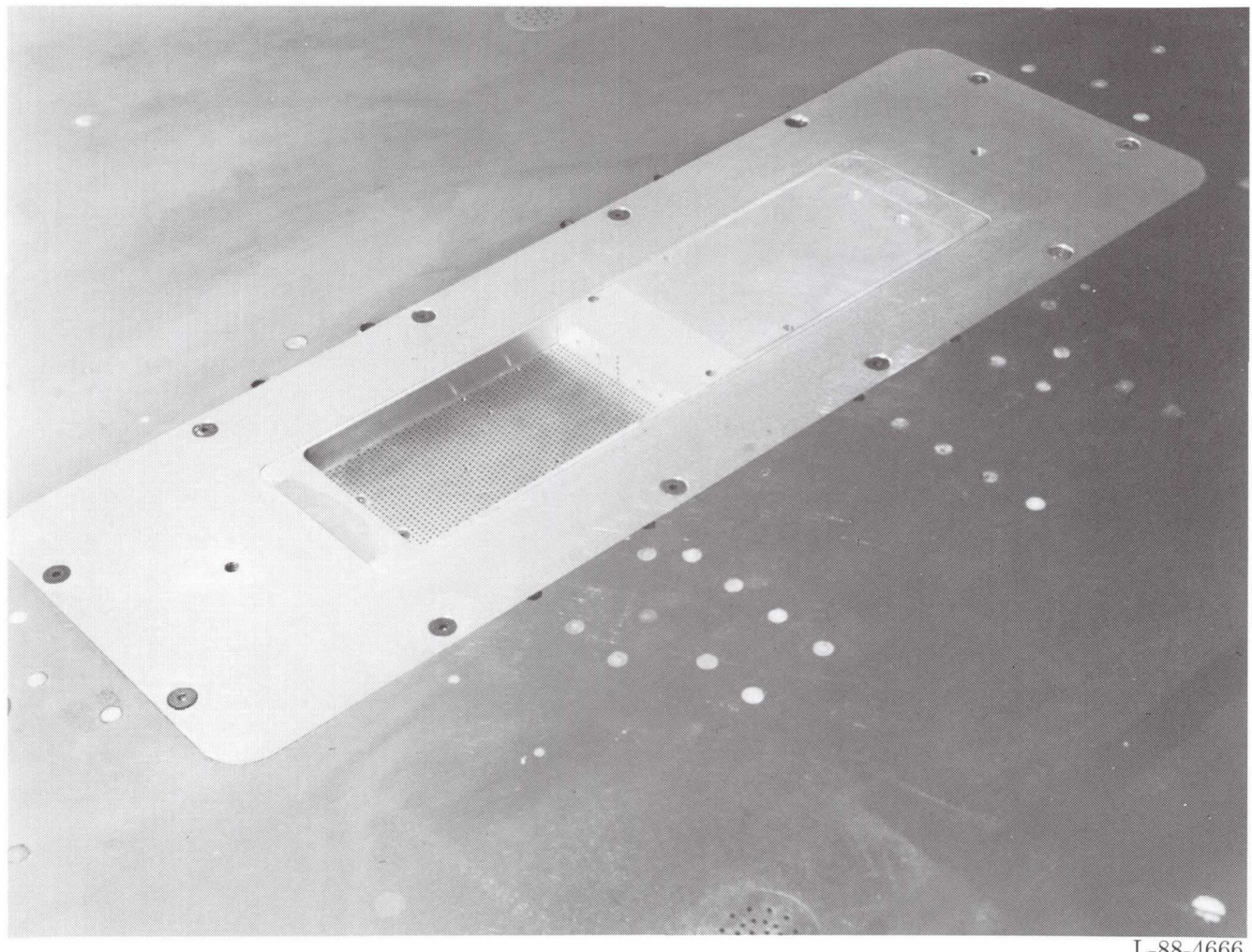


Block length, in.      Cavity L/h

None	17.500
1.062	14.845
1.842	12.895
2.232	11.920
2.622	10.945
3.012	9.970
3.402	8.995
3.792	8.020
4.572	6.070
5.352	4.120

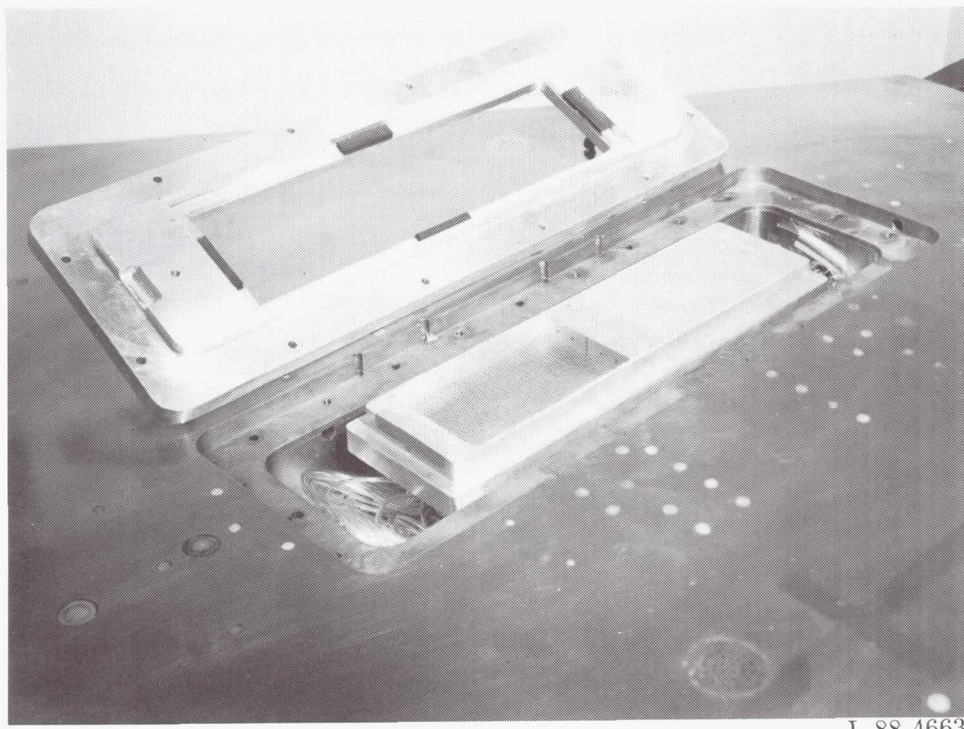
(b) Sketch of inserts (dimensions in inches).

Figure 10. Concluded.



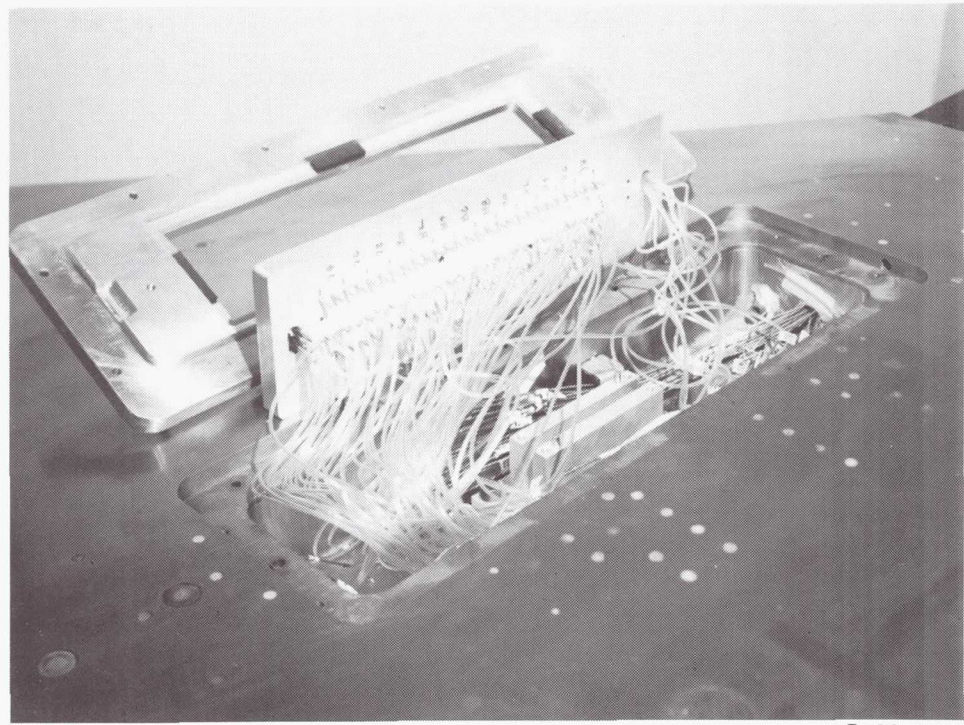
L-88-4666

Figure 11. Photograph of cavity pressure model.



L-88-4663

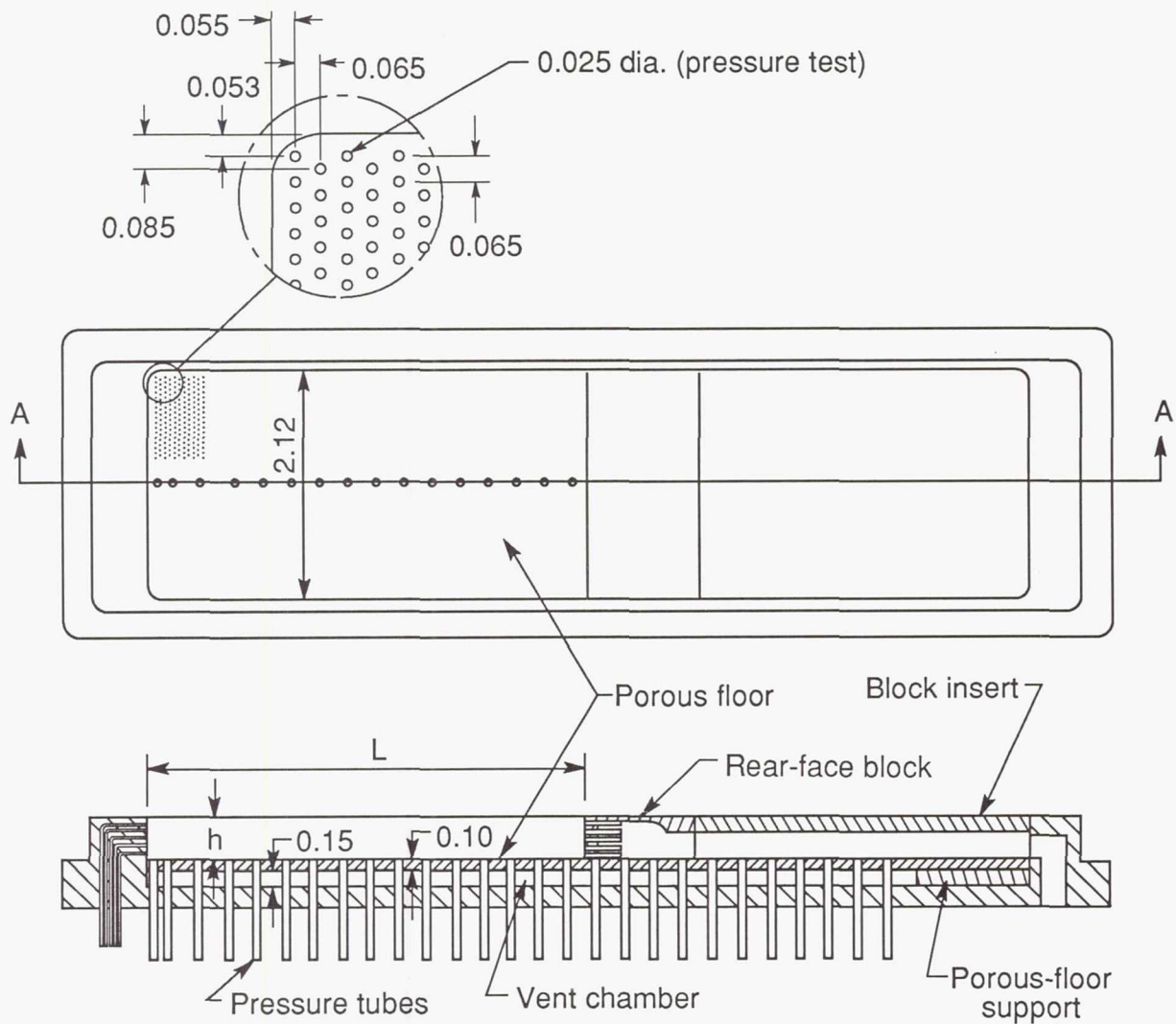
(a) Pallet installed.



L-88-4664

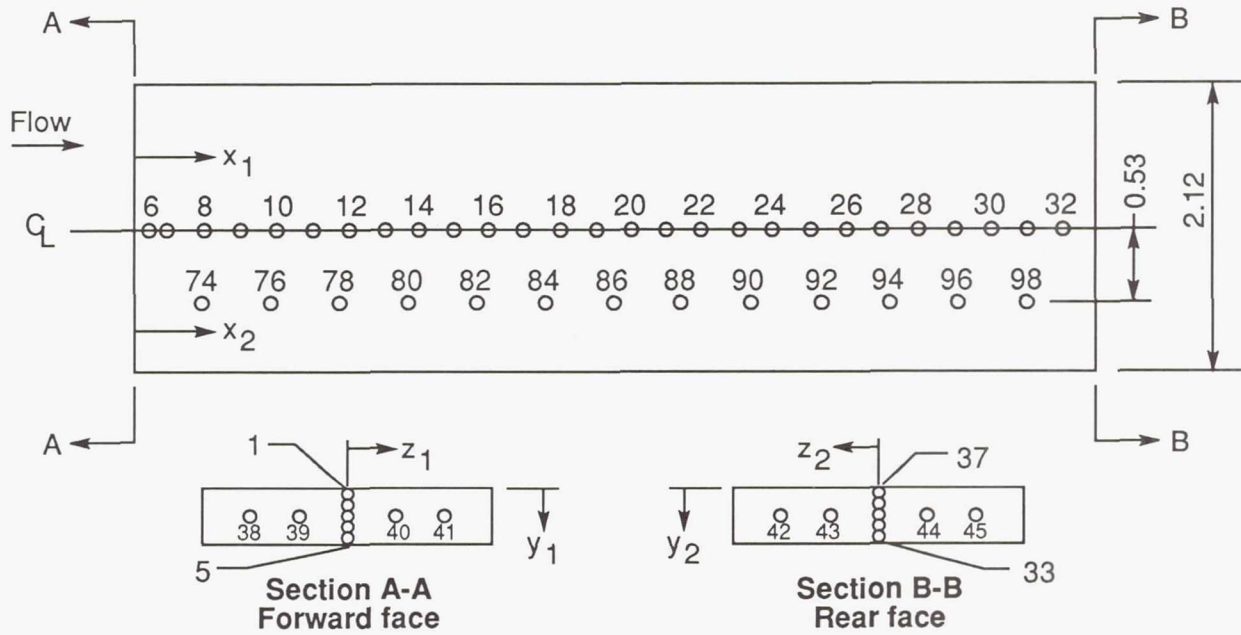
(b) Pallet removed.

Figure 12. Photograph of pressure test instrumentation area.



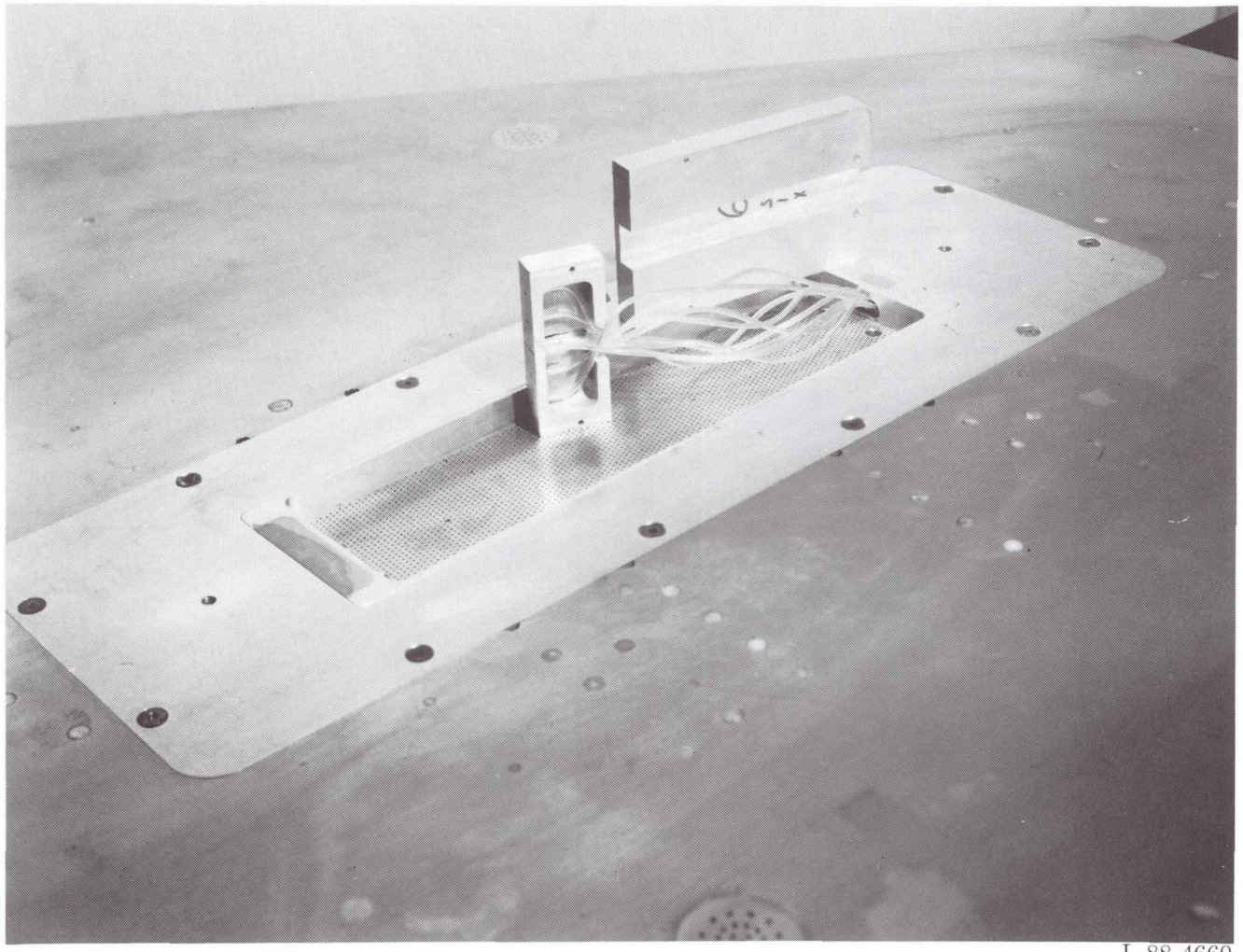
**Section A-A**

Figure 13. Cavity pressure pallet details. All dimensions are in inches.



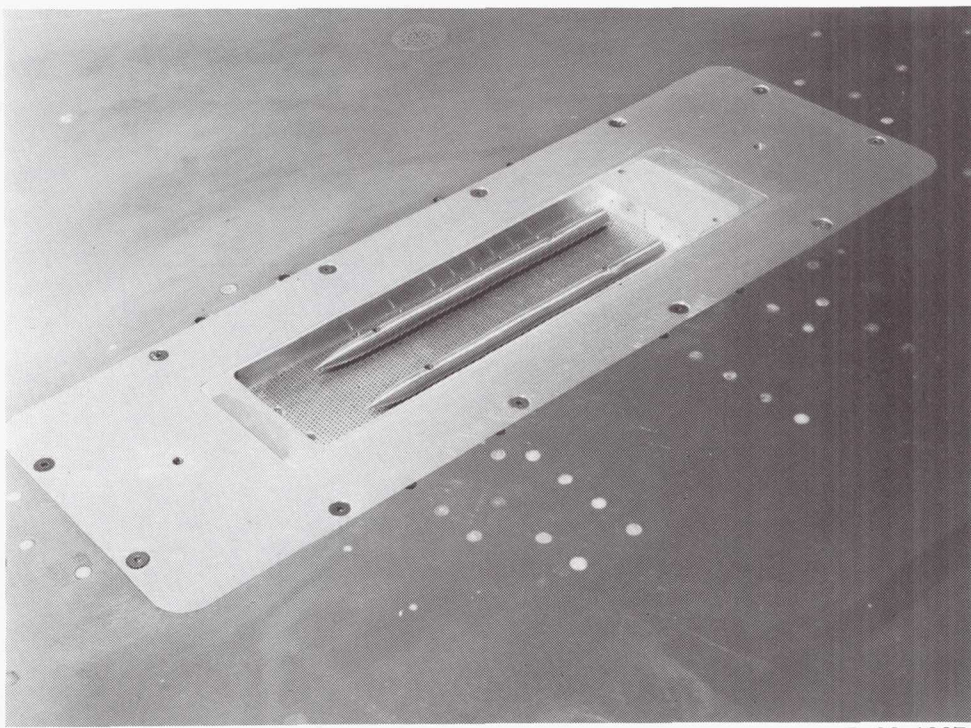
Cavity floor		Vent chamber floor		Forward face			Rear face		
Orifice	$x_1$	Orifice	$x_2$	Orifice	$y_1$	$z_1$	Orifice	$y_2$	$z_2$
6	0.120	74	0.500	1	0.050	0	33	0.350	0
7	0.250	76	1.000	2	.125	0	34	.275	0
8	0.510	78	1.500	3	.200	0	35	.200	0
9	0.770	80	2.000	4	.275	0	36	.125	0
10	1.030	82	2.500	5	.350	0	37	.050	0
11	1.290	84	3.000						
12	1.550	86	3.500	38	.200	-.700	42	.200	-.700
13	1.810	88	4.000	39	.200	-.350	43	.200	-.350
14	2.070	90	4.500	40	.200	0.350	44	.200	0.350
15	2.330	92	5.000	41	.200	.700	45	.200	.700
16	2.590	94	5.500						
17	2.850	96	6.000						
18	3.110	98	6.500						
19	3.370								
20	3.630								
21	3.890								
22	4.150								
23	4.410								
24	4.670								
25	4.930								
26	5.190								
27	5.450								
28	5.710								
29	5.970								
30	6.230								
31	6.490								
32	6.750								

Figure 14. Pressure pallet orifice locations. (All dimensions are in inches.)



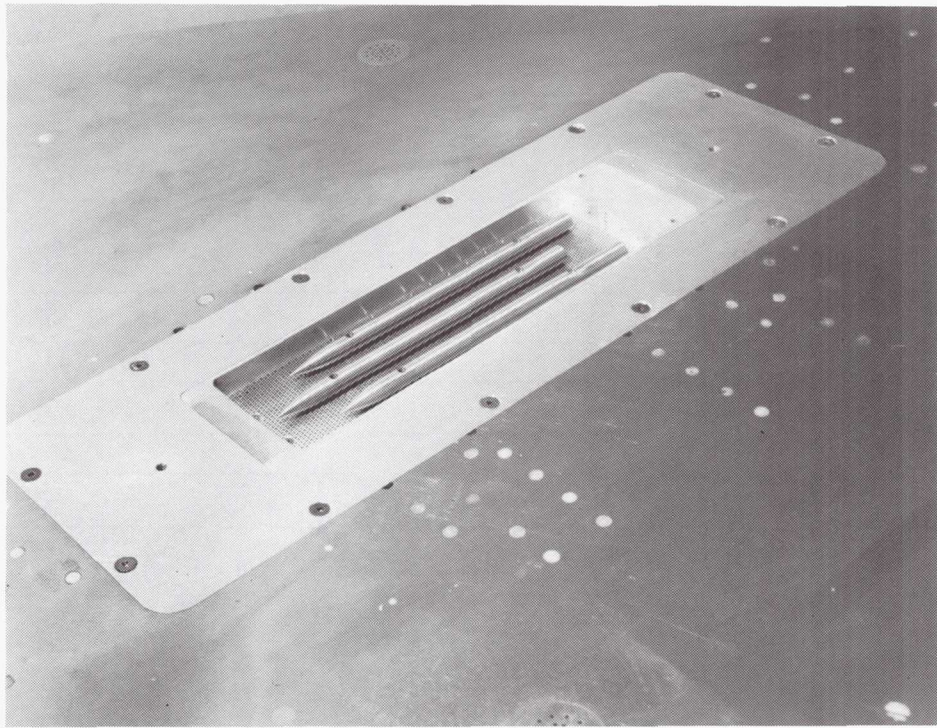
L-88-4660

Figure 15. Photograph of movable rear-face block.



L-88-4667

(a) Two stores.



L-88-4662

(b) Three stores.

Figure 16. Photograph of store arrangements.

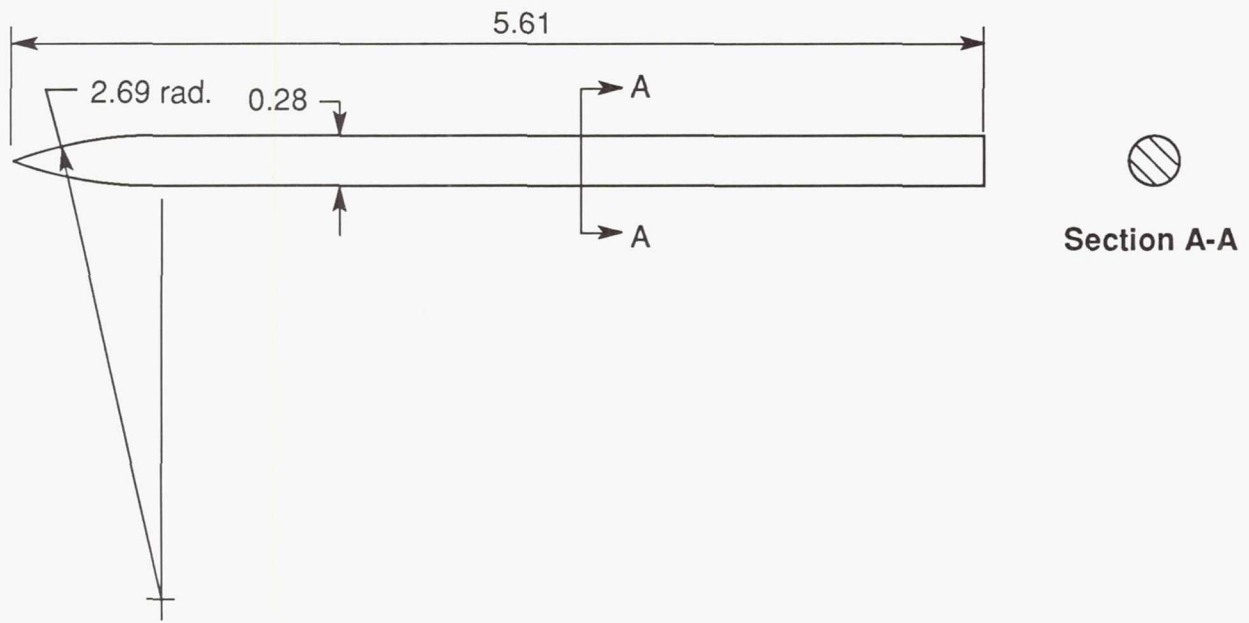


Figure 17. Store details. (Dimensions are in inches.)

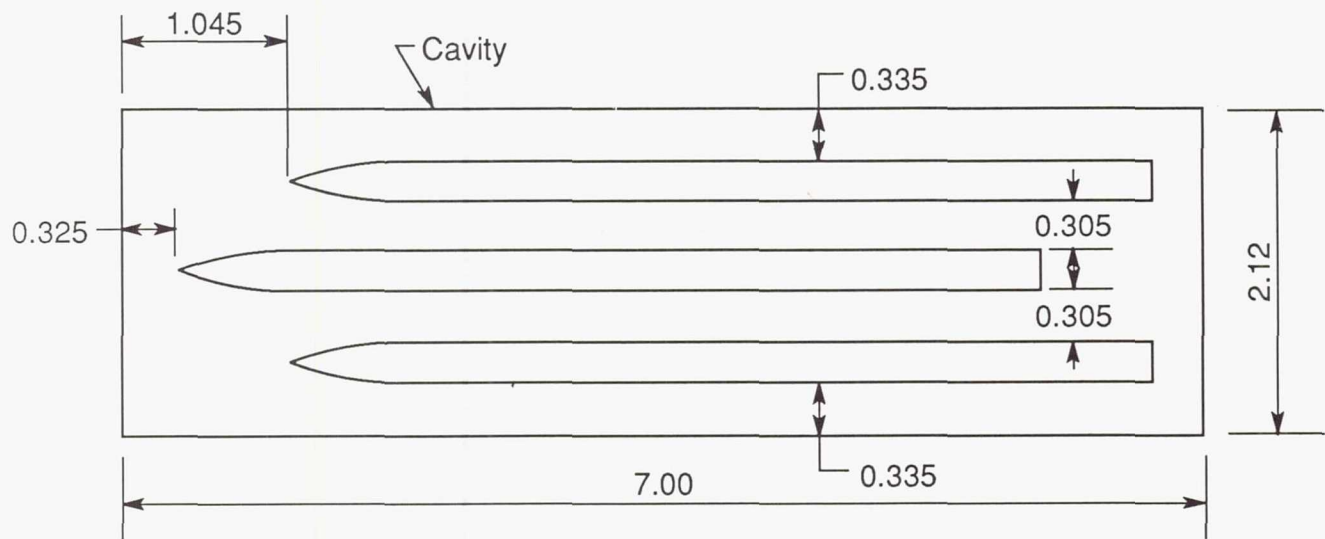
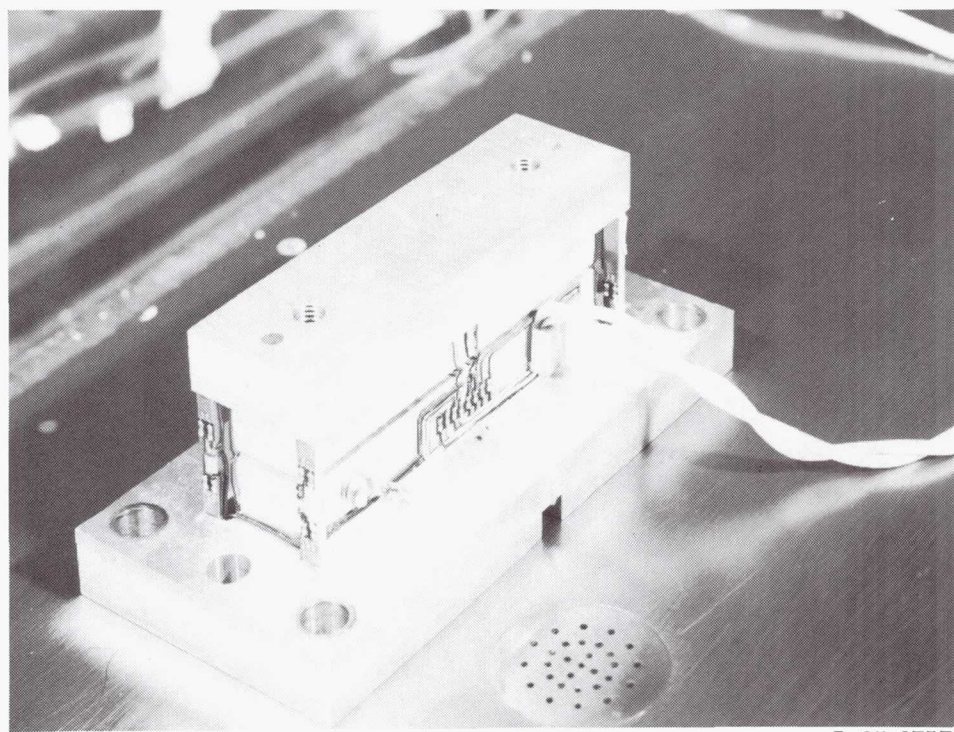


Figure 18. Location of stores in cavity. (All dimensions are in inches.) The two-store configuration was obtained by removing center store.



L-85-6757

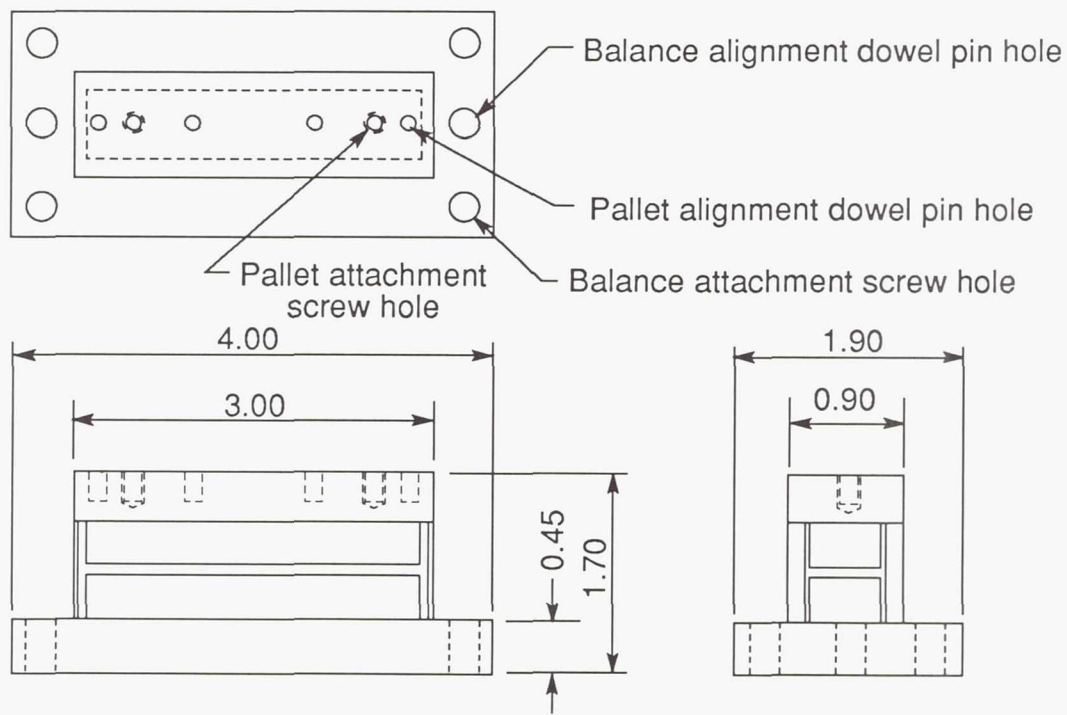
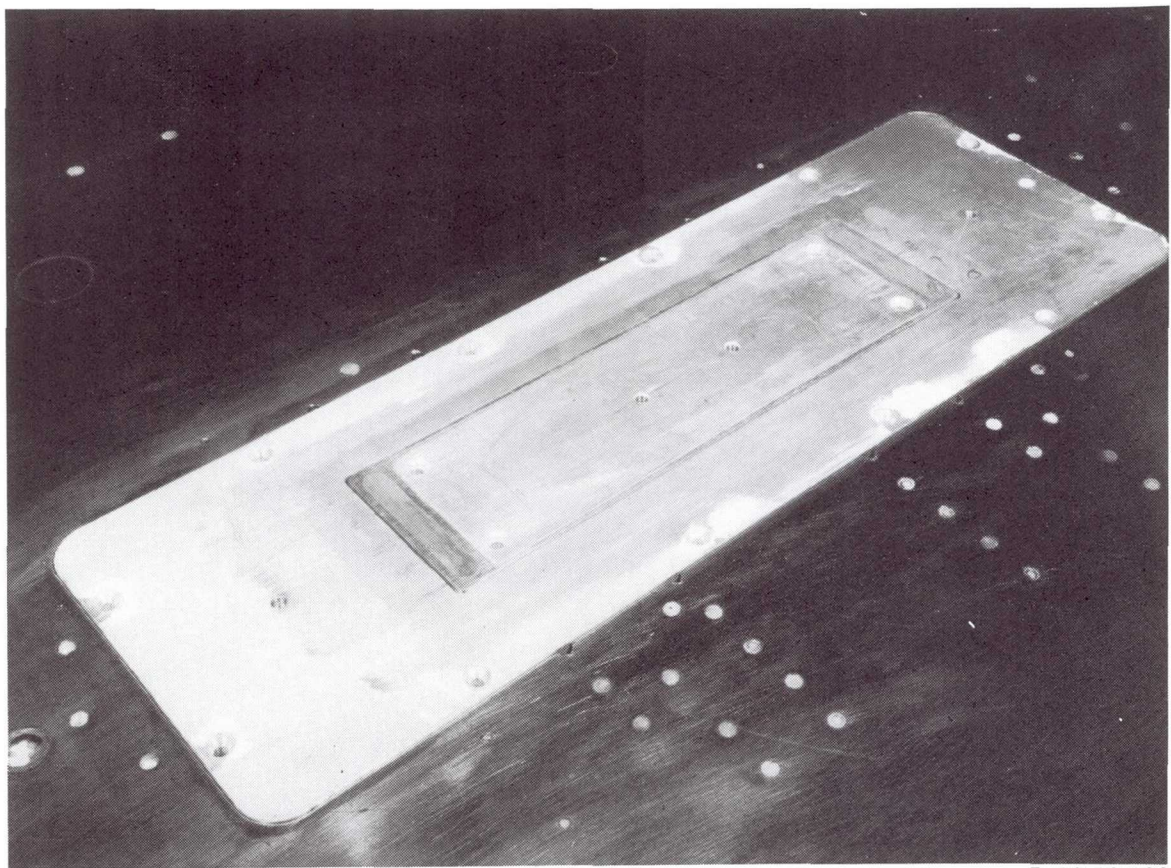
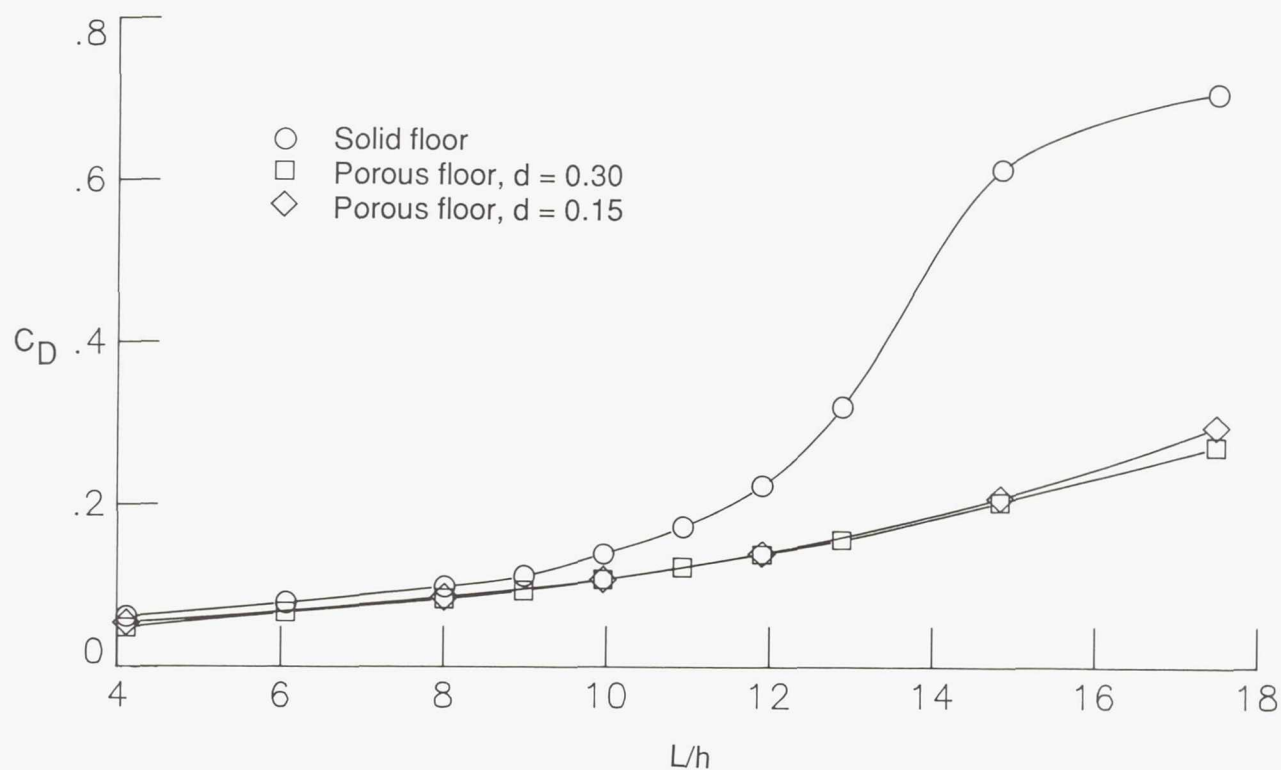


Figure 19. Details of strain-gage balance. All dimensions are in inches.

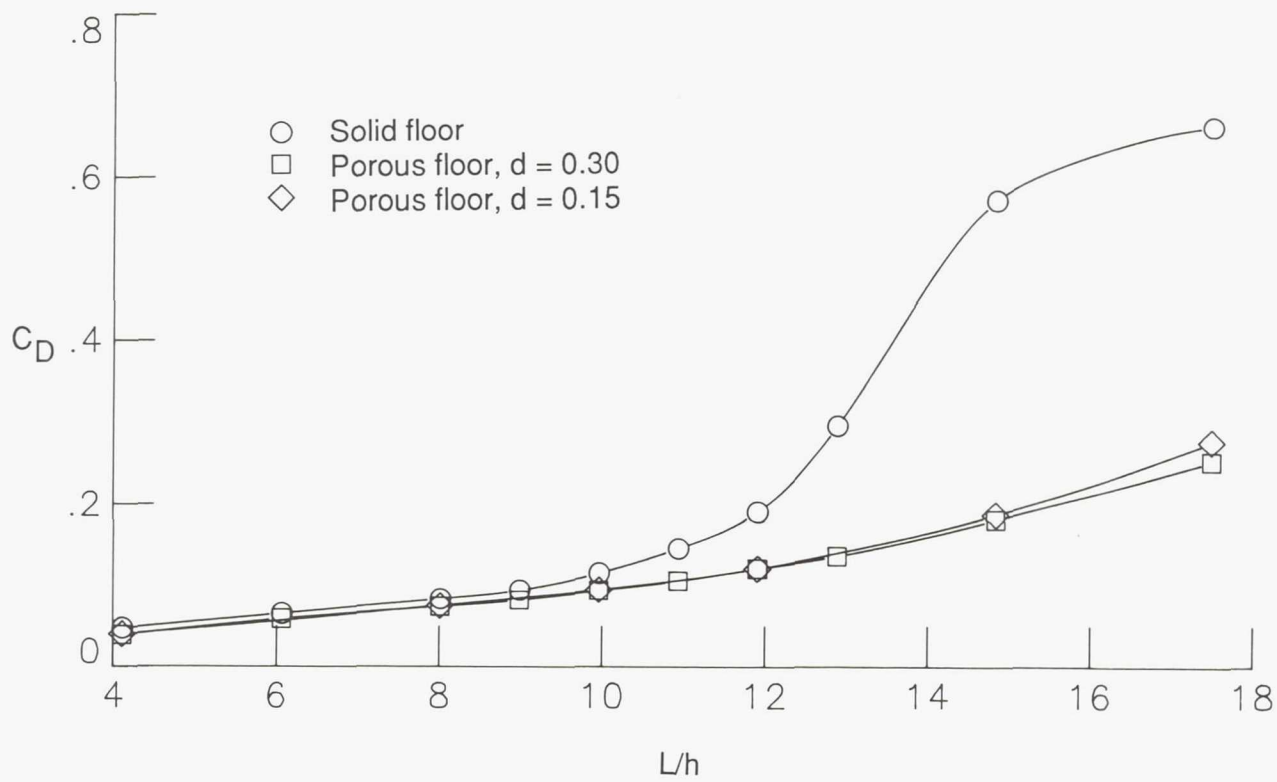


L-88-12,130

Figure 20. Photograph of cavity insert.

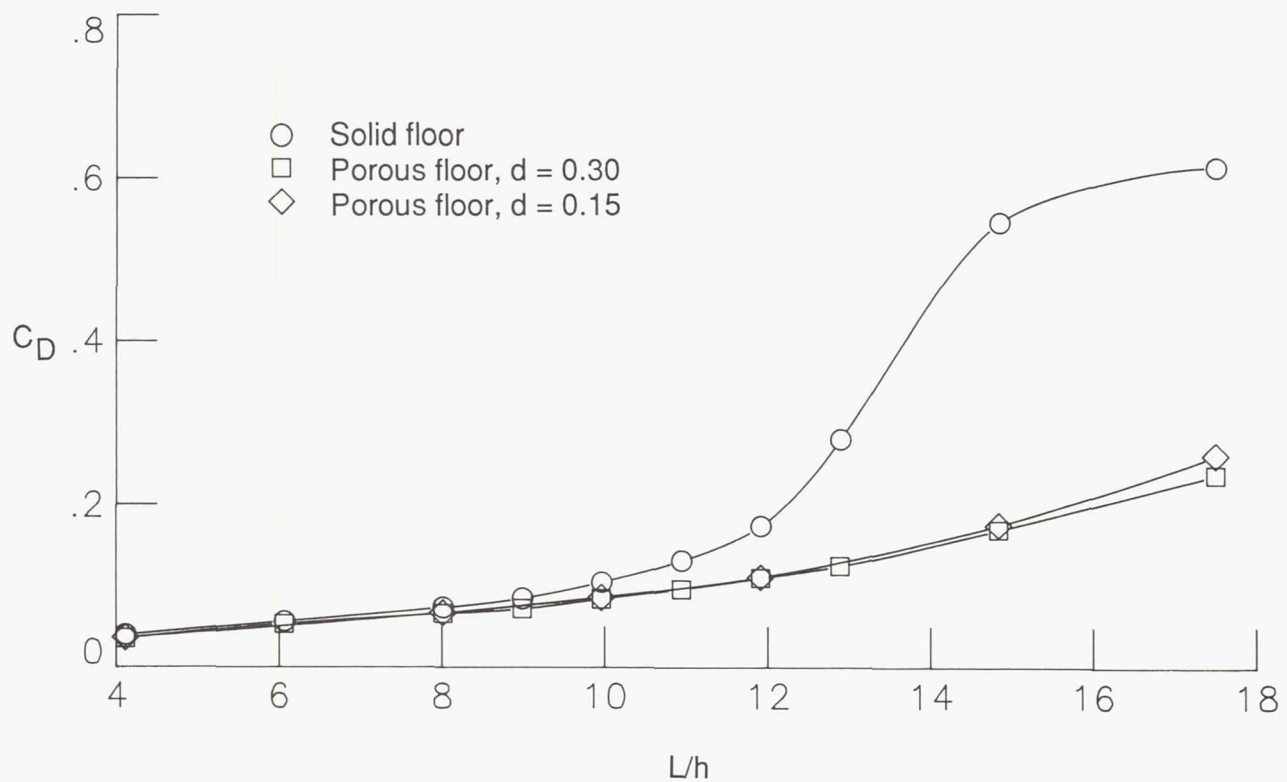


(a)  $M_\infty = 1.60$ .

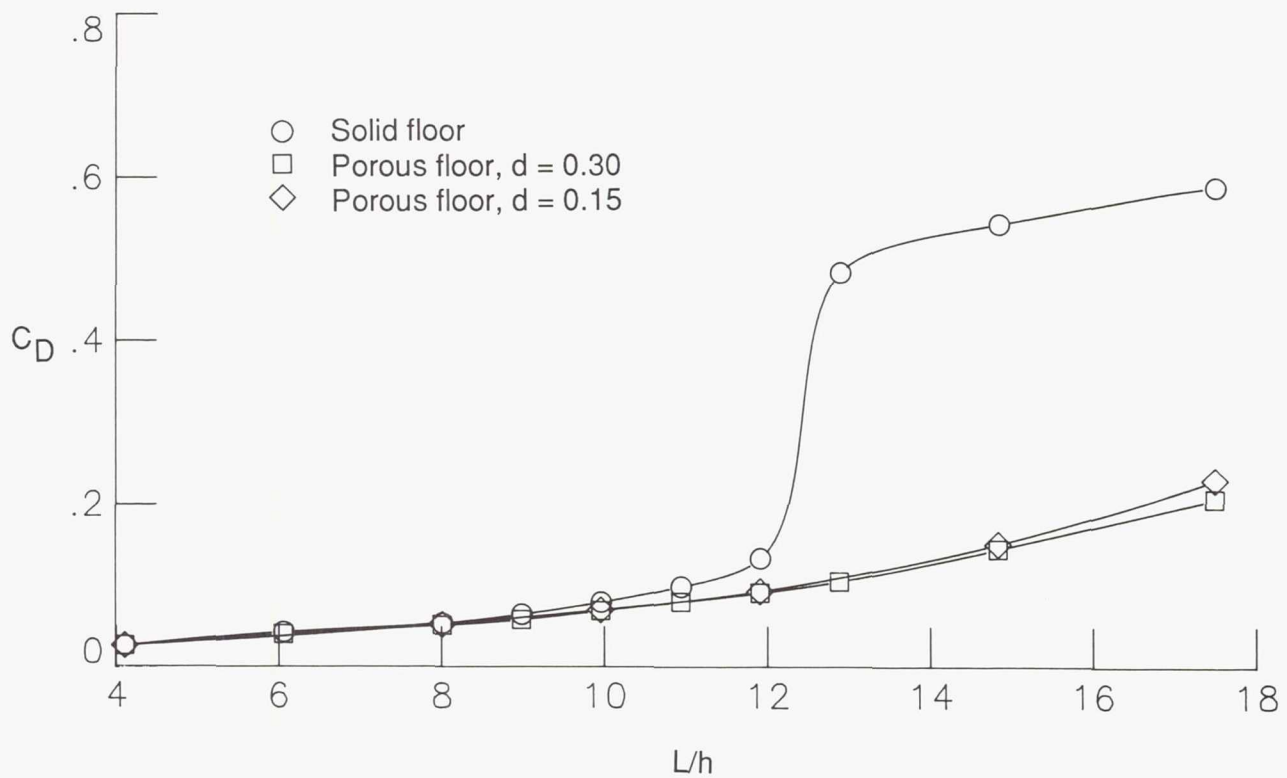


(b)  $M_\infty = 1.90$ .

Figure 21. Effect of porosity on cavity drag.



(c)  $M_\infty = 2.16$ .



(d)  $M_\infty = 2.86$ .

Figure 21. Concluded.

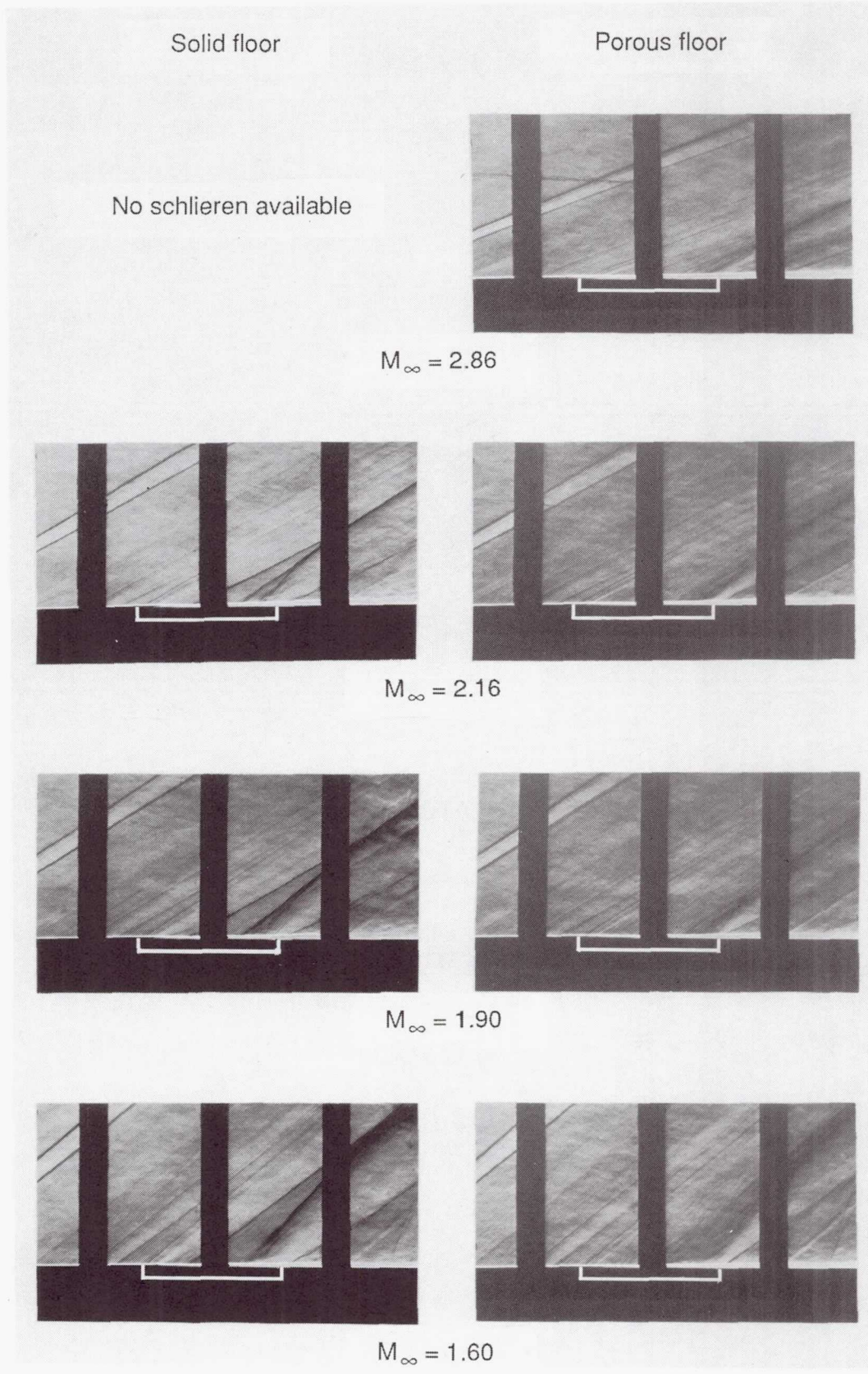
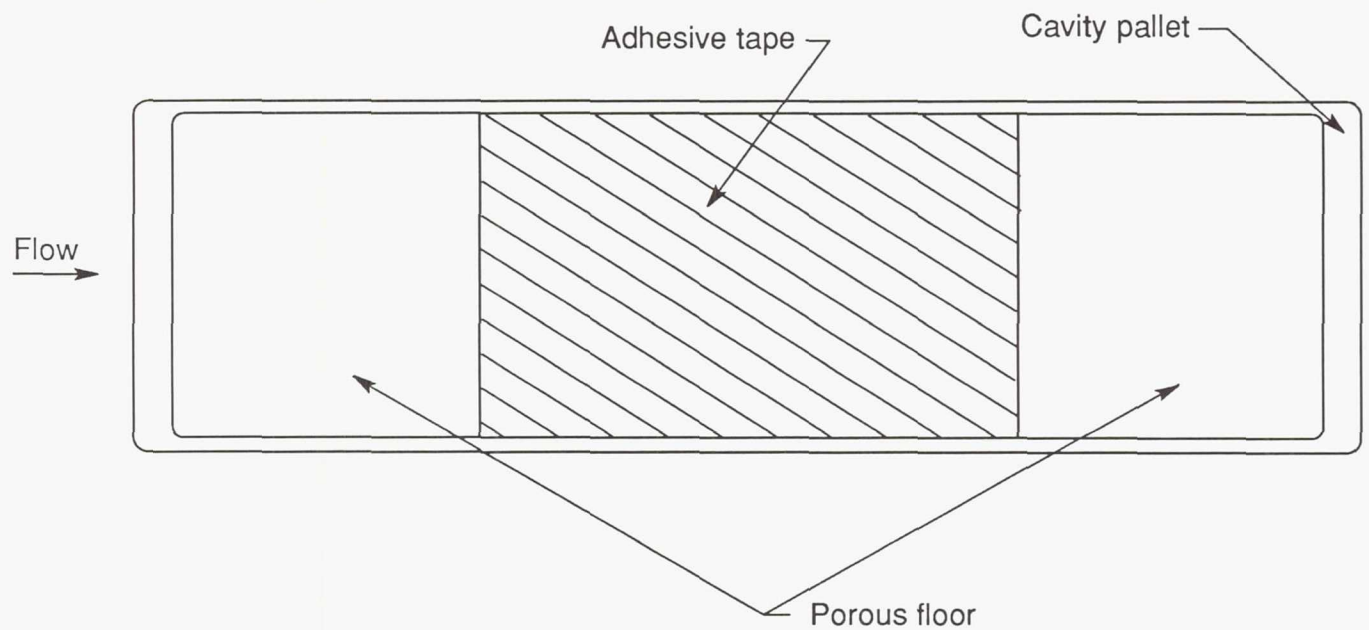
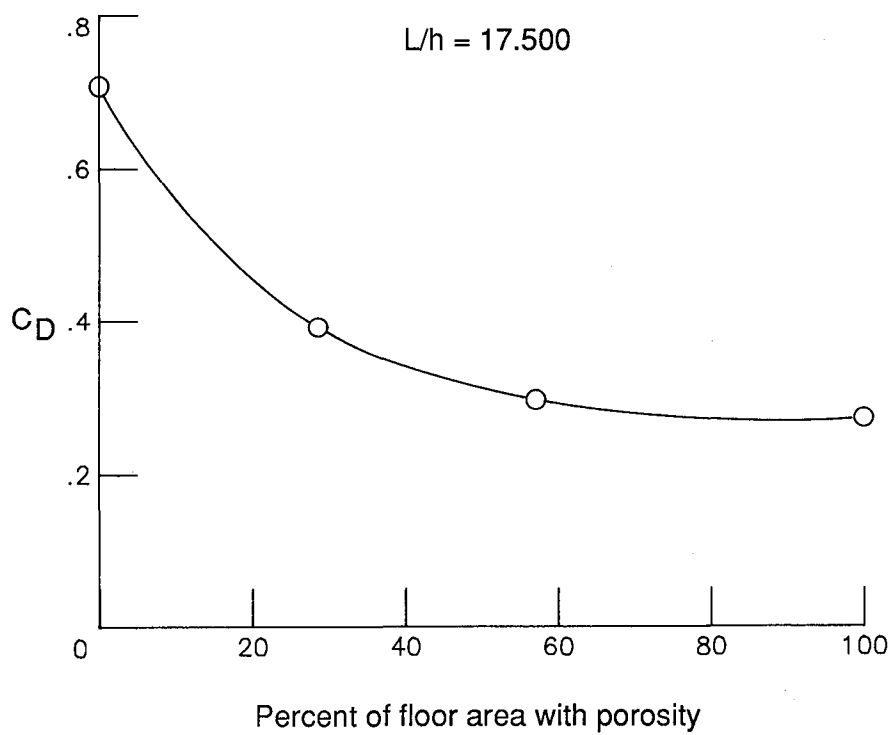


Figure 22. Schlieren photographs of solid- and porous-floor cavities ( $L/h = 17.500$  and  $d = 0.30$  in.).

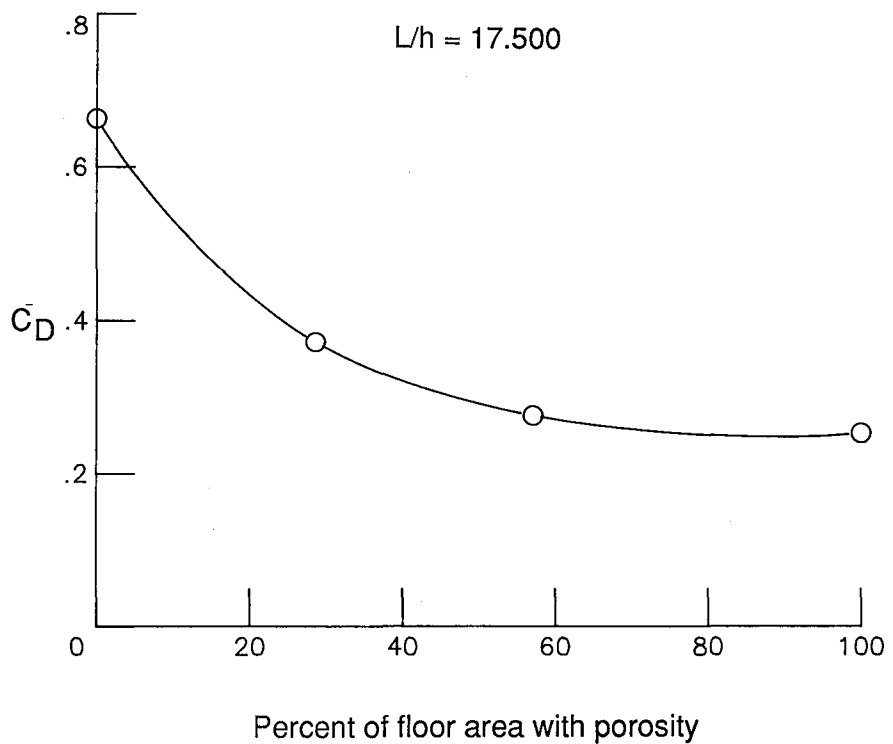


Cavity length, in.	Adhesive tape length, in.	Porous-floor length, in. (forward and rear)	Percent of floor area with porosity
7	none	—	100.0
7	3	2	57.1
7	5	1	28.6
7	7	0	0

Figure 23. Details of adhesive tape placement on cavity floor.

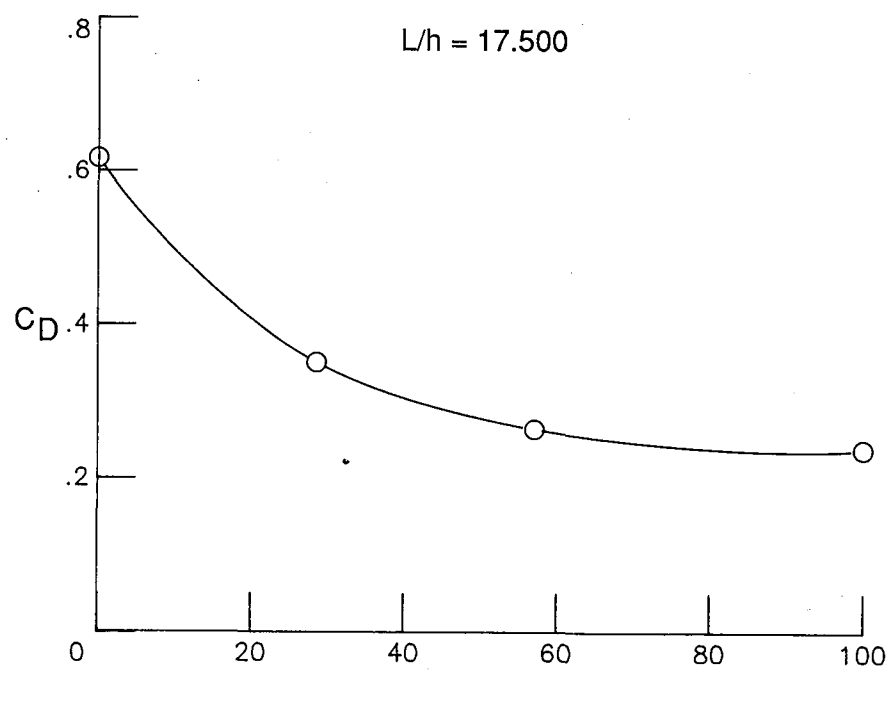


(a)  $M_\infty = 1.60.$

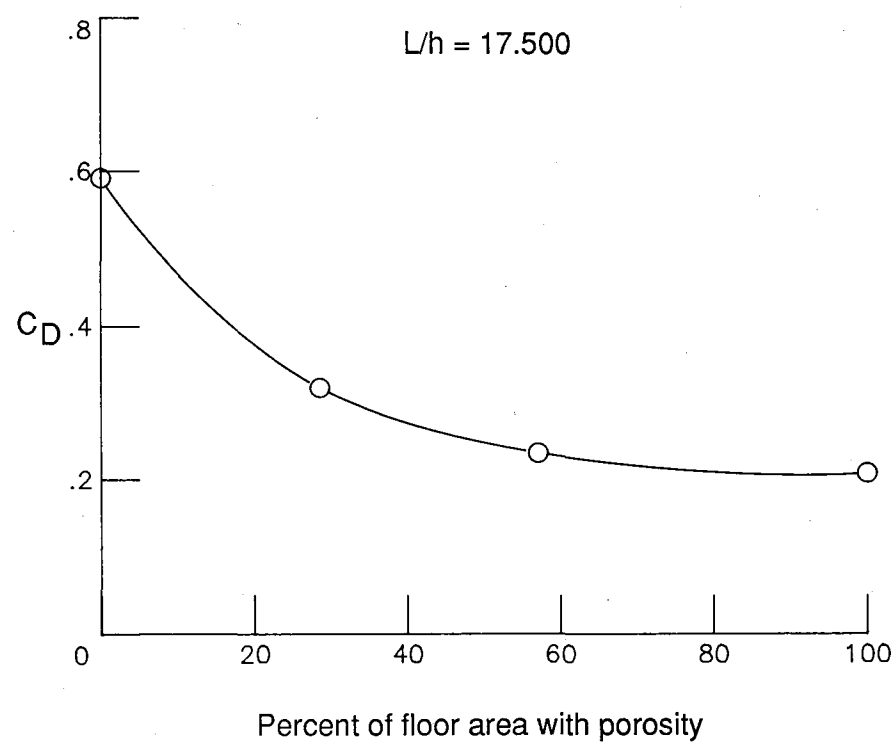


(b)  $M_\infty = 1.90.$

Figure 24. Effect of porosity in forward and rear sections of cavity.

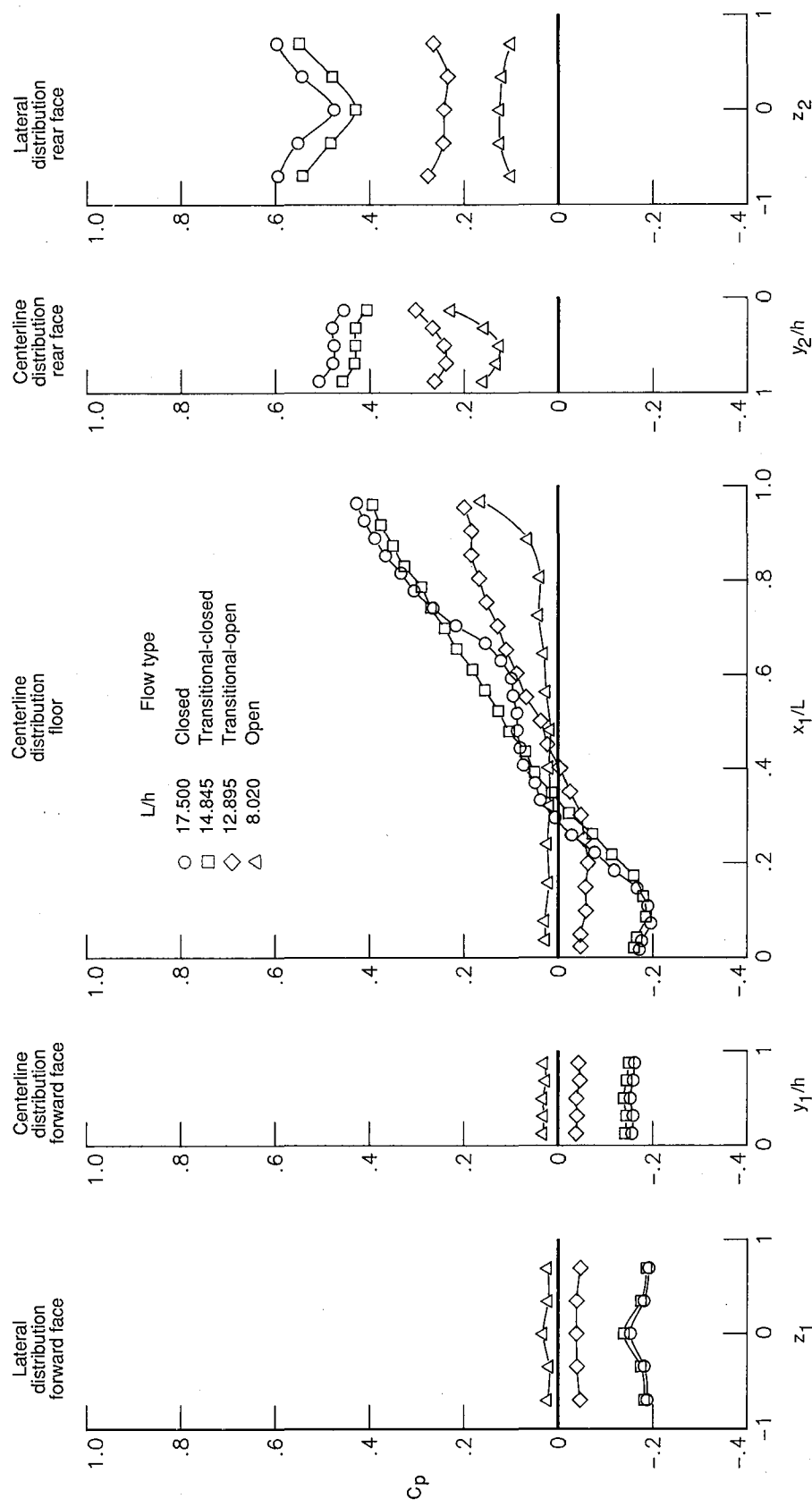


(c)  $M_\infty = 2.16.$



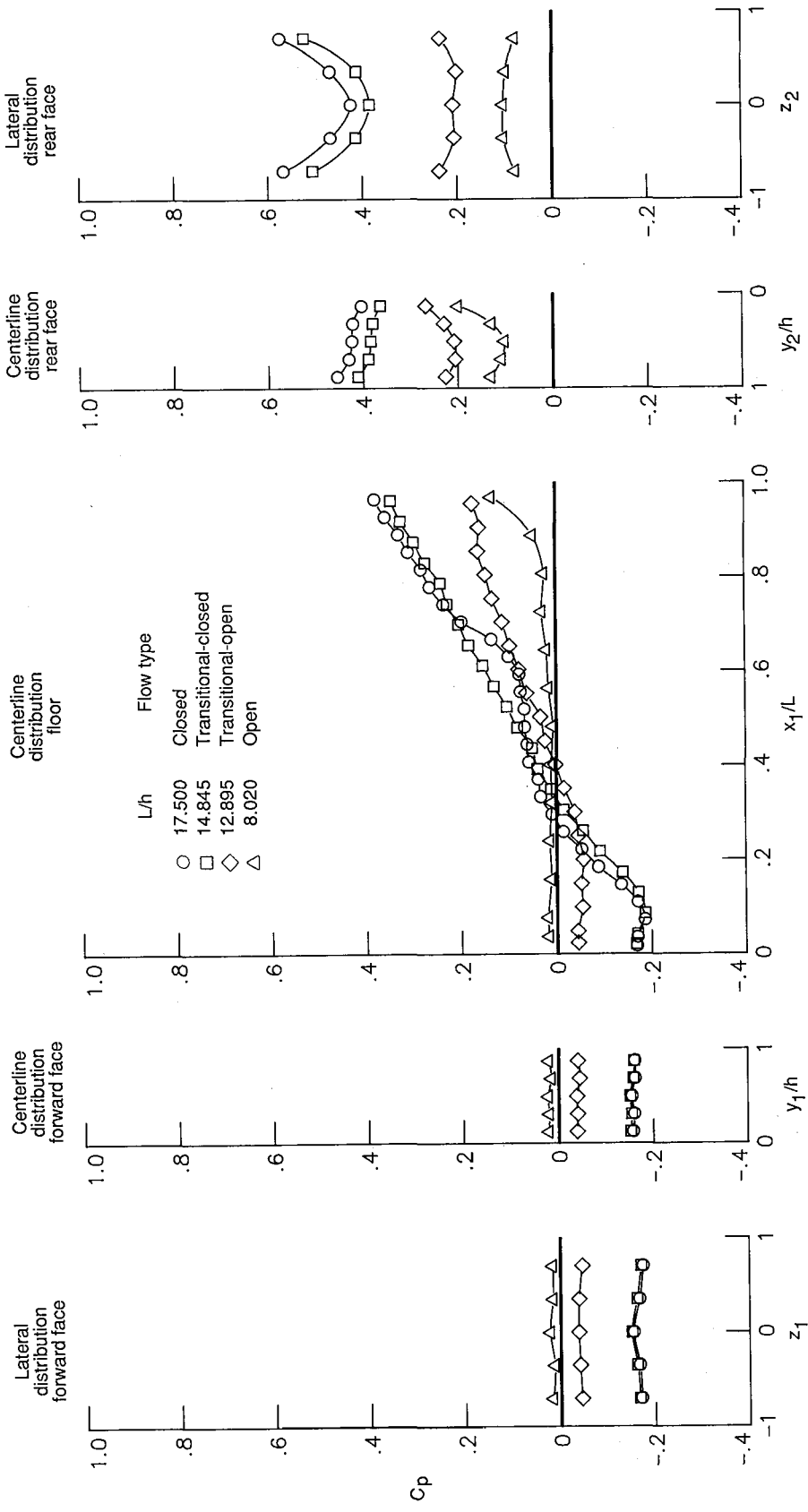
(d)  $M_\infty = 2.86.$

Figure 24. Concluded.



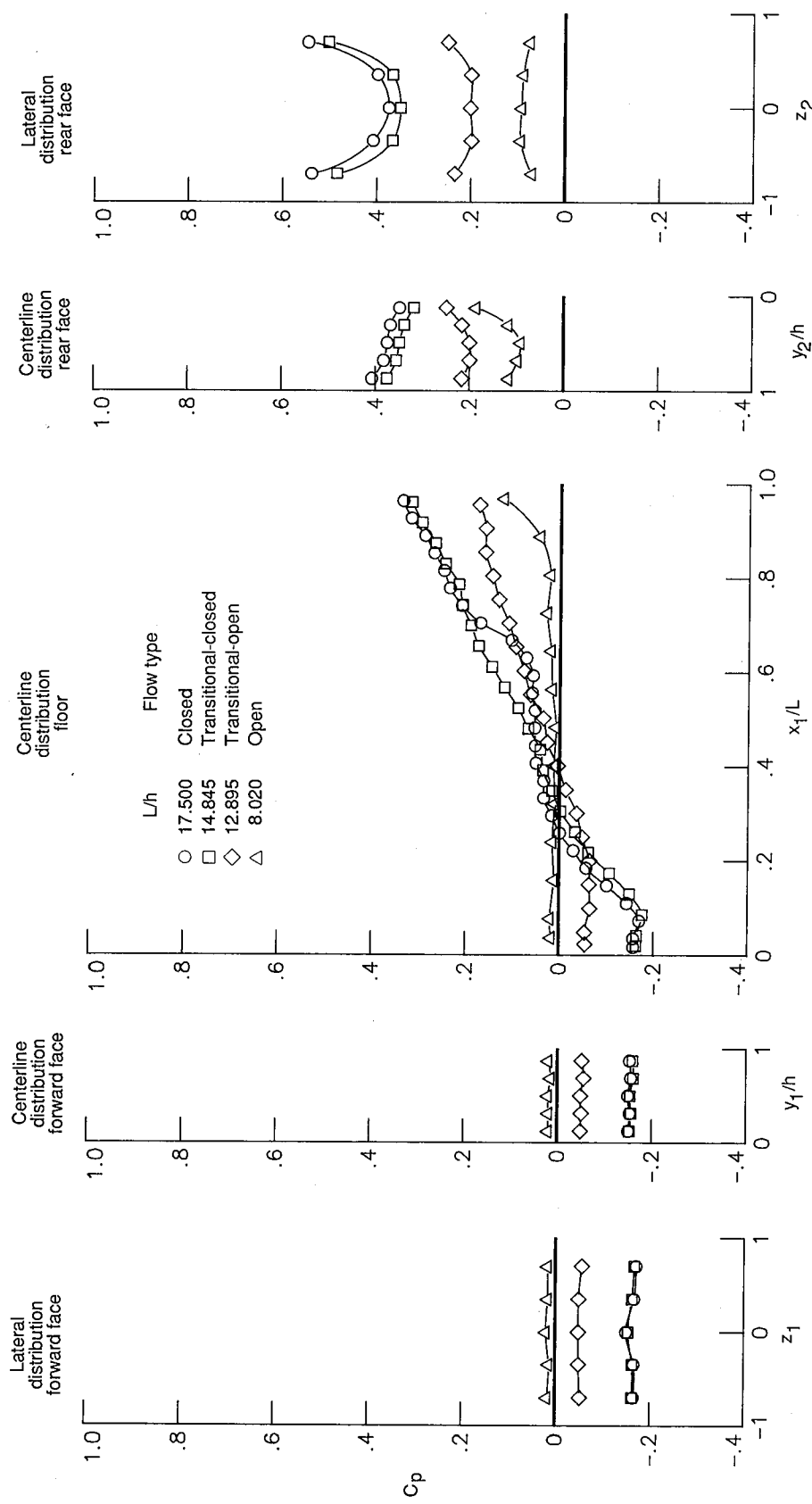
(a)  $M_{\infty} = 1.60$ .

Figure 25. Solid-floor cavity pressure distributions.



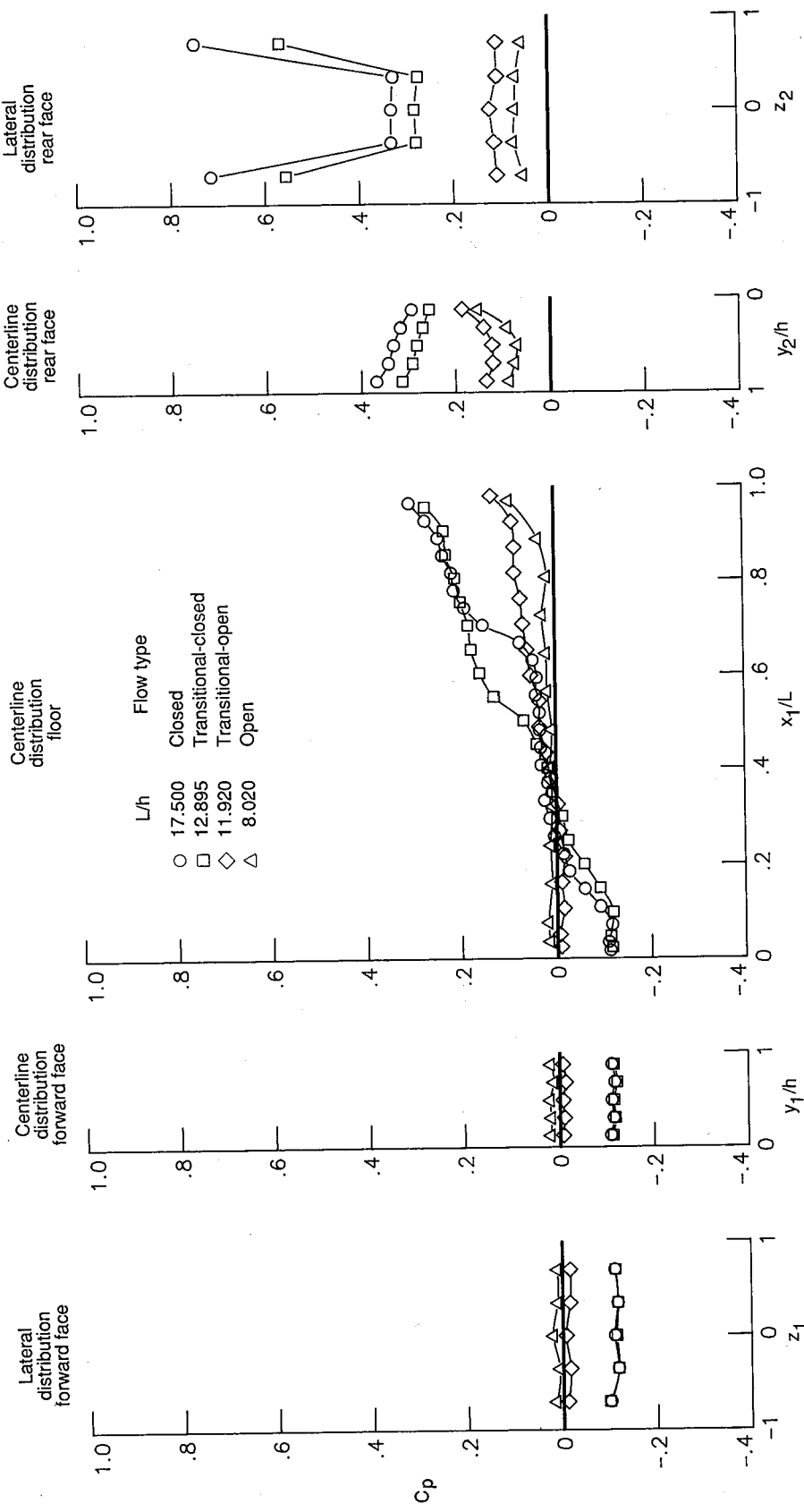
(b)  $M_\infty = 1.90$ .

Figure 25. Continued.



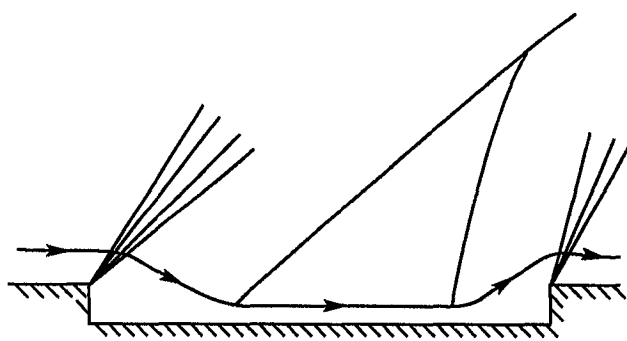
(c)  $M_\infty = 2.16$ .

Figure 25. Continued.

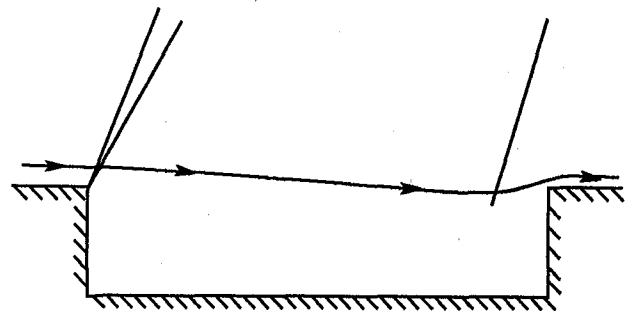


(d)  $M_\infty = 2.86$ .

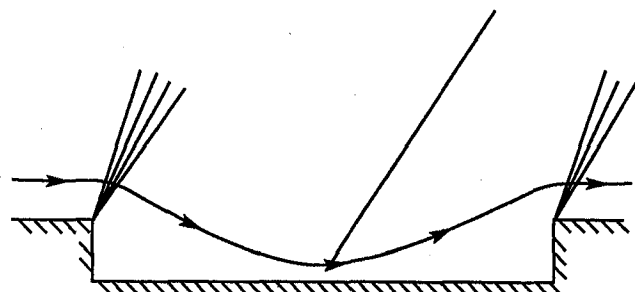
Figure 25. Concluded.



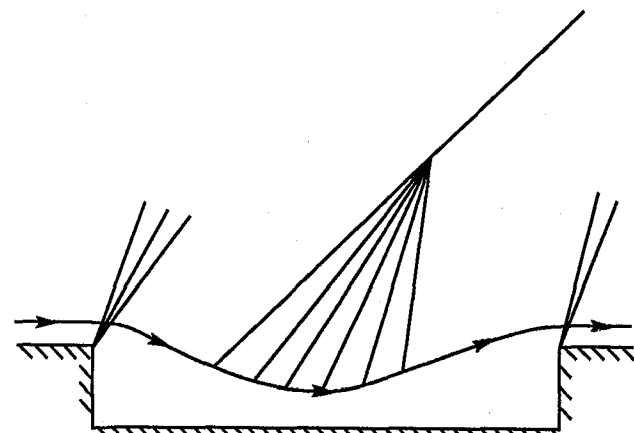
Closed-cavity flow  
 $L/h \gtrsim 13$



Open-cavity flow  
 $L/h \lesssim 10$



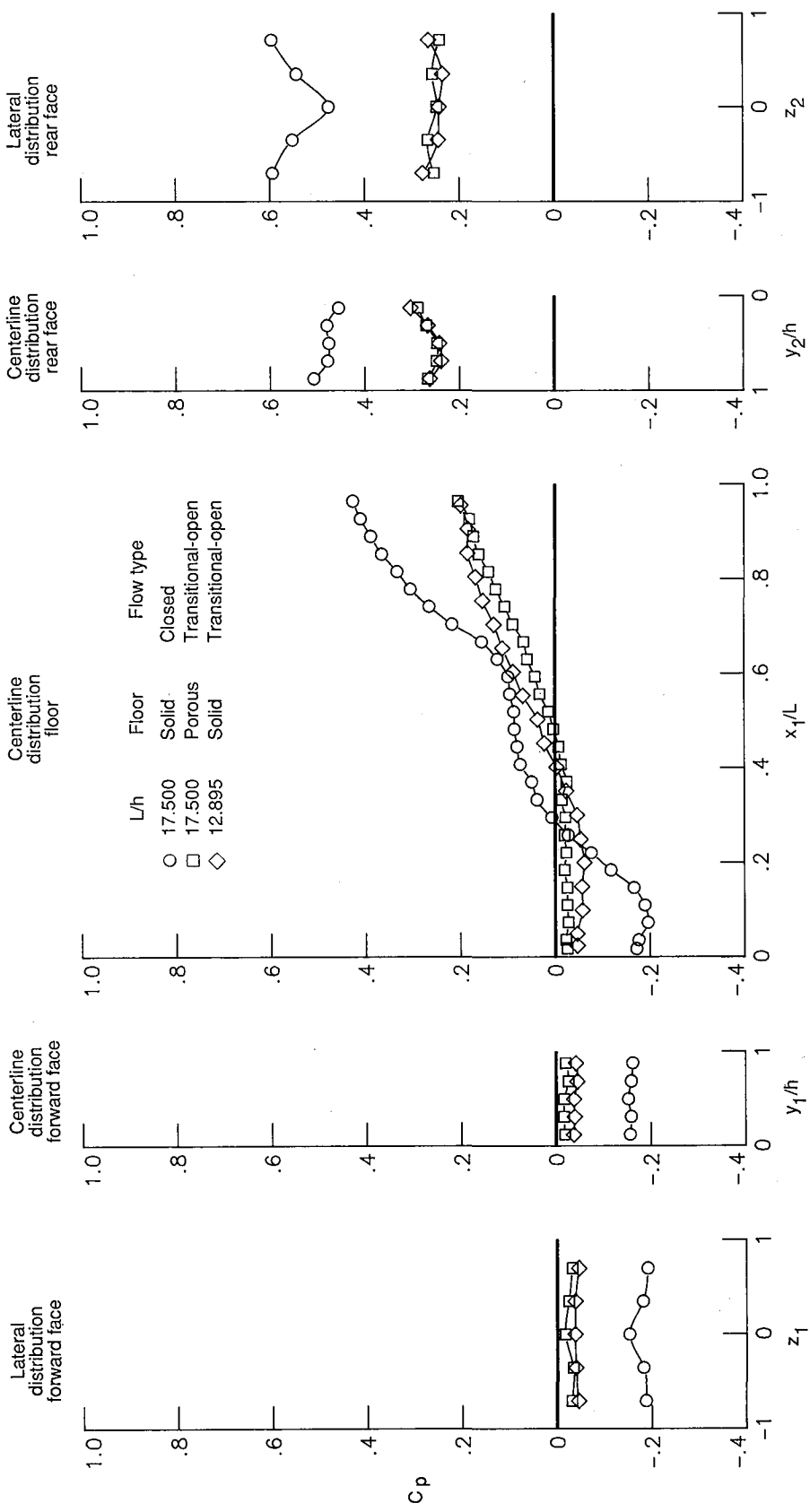
Transitional-closed-cavity flow



Transitional-open-cavity flow

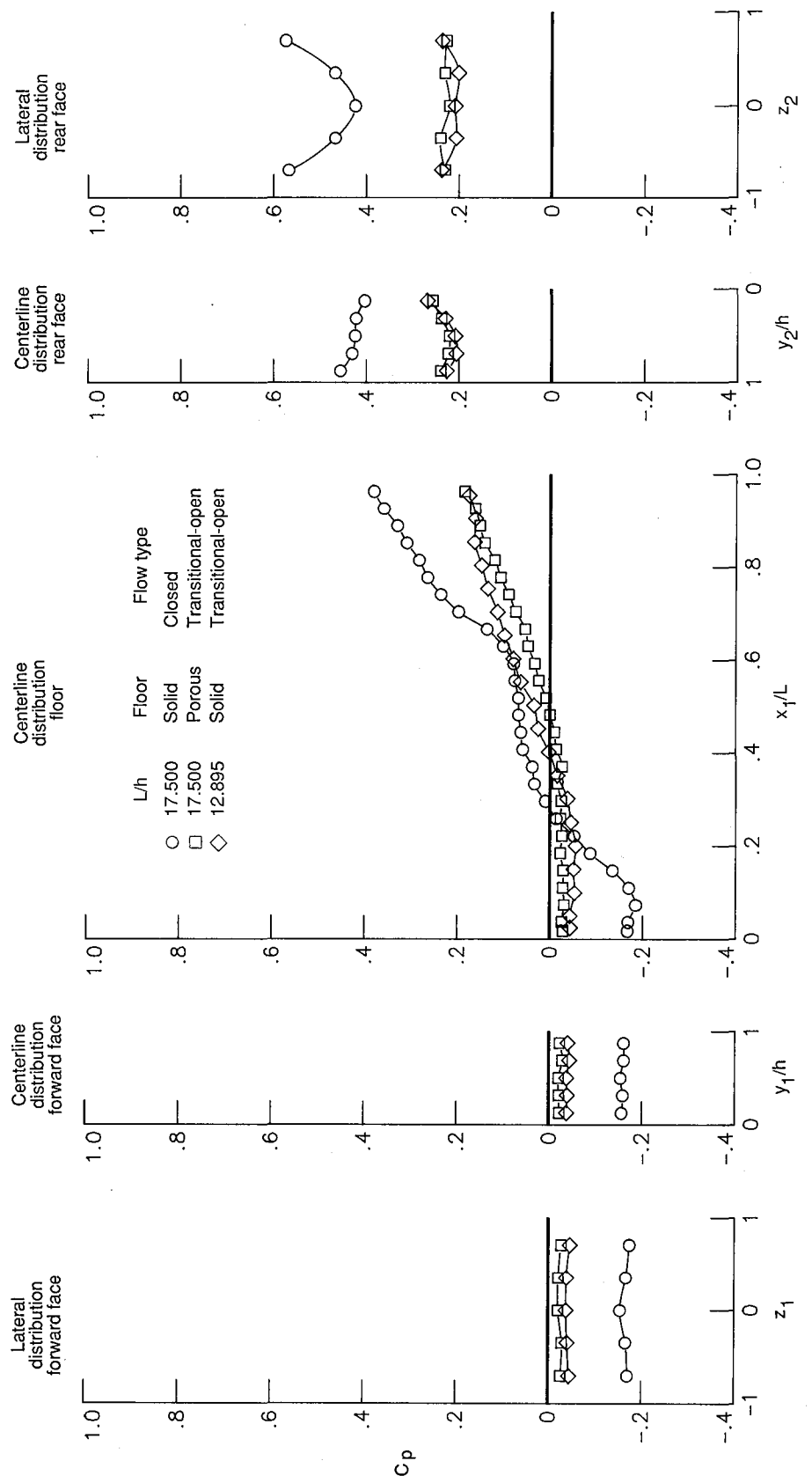
$$10 \lesssim L/h \lesssim 13$$

Figure 26. Cavity flow field characteristics and terminology.



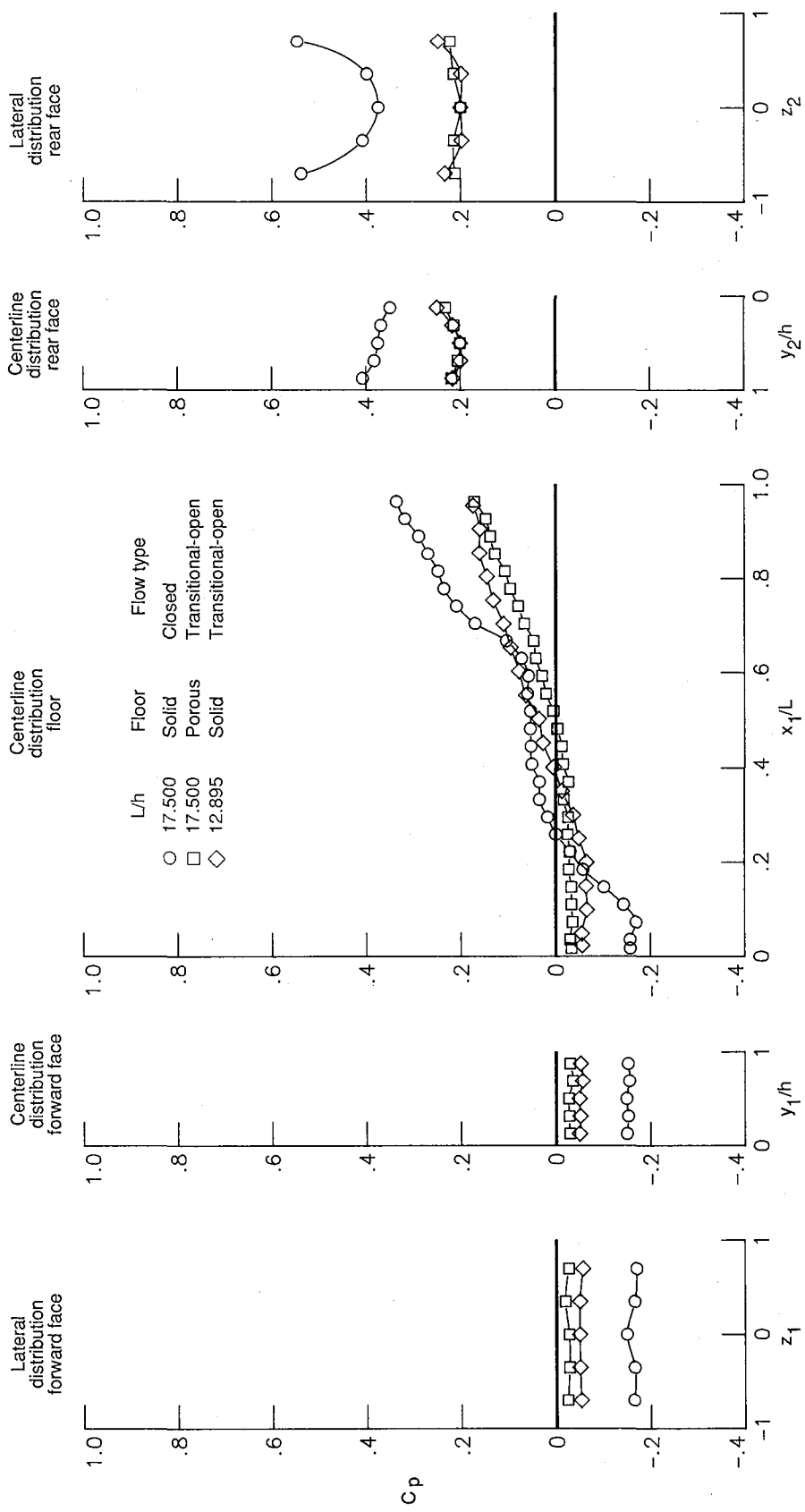
(a)  $M_{\infty} = 1.60$ .

Figure 27. Solid- and porous-floor cavity pressure distribution comparisons.



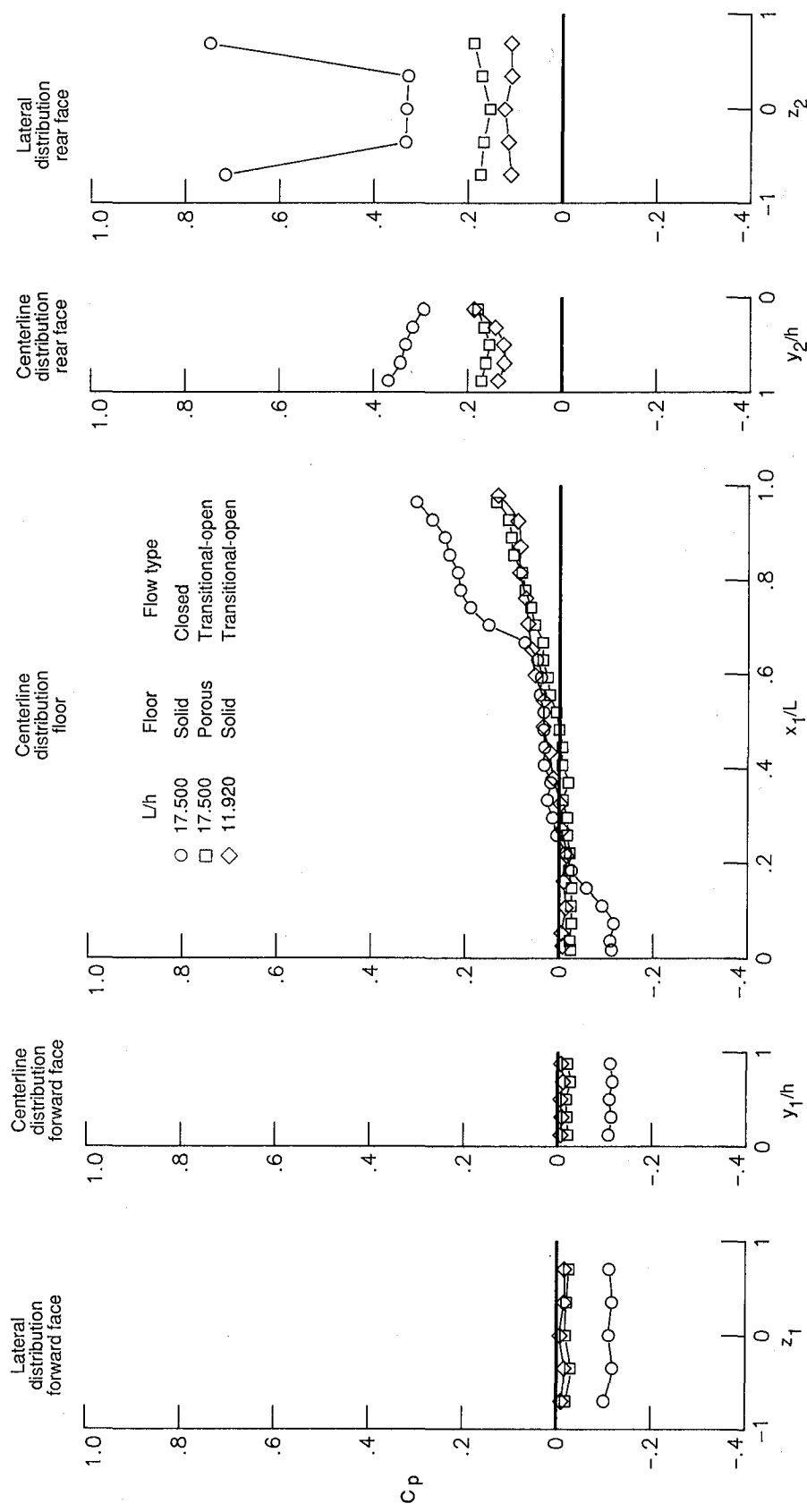
(b)  $M_\infty = 1.90$ .

Figure 27. Continued.



(c)  $M_\infty = 2.16$ .

Figure 27. Continued.



(d)  $M_\infty = 2.86$ .

Figure 27. Concluded.

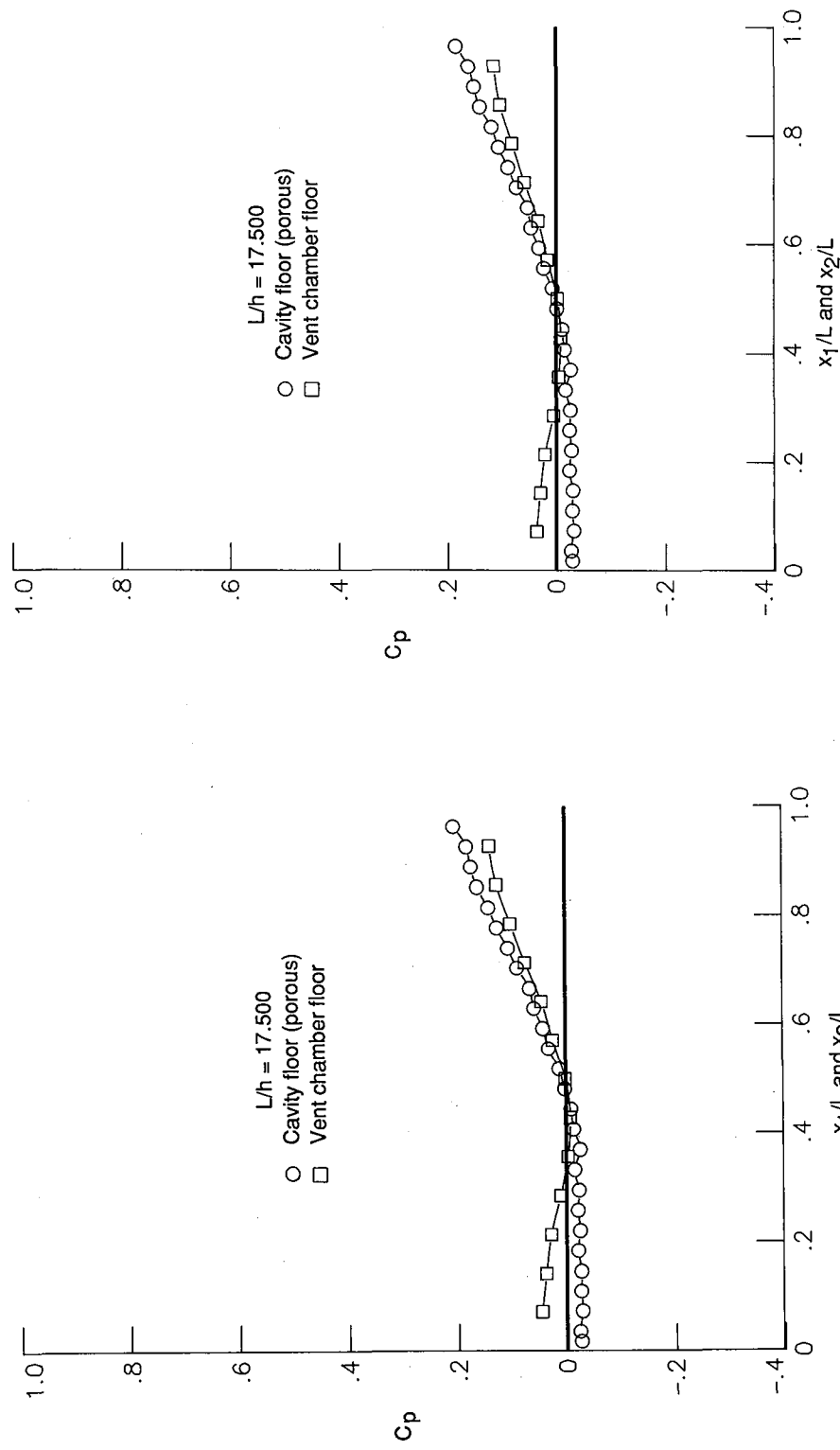


Figure 28. Comparison of cavity floor and vent chamber floor pressure distributions (closed flow).

(a)  $M_\infty = 1.60$ .  
 (b)  $M_\infty = 1.90$ .

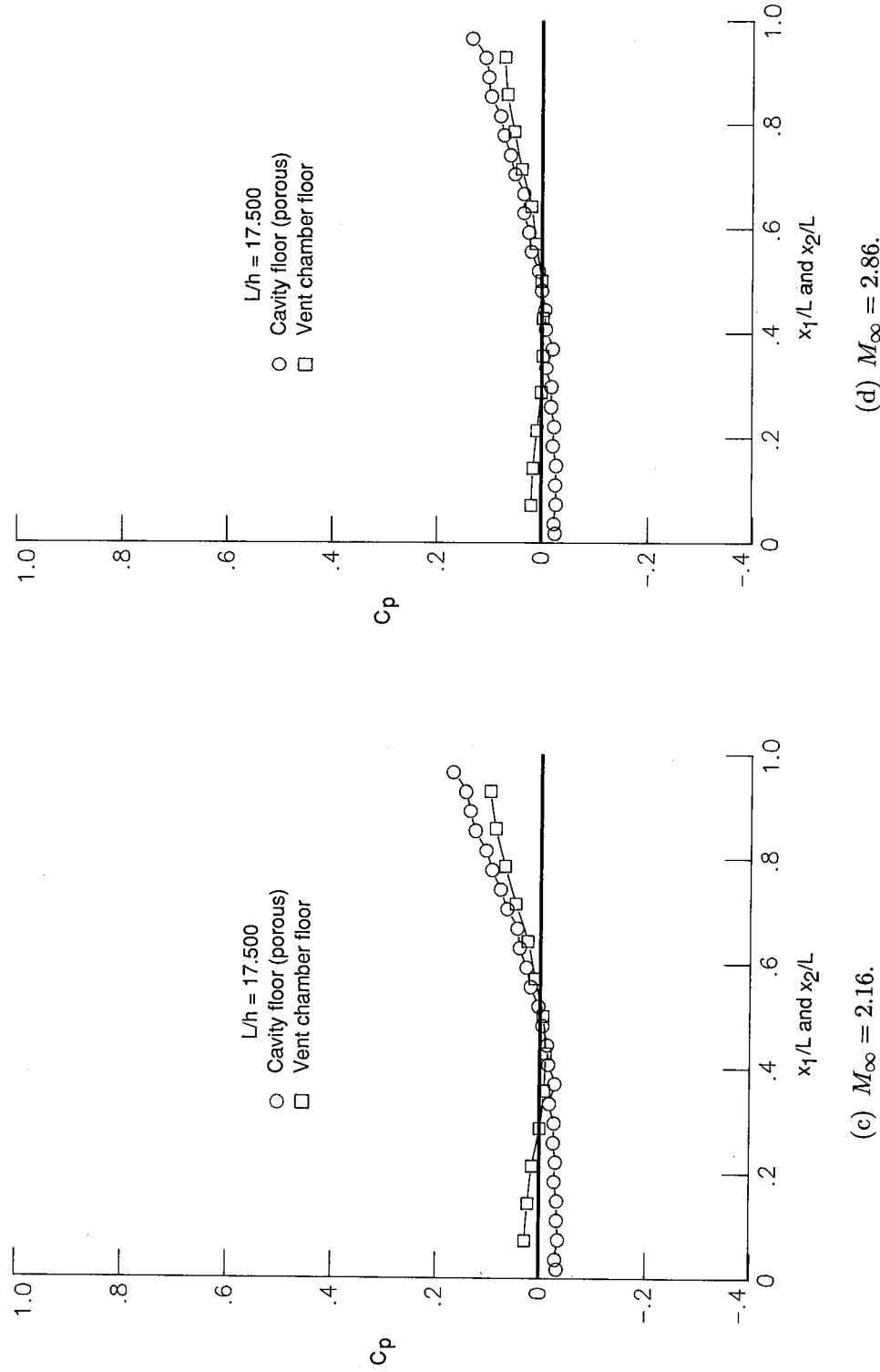
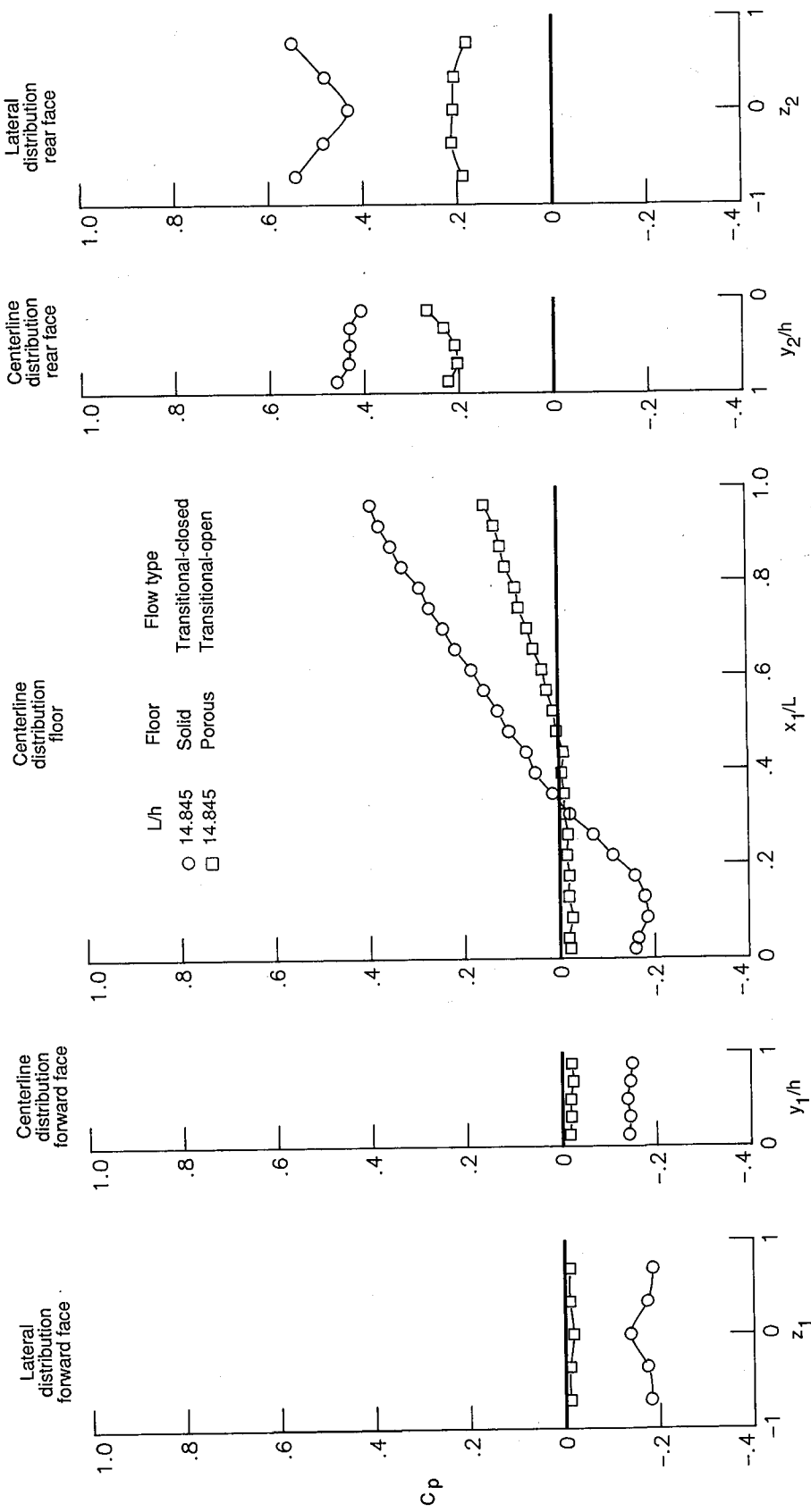
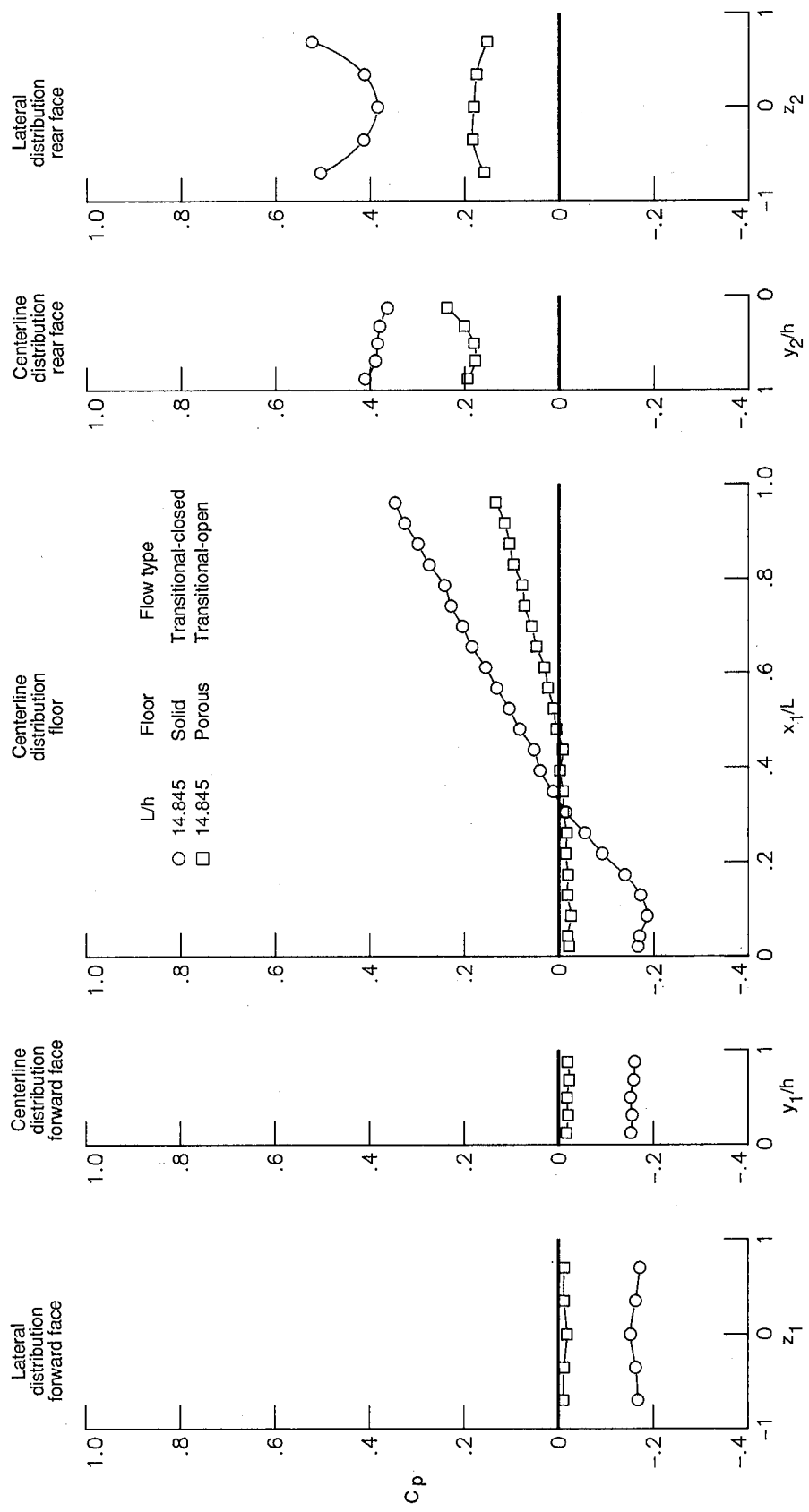


Figure 28. Concluded.



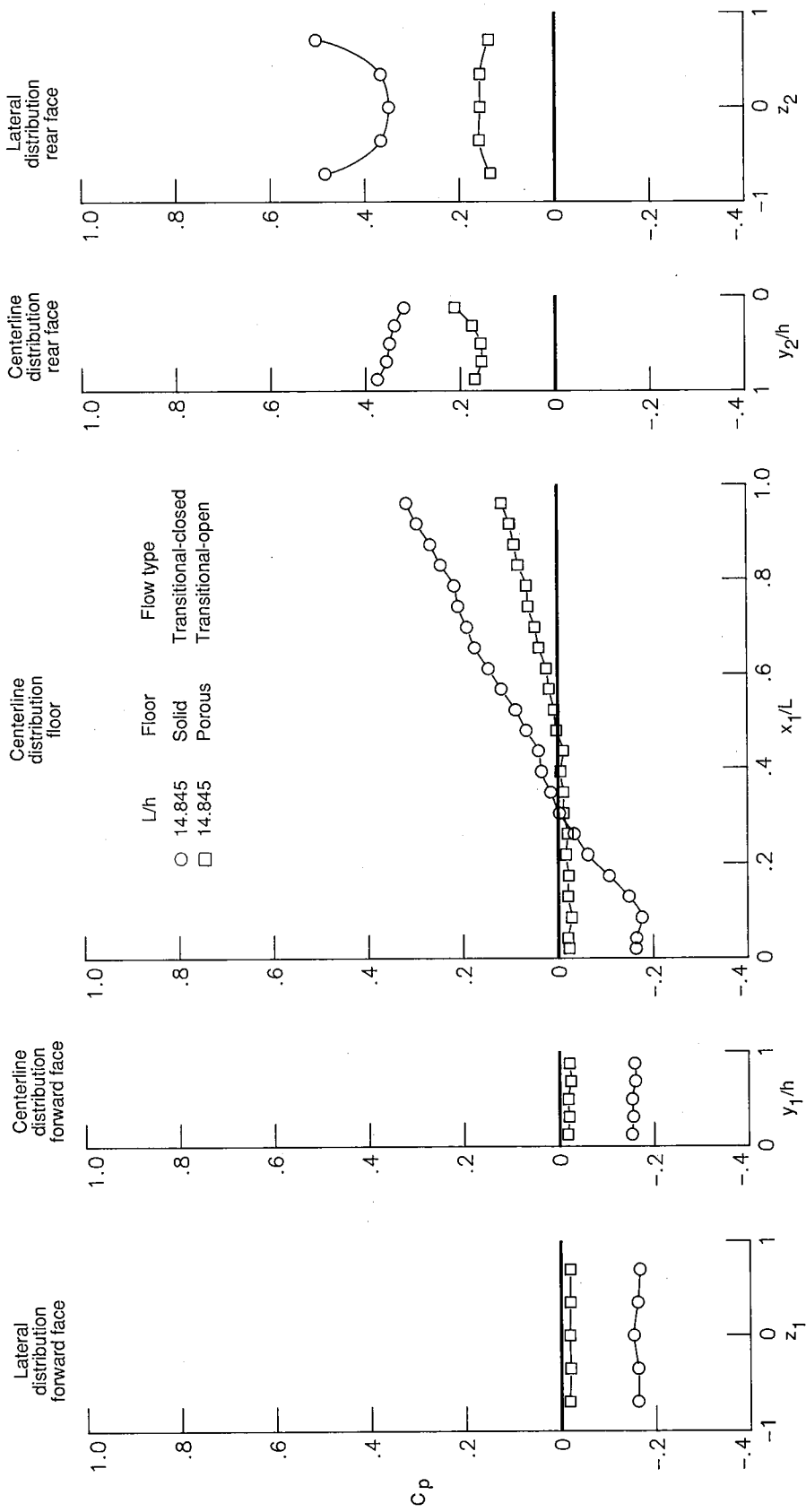
(a)  $M_{\infty} = 1.60$ .

Figure 29. Solid- and porous-floor cavity pressure distribution comparisons (transitional-closed flow).



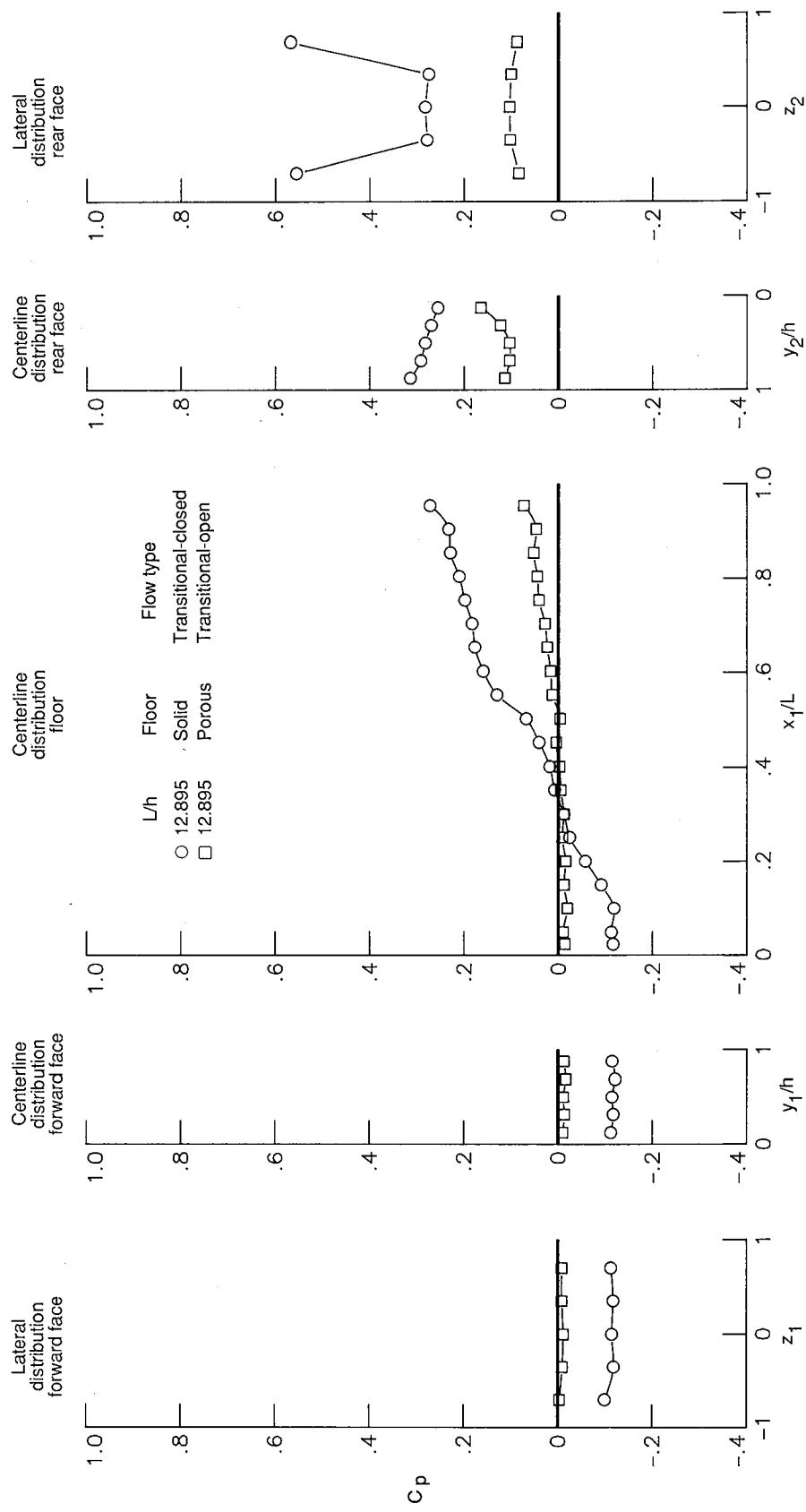
(b)  $M_\infty = 1.90$ .

Figure 29. Continued.



(c)  $M_\infty = 2.16$ .

Figure 29. Continued.



(d)  $M_\infty = 2.86$ .

Figure 29. Concluded.

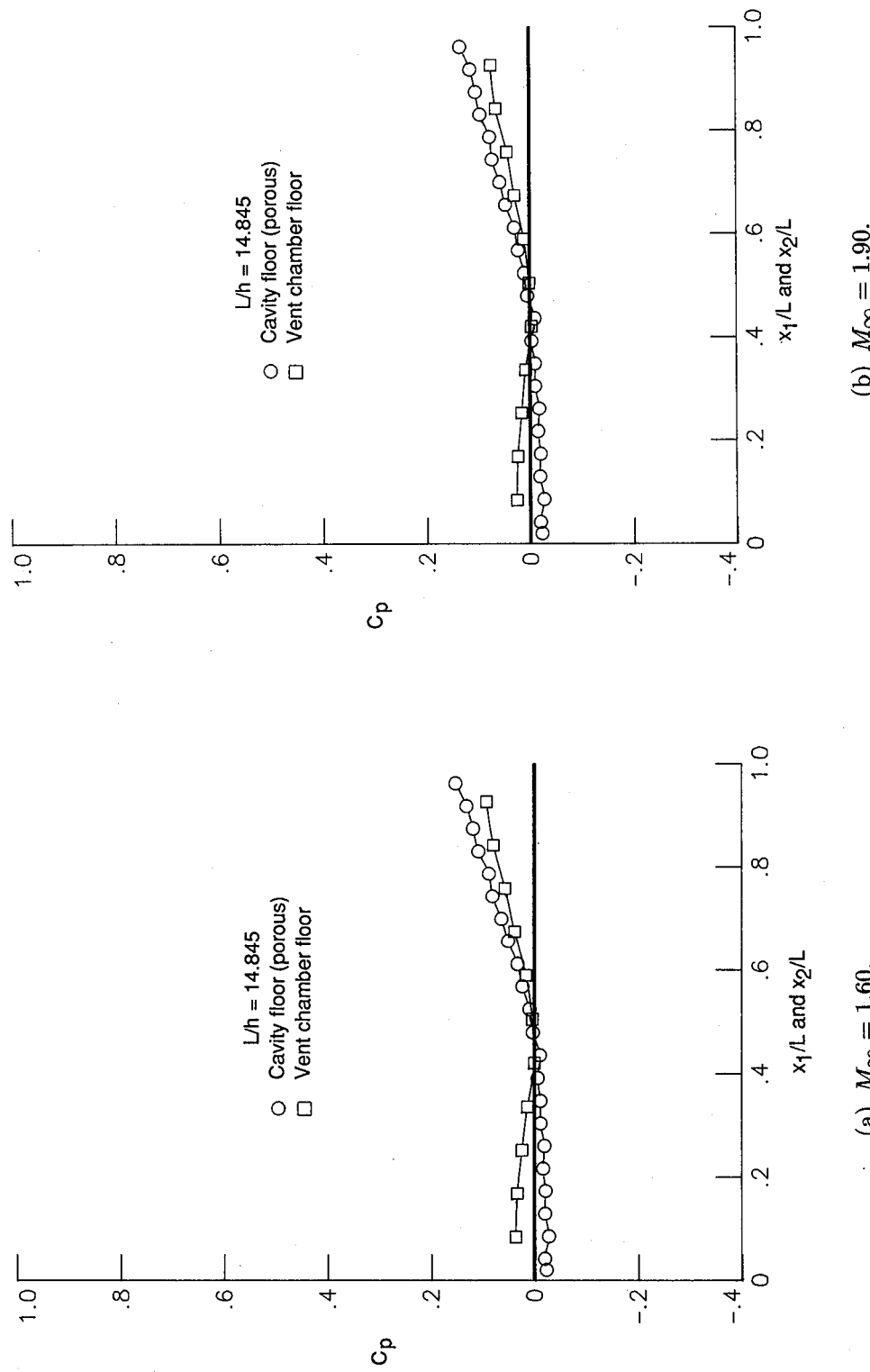


Figure 30. Comparison of cavity and vent chamber floor pressure distributions (transitional-closed flow).

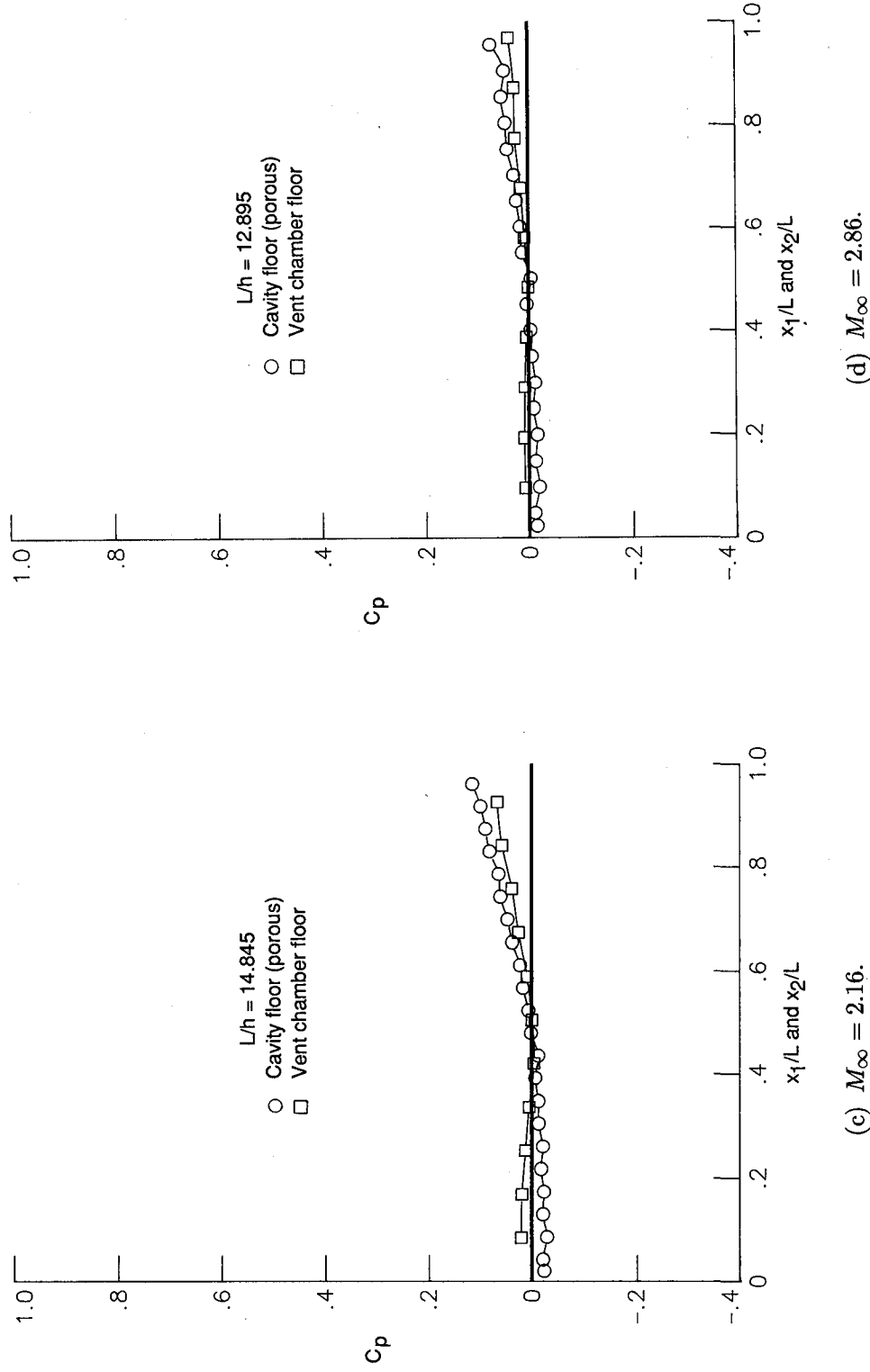
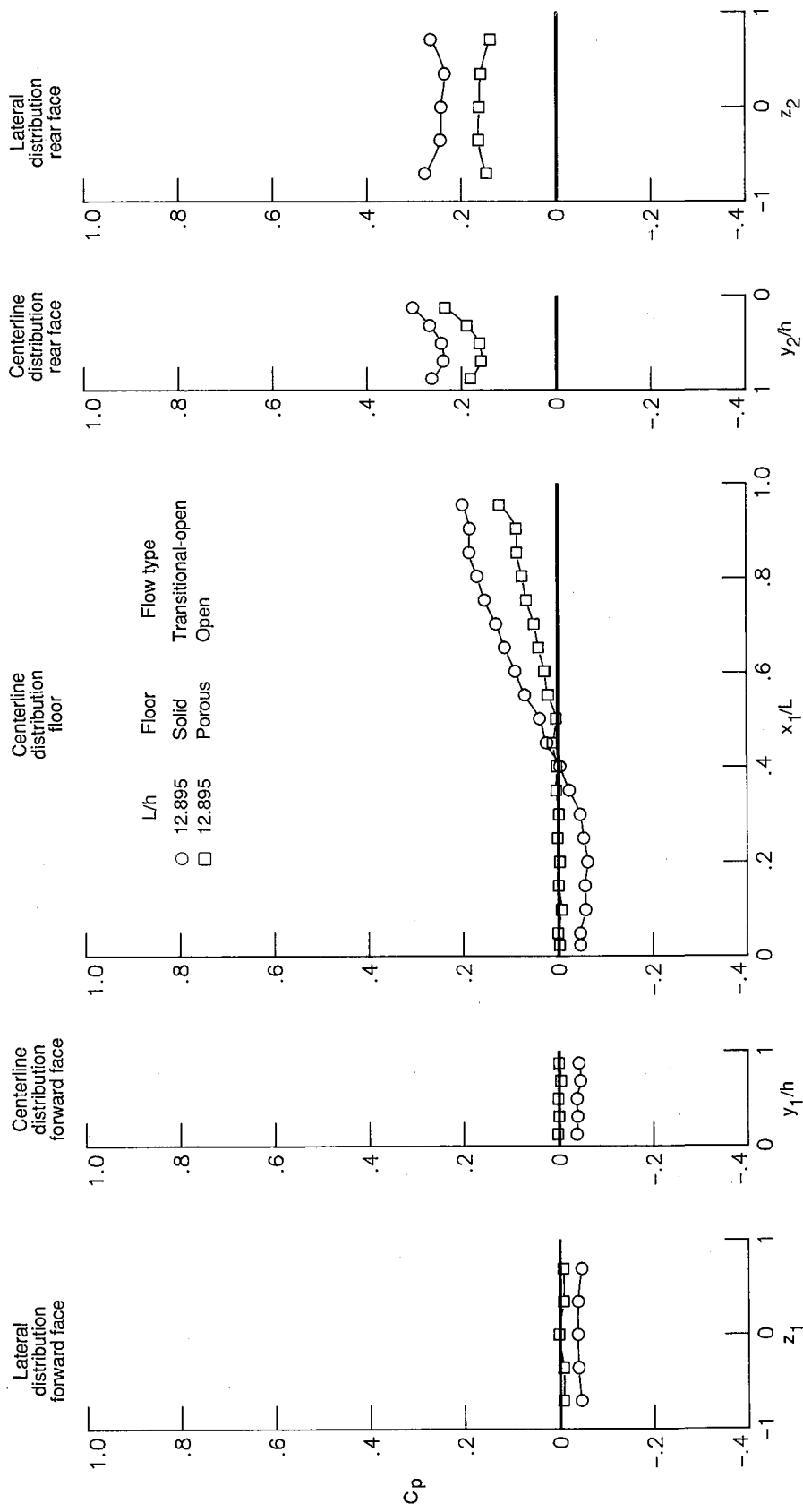
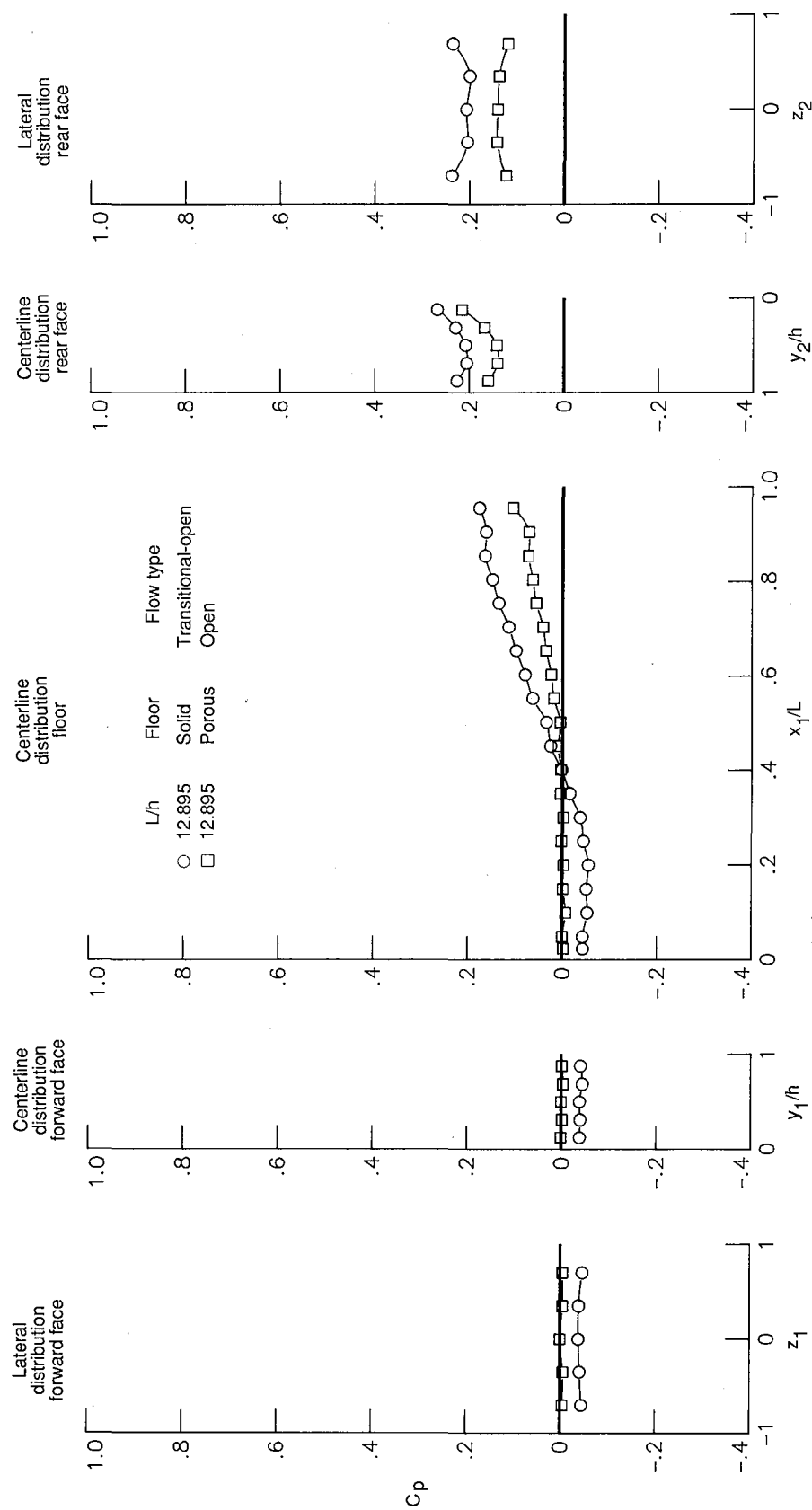


Figure 30. Concluded.



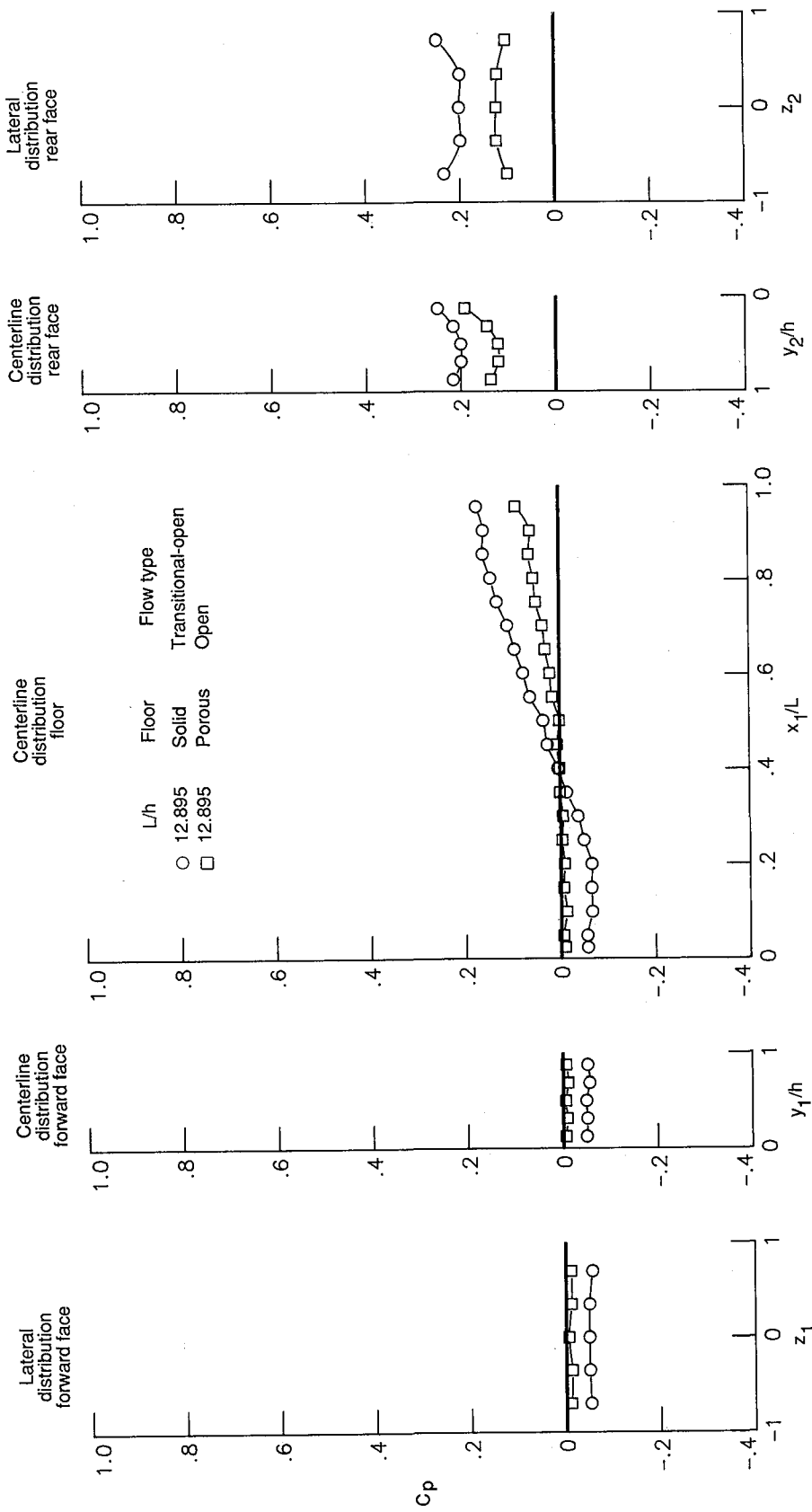
(a)  $M_\infty = 1.60$ .

Figure 31. Solid- and porous-floor cavity pressure distributions (transitional-open flow).



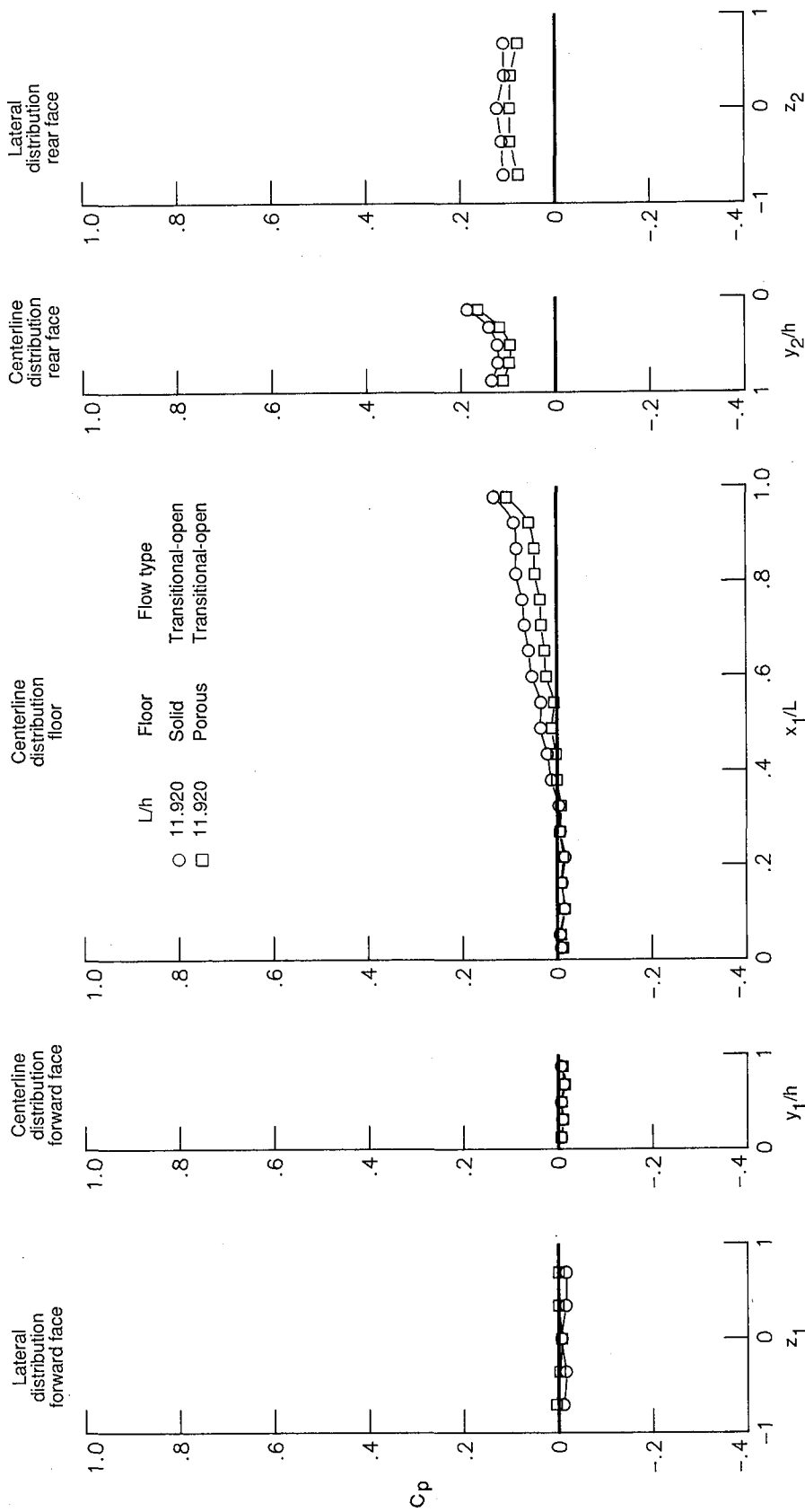
(b)  $M_\infty = 1.90$ .

Figure 31. Continued.



(c)  $M_\infty = 2.16$ .

Figure 31. Continued.



(d)  $M_\infty = 2.86$ .

Figure 31. Concluded.

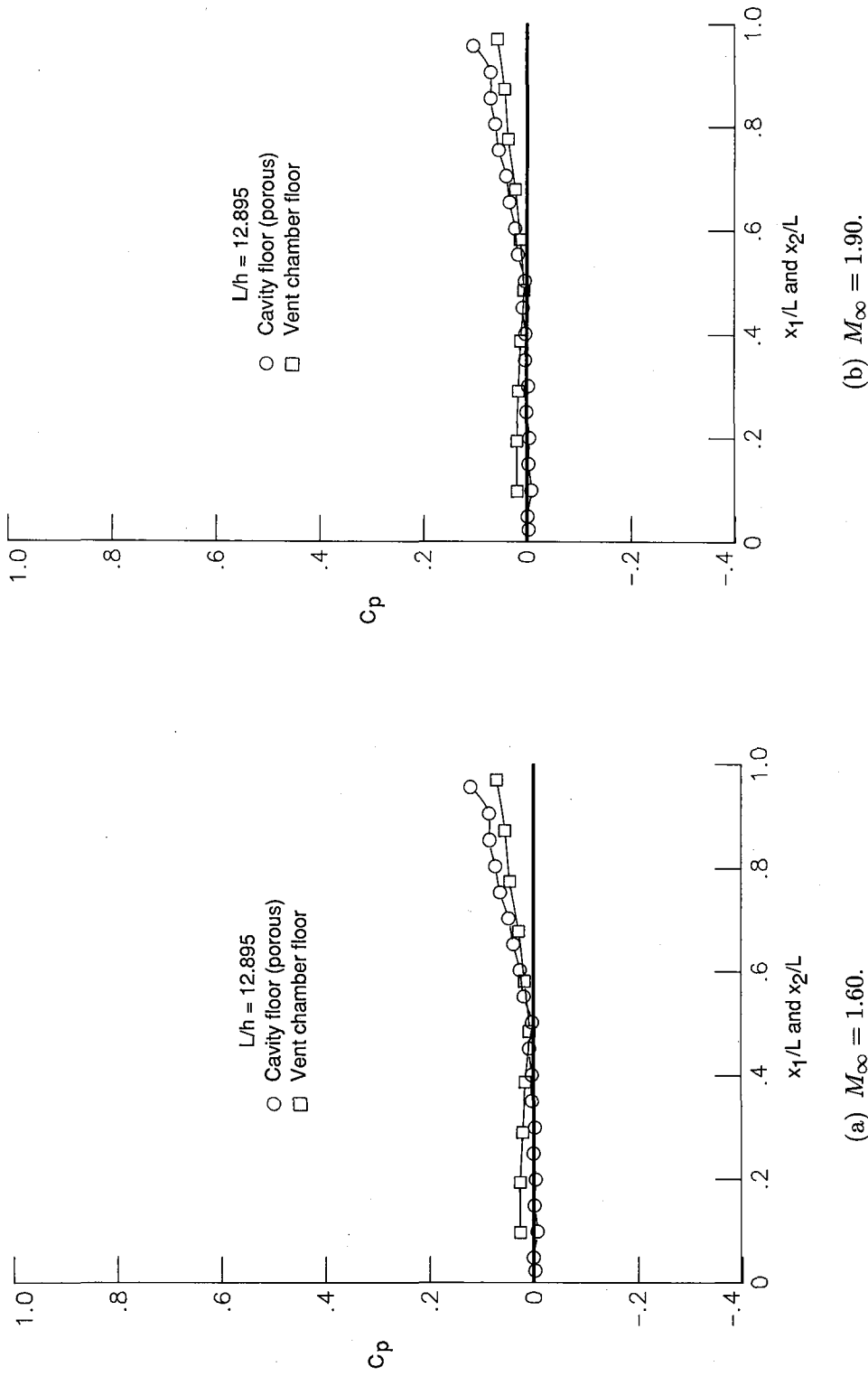


Figure 32. Comparison of cavity and vent chamber floor pressure distributions (transitional-open flow).

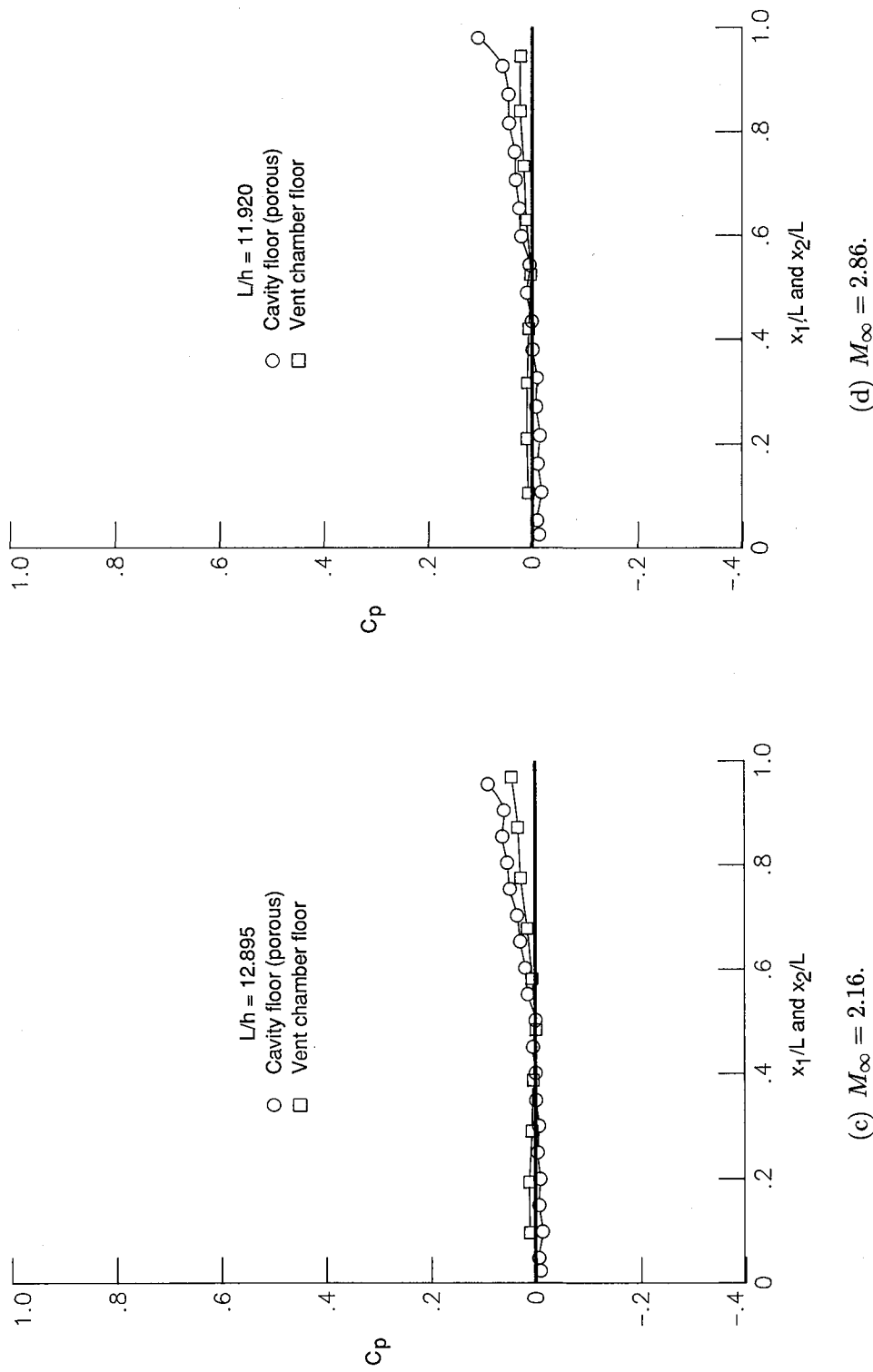
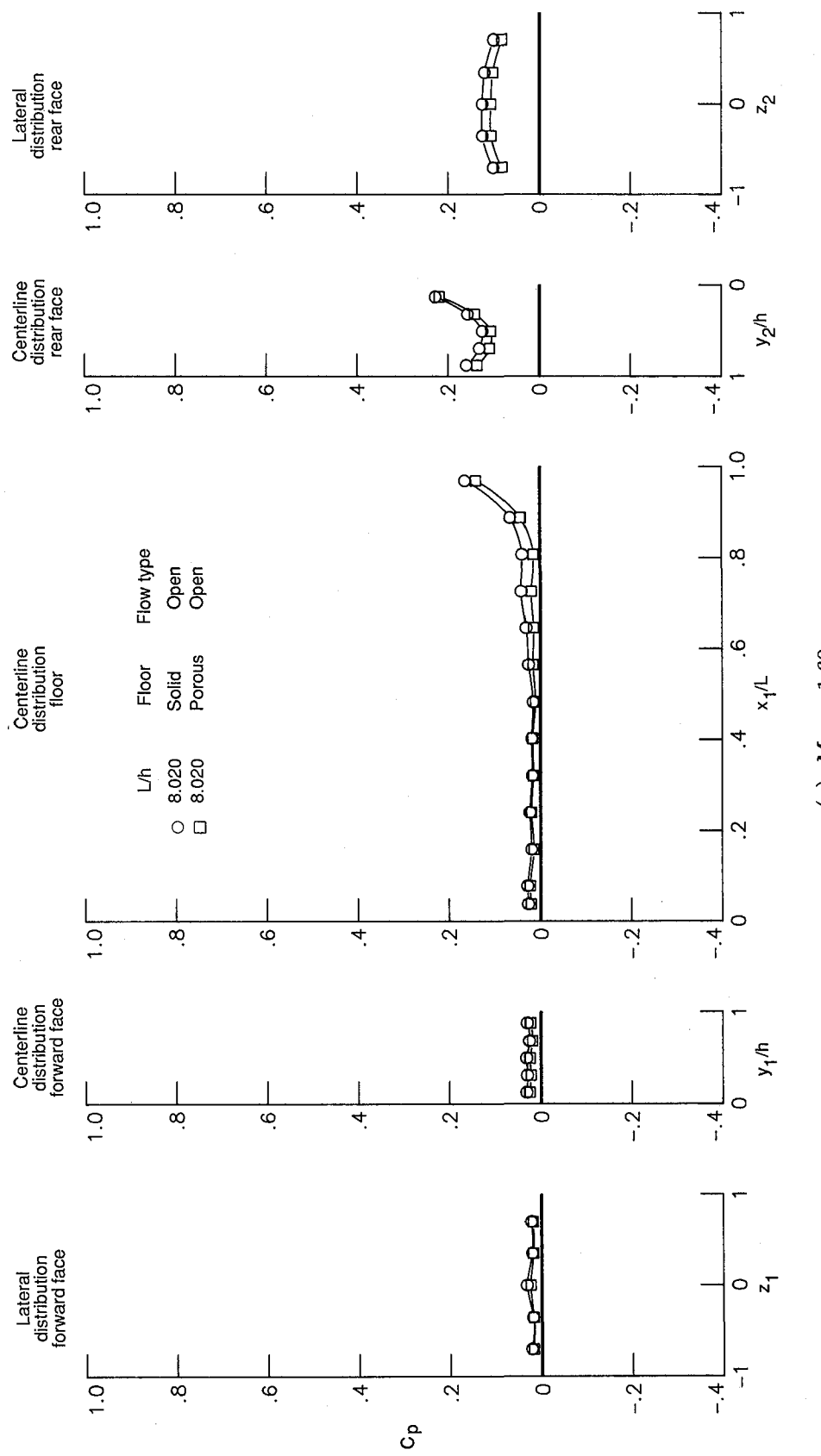
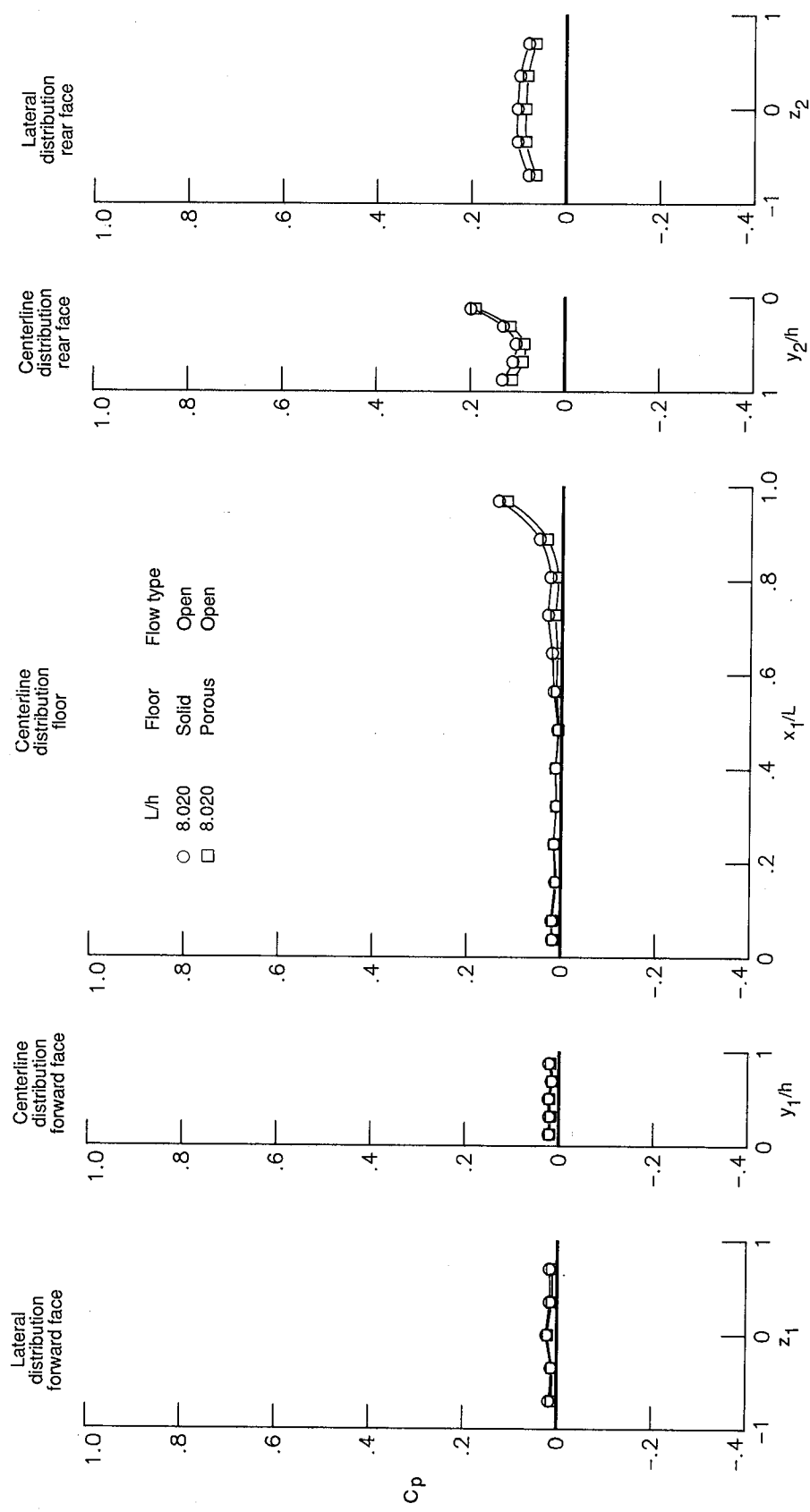


Figure 32. Concluded.



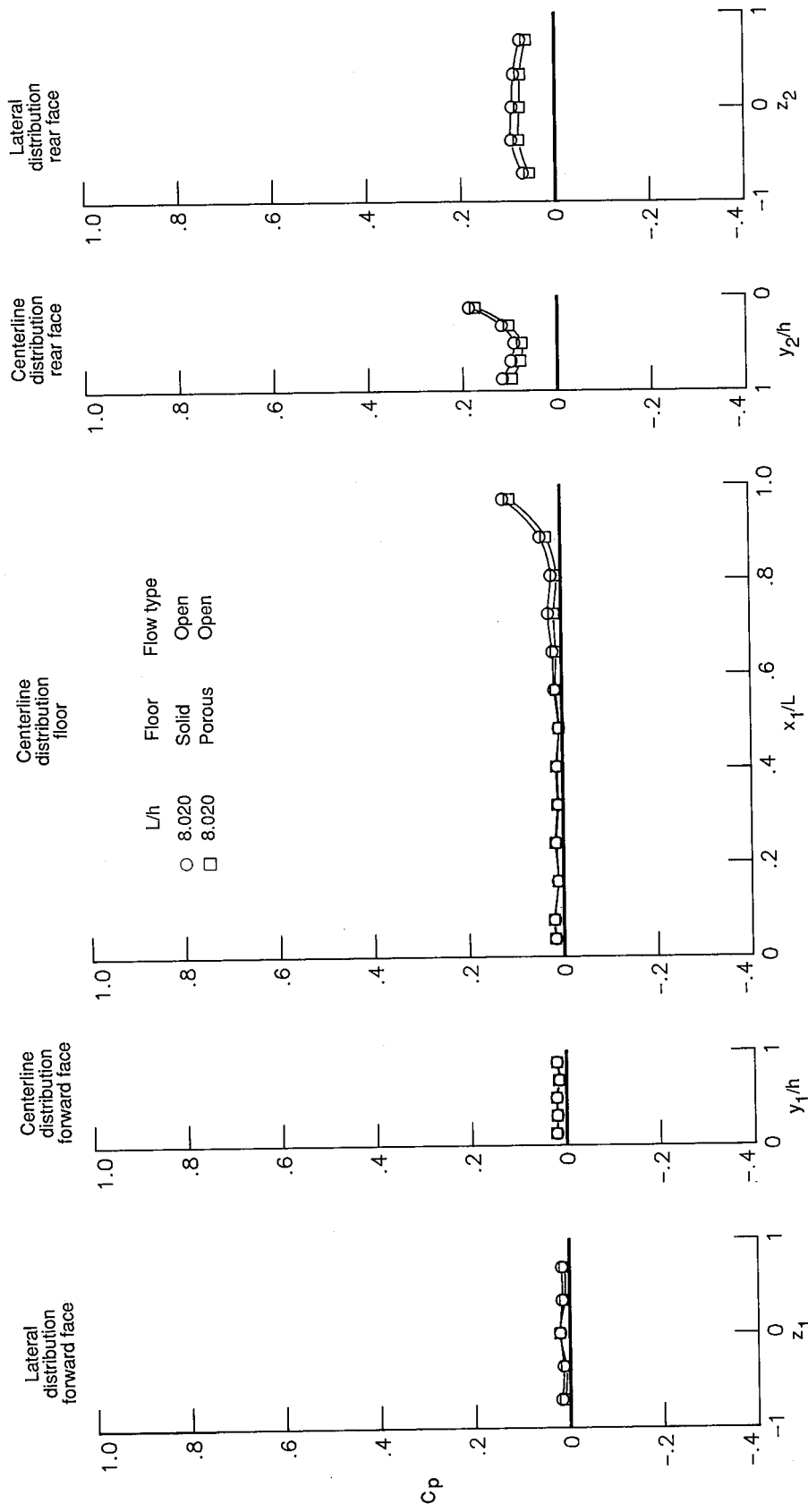
(a)  $M_\infty = 1.60$ .

Figure 33. Solid- and porous-floor cavity pressure distributions (open flow).



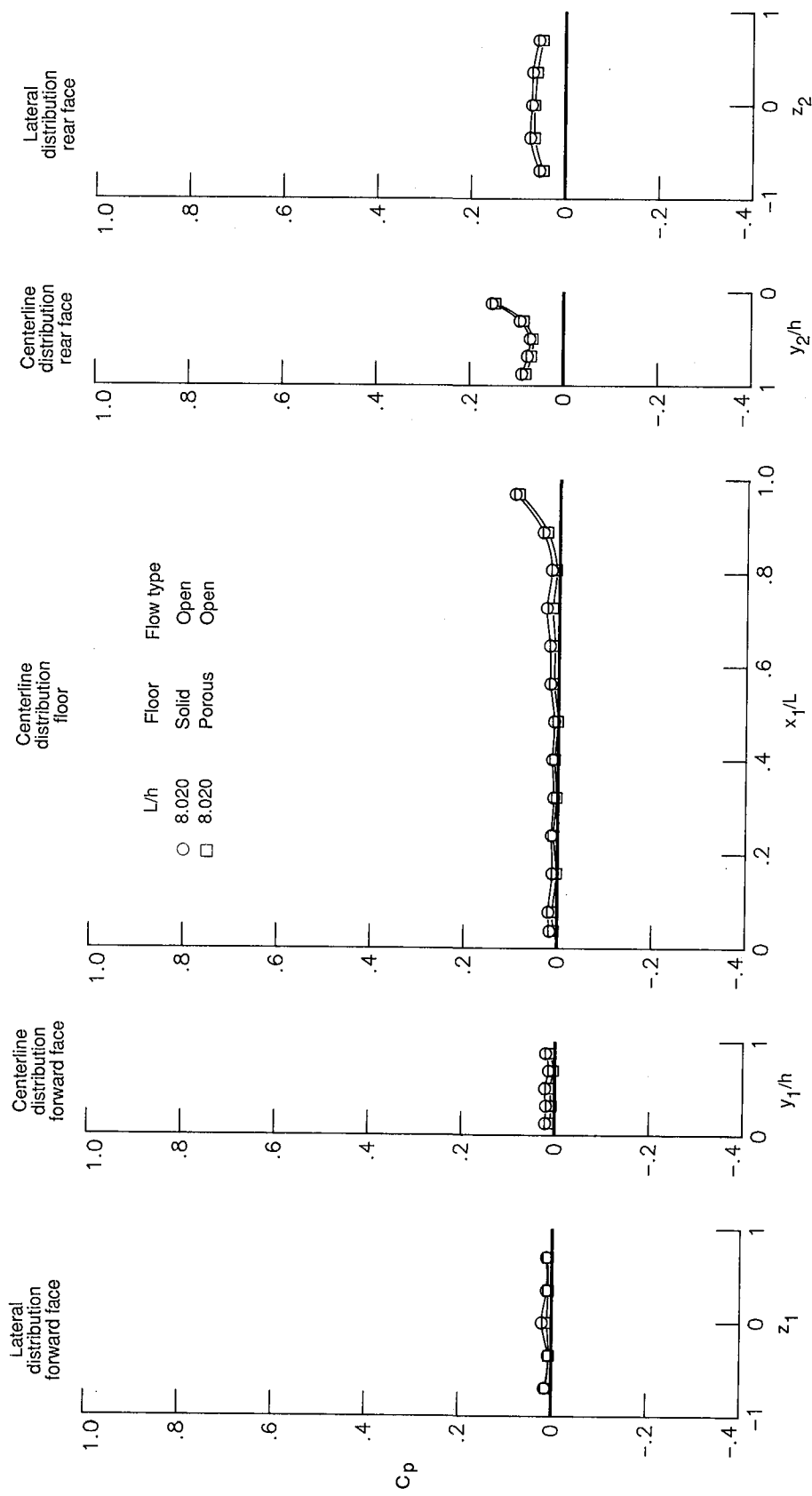
(b)  $M_\infty = 1.90$ .

Figure 33. Continued.



(c)  $M_\infty = 2.16$ .

Figure 33. Continued.



(d)  $M_\infty = 2.86$ .

Figure 33. Concluded.

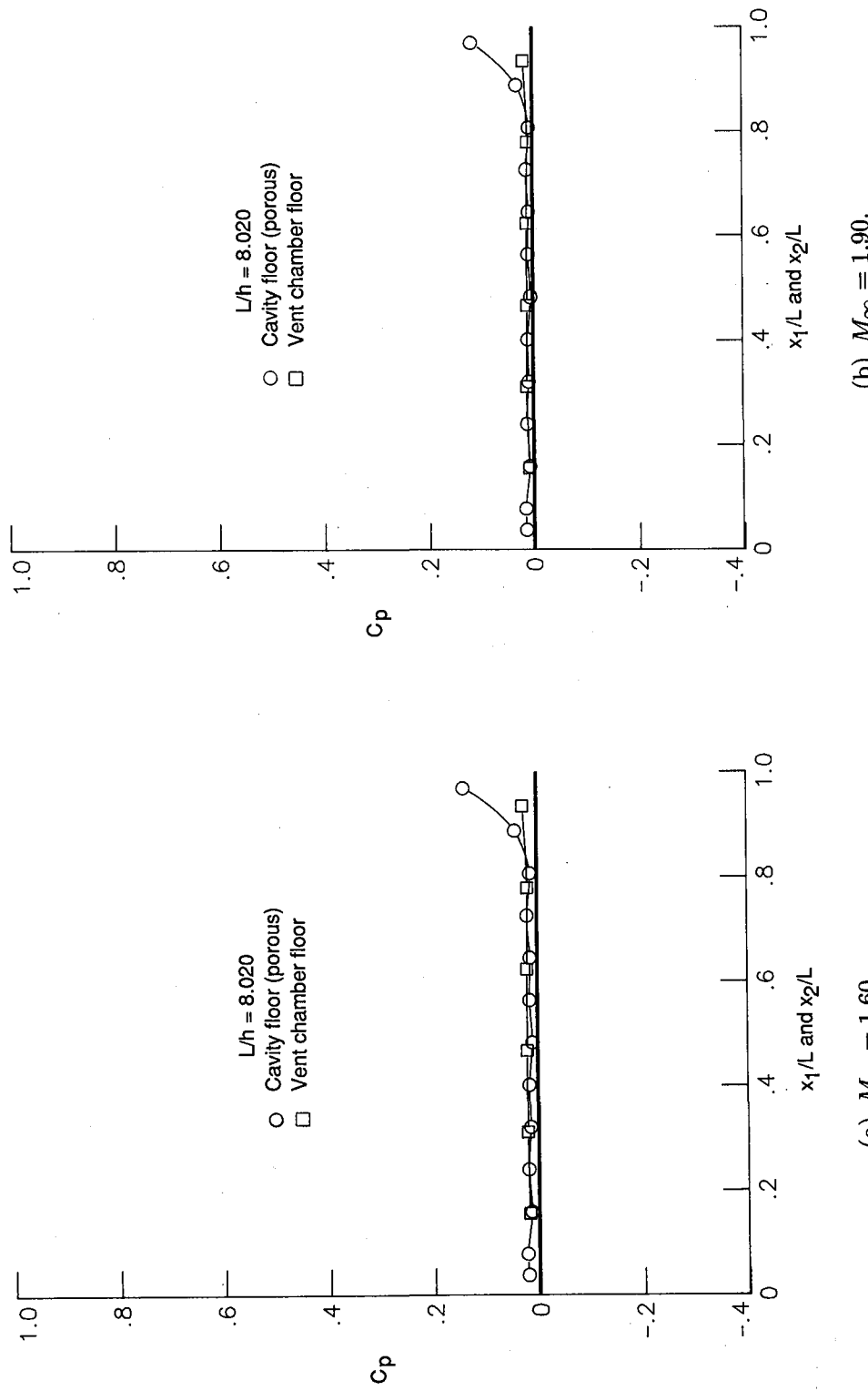


Figure 34. Comparison of cavity and vent chamber floor pressure distributions (open flow).

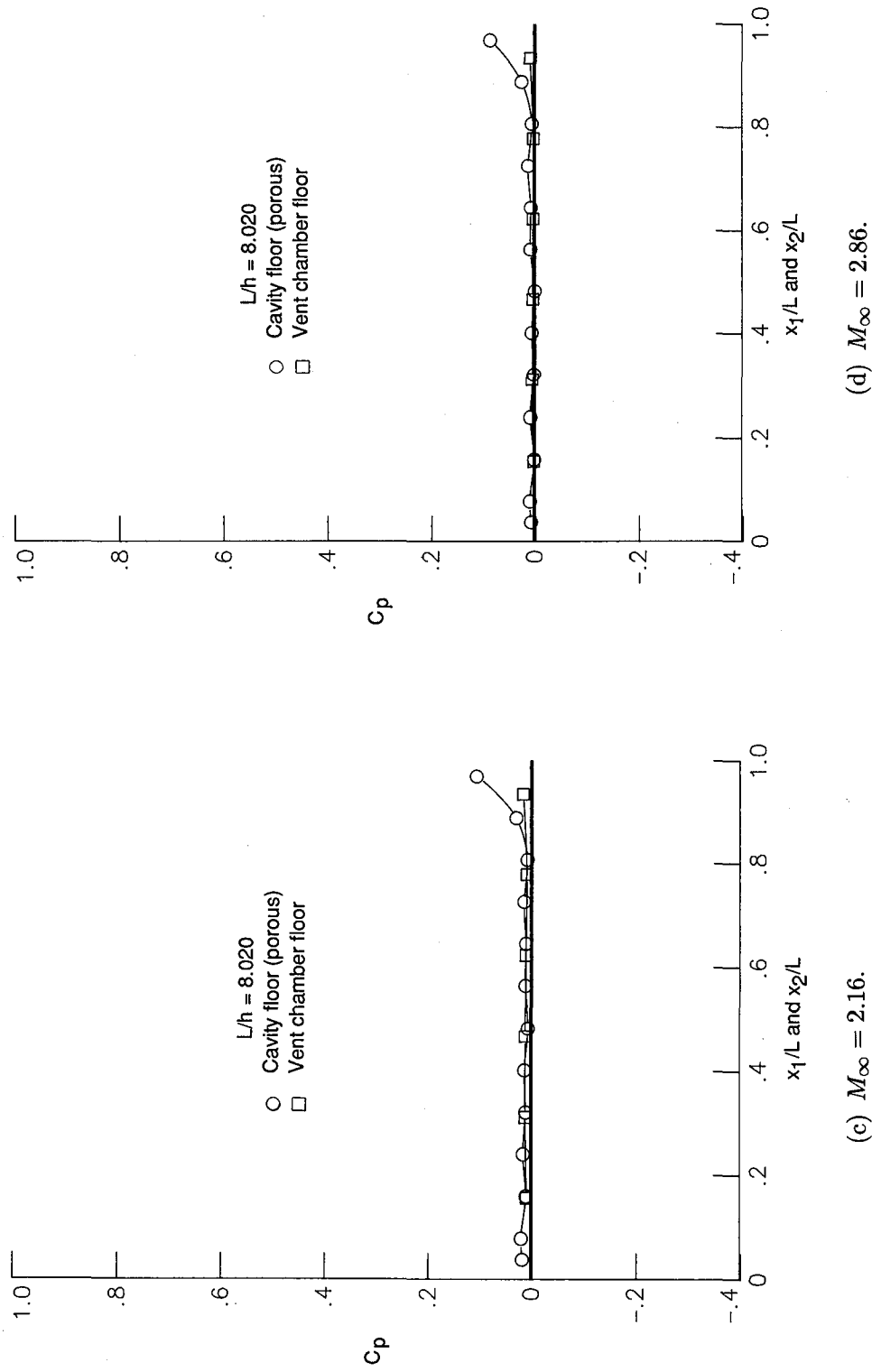
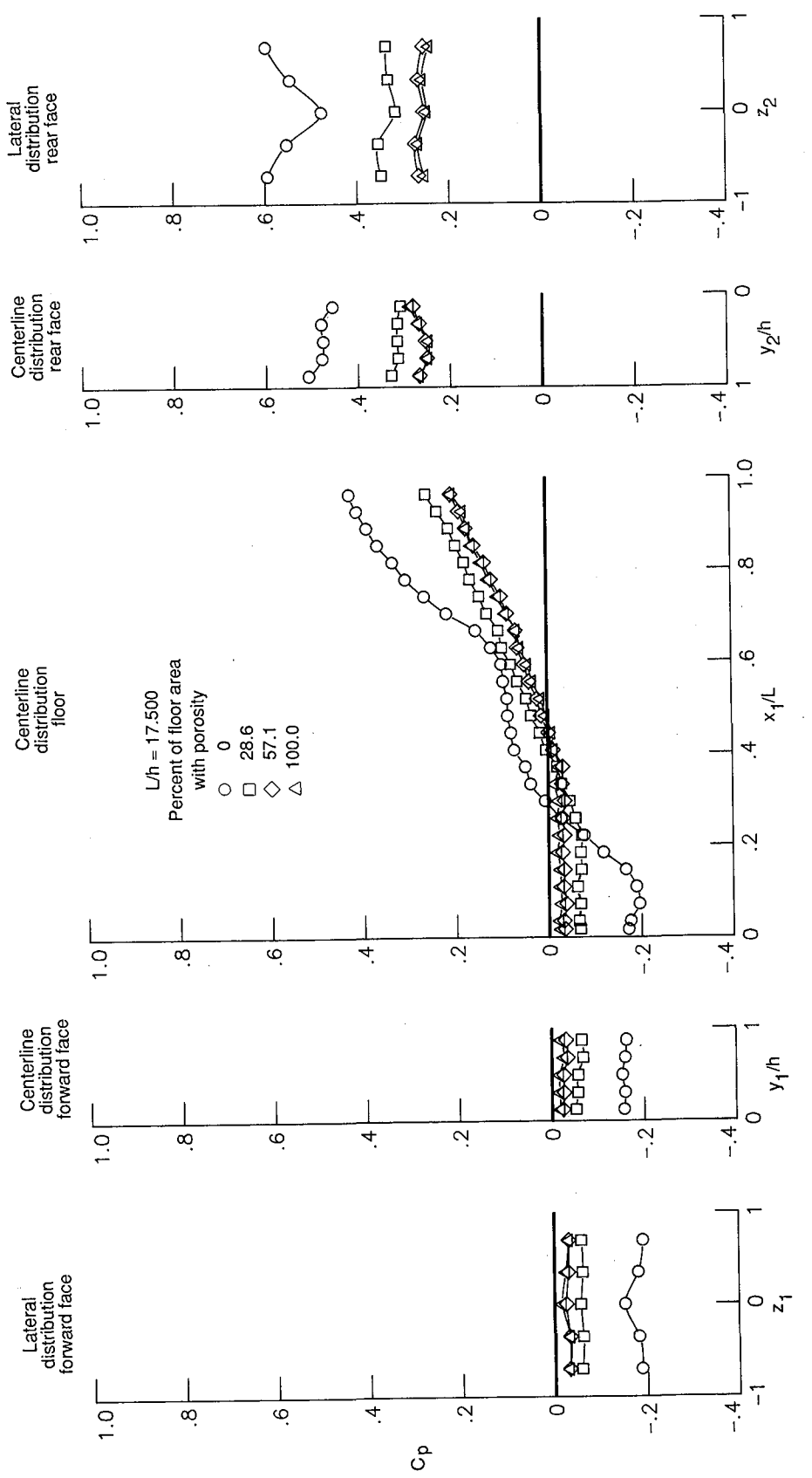
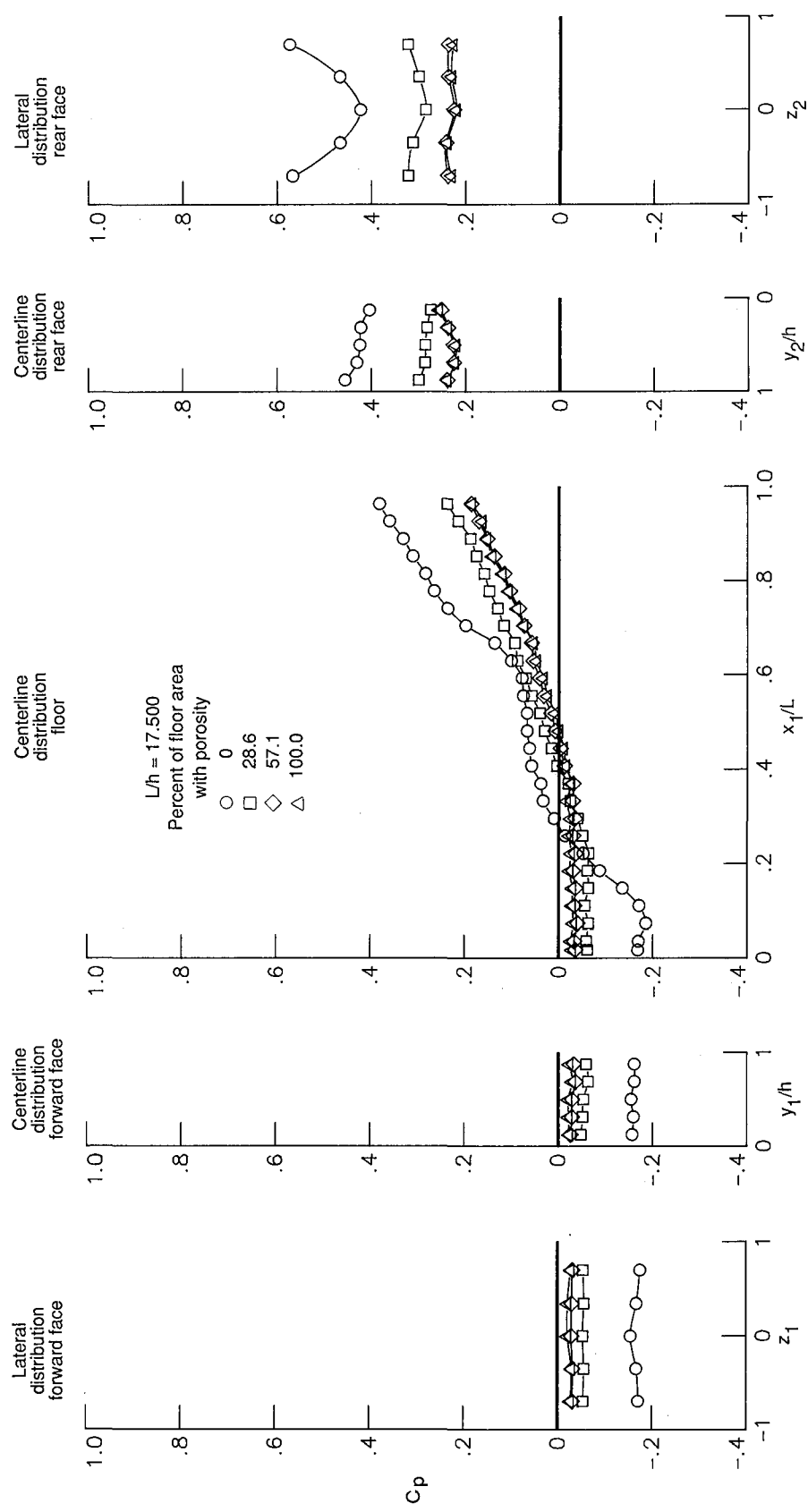


Figure 34. Concluded.



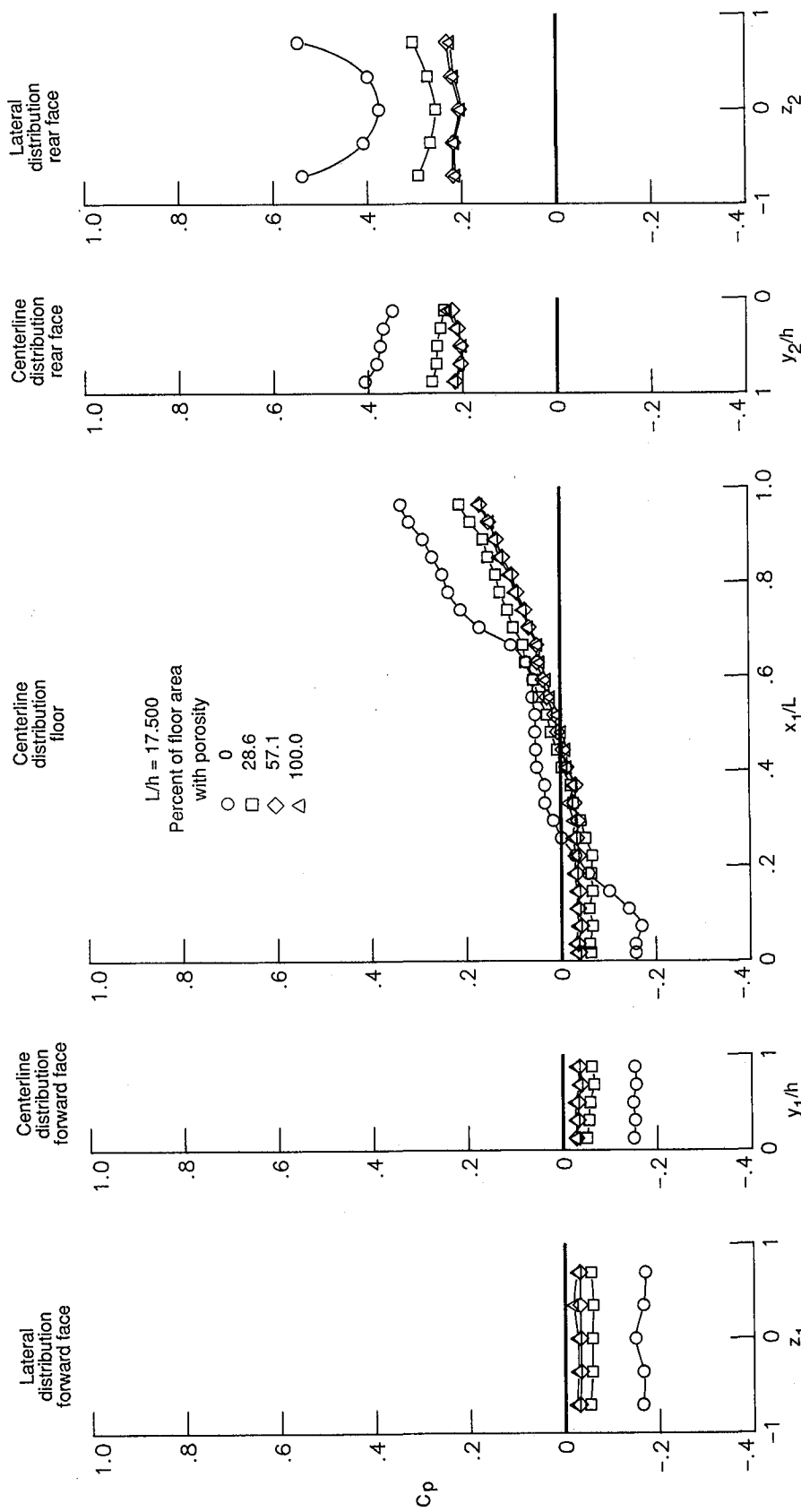
(a)  $M_\infty = 1.60$ .

Figure 35. Effect of porosity in the cavity forward and rear sections on the cavity pressure distributions.



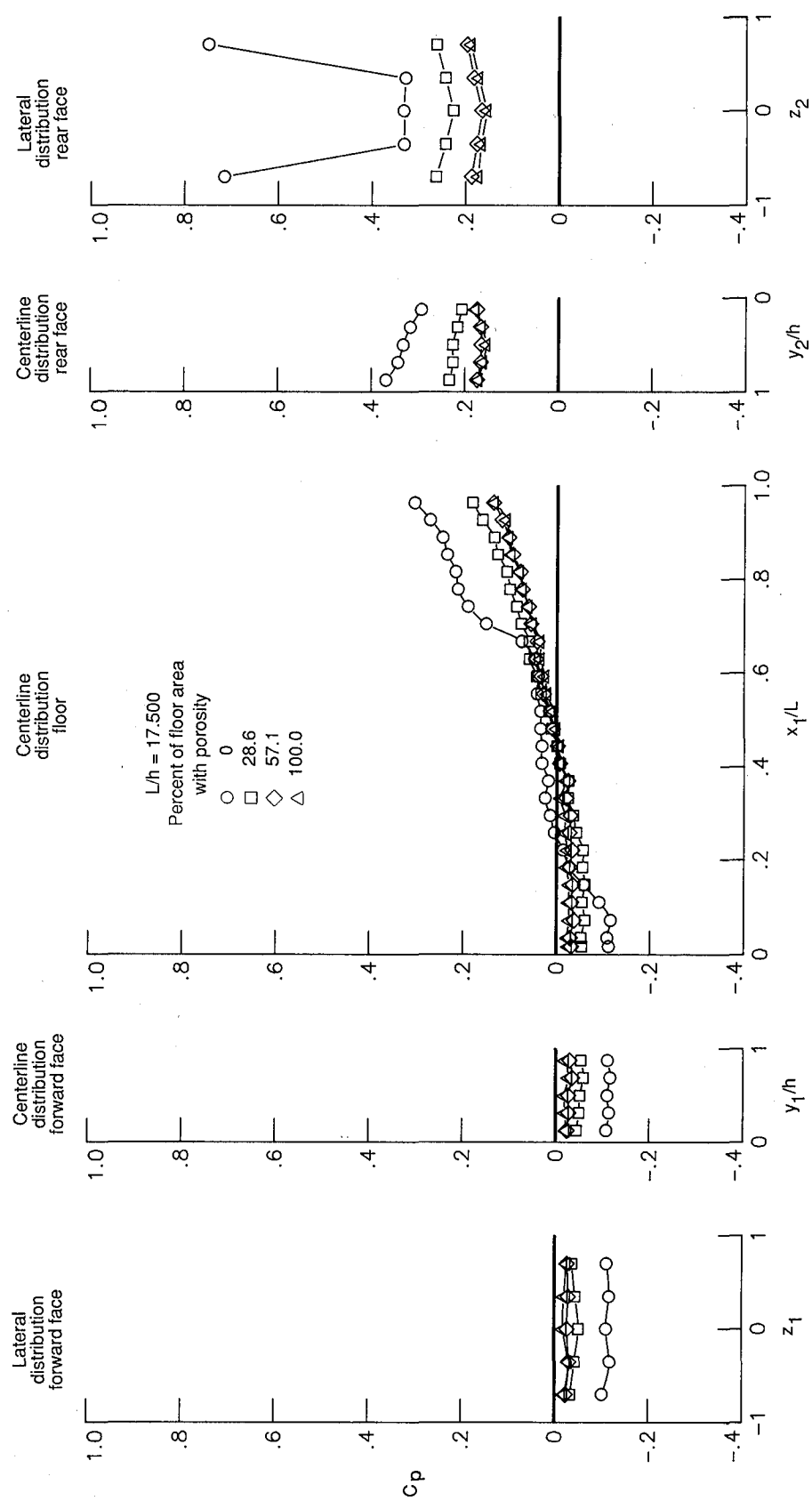
(b)  $M_\infty = 1.90$ .

Figure 35. Continued.



(c)  $M_\infty = 2.16$ .

Figure 35. Continued.



(d)  $M_\infty = 2.86$ .

Figure 35. Concluded.

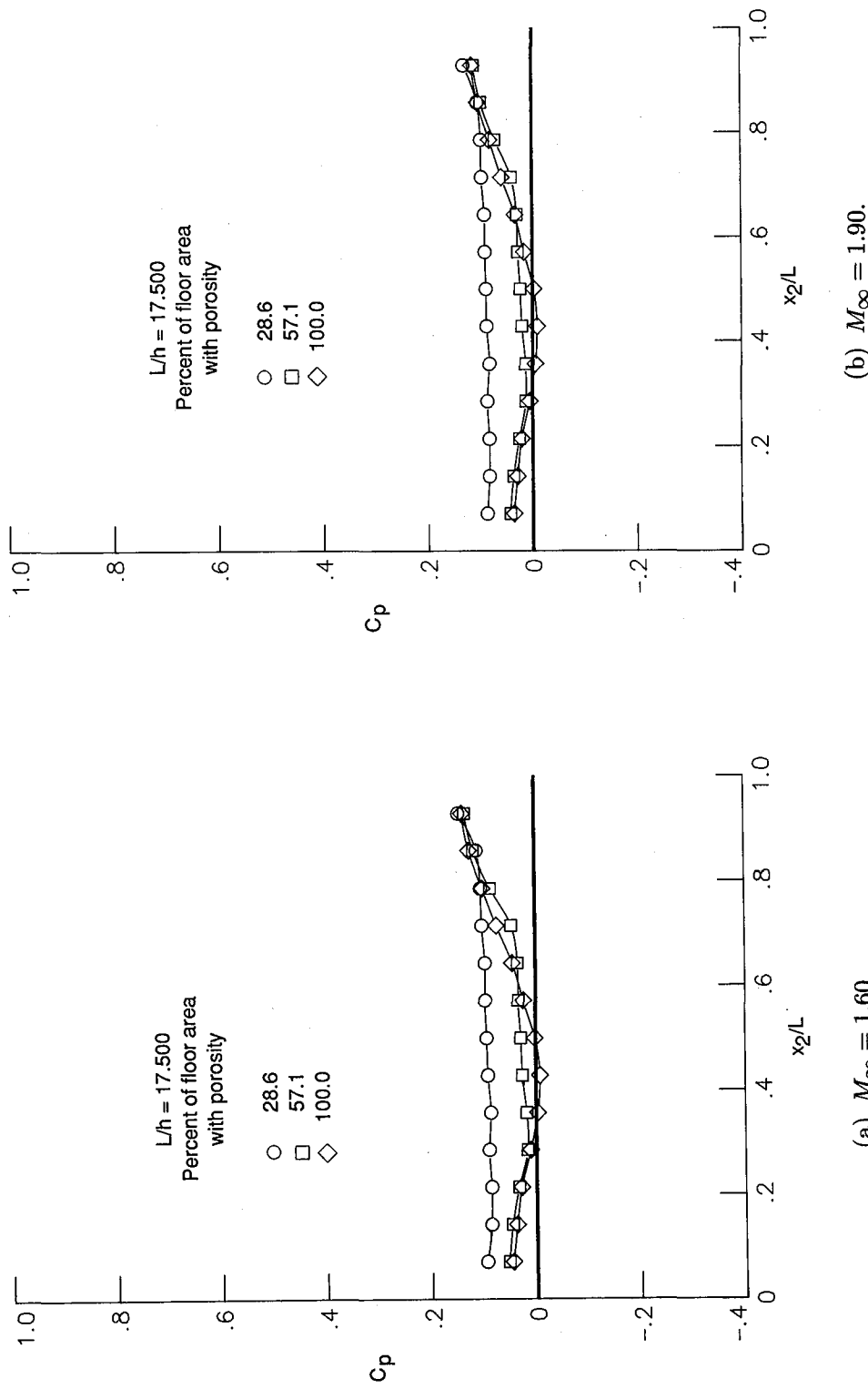


Figure 36. Effect of porosity in the cavity forward and rear sections on the vent chamber pressure distributions.

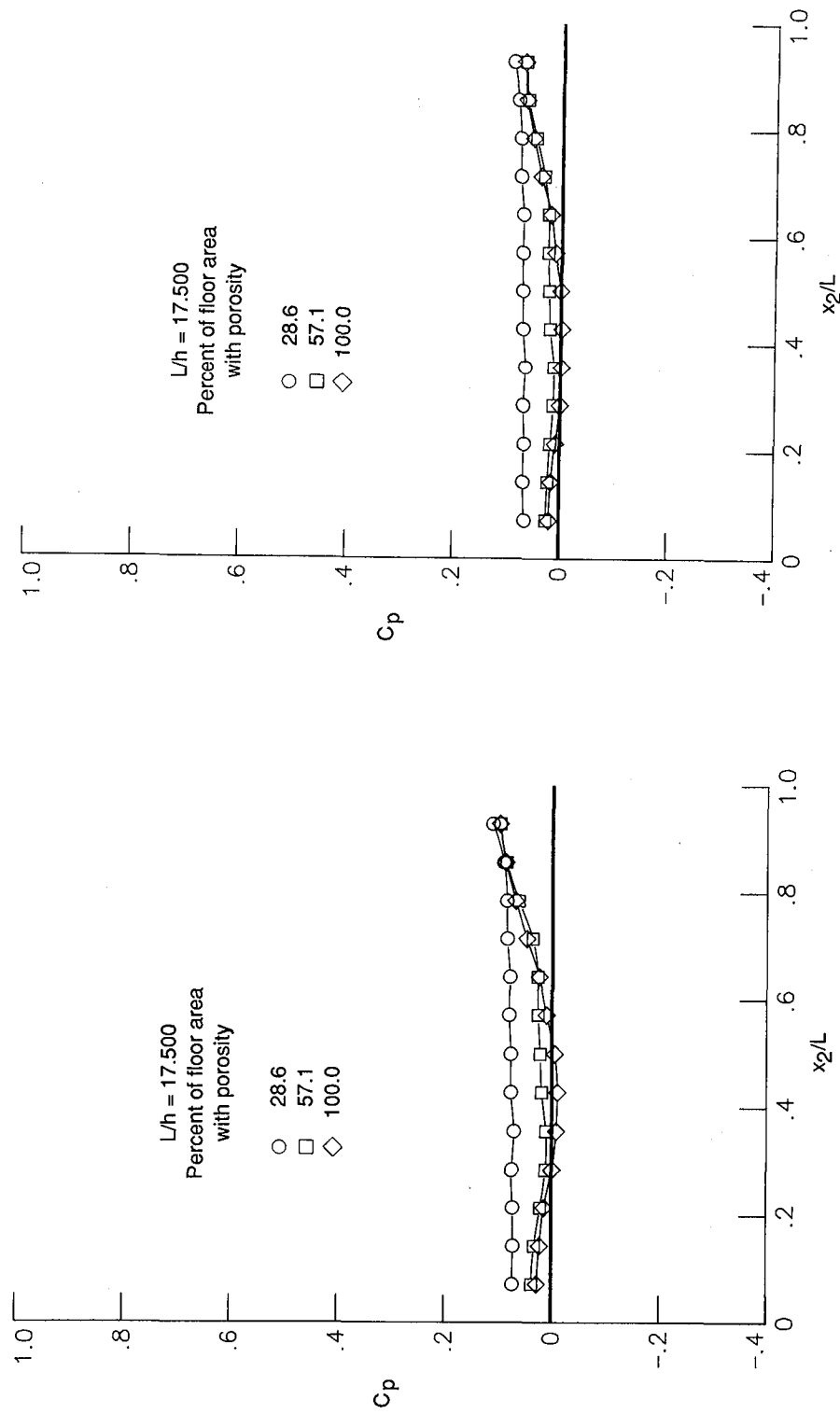
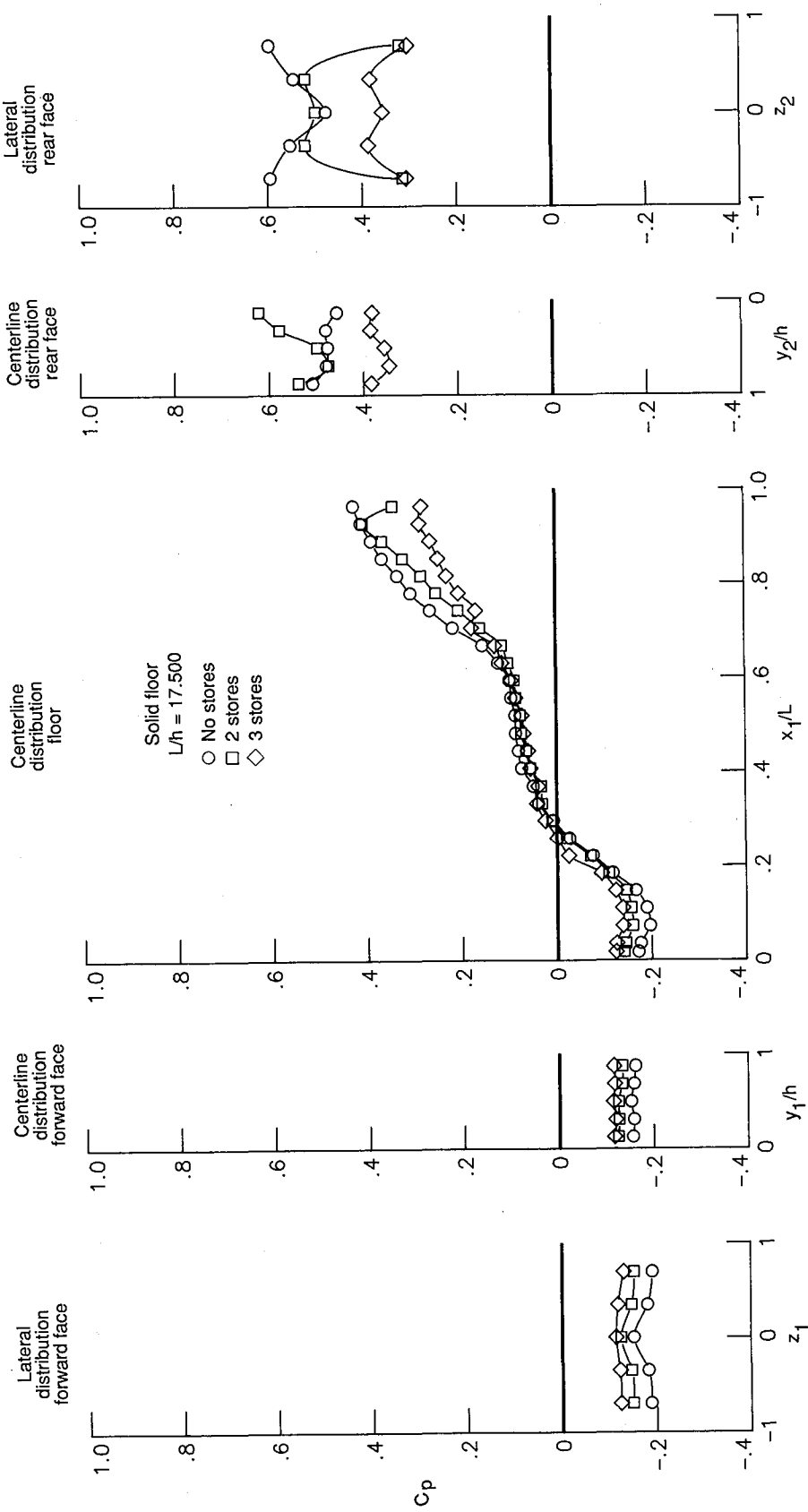
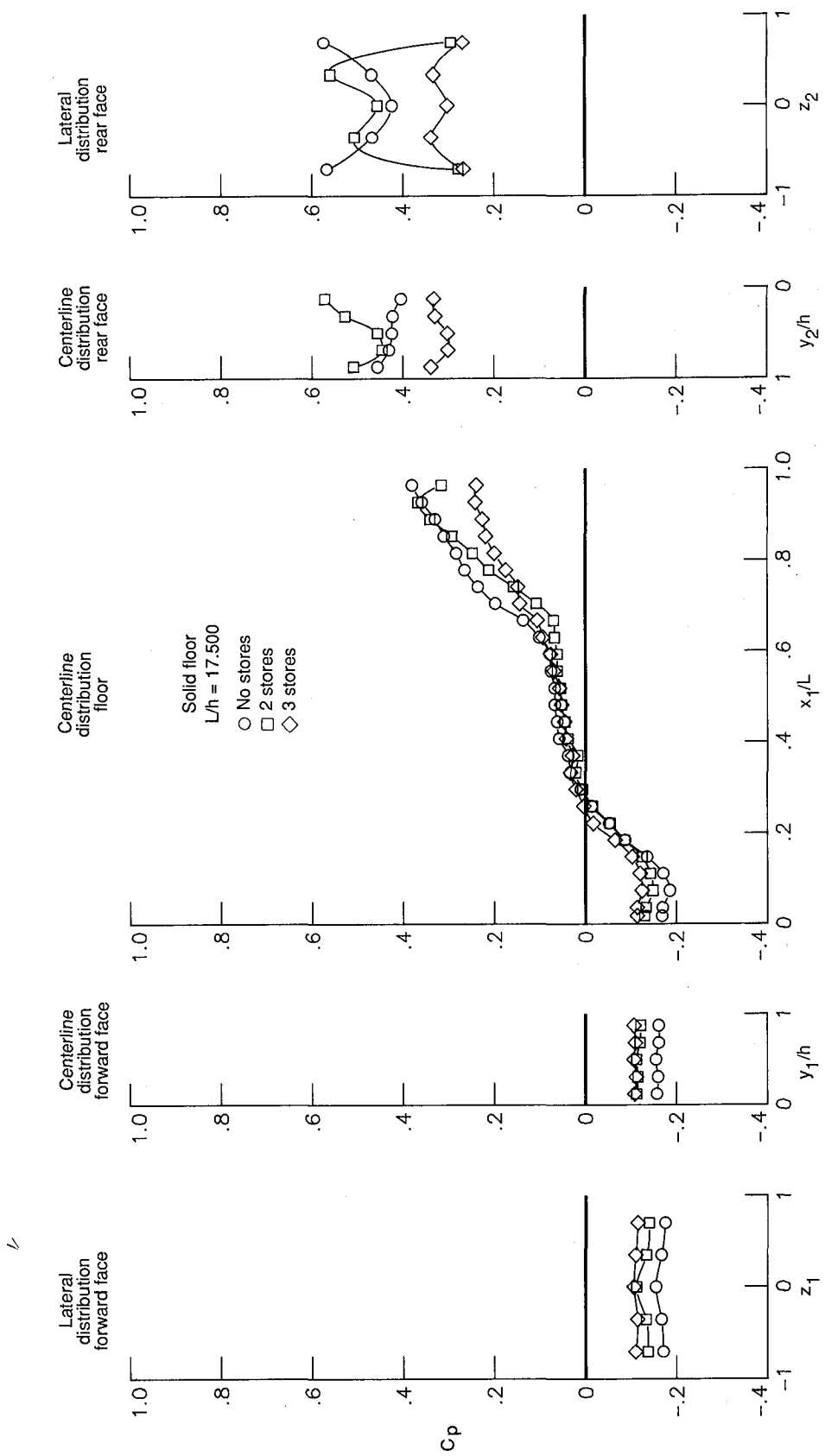


Figure 36. Concluded.



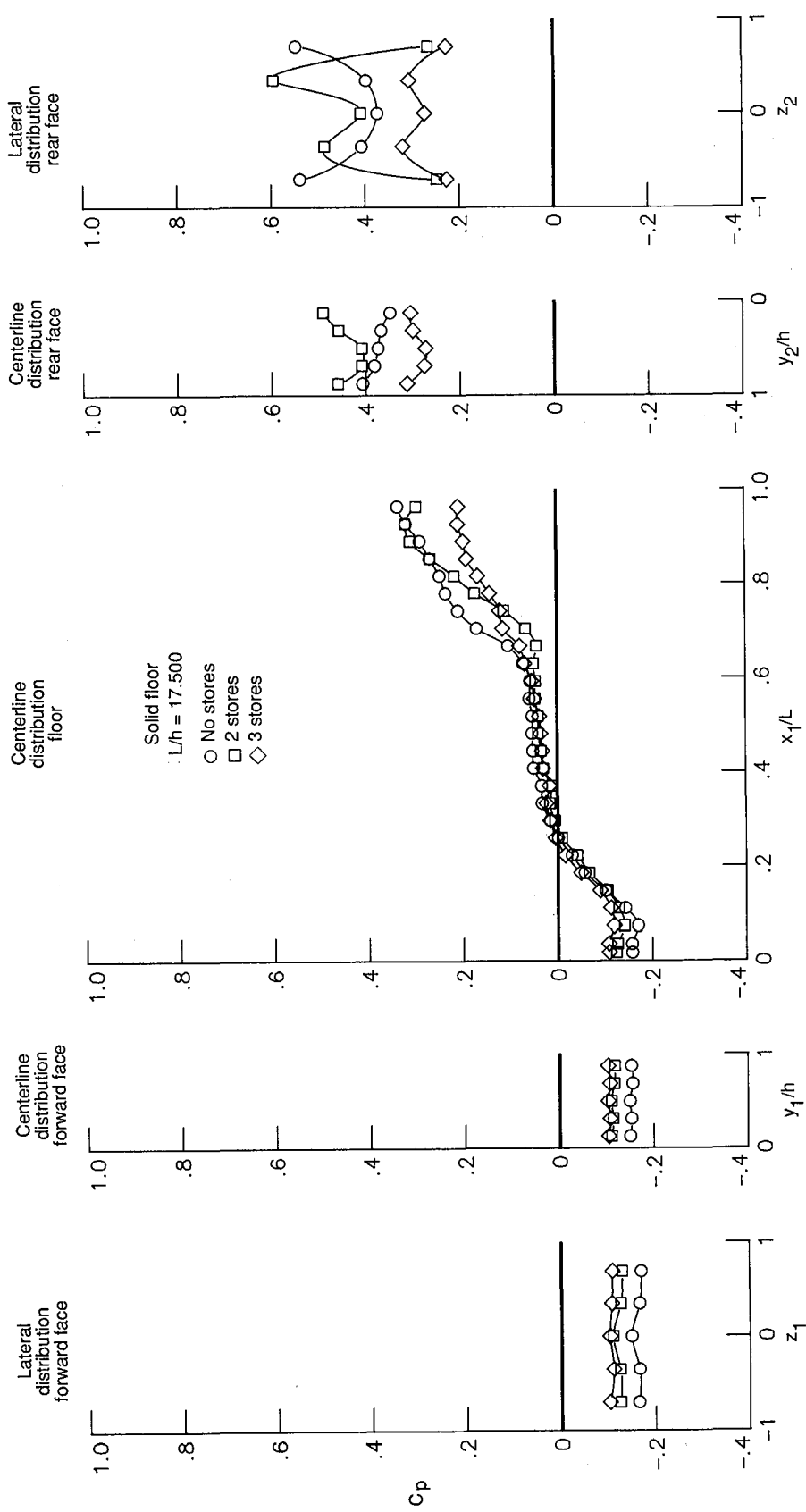
(a)  $M_\infty = 1.60$ .

Figure 37. Effect of stores on the solid-floor cavity pressure distributions.



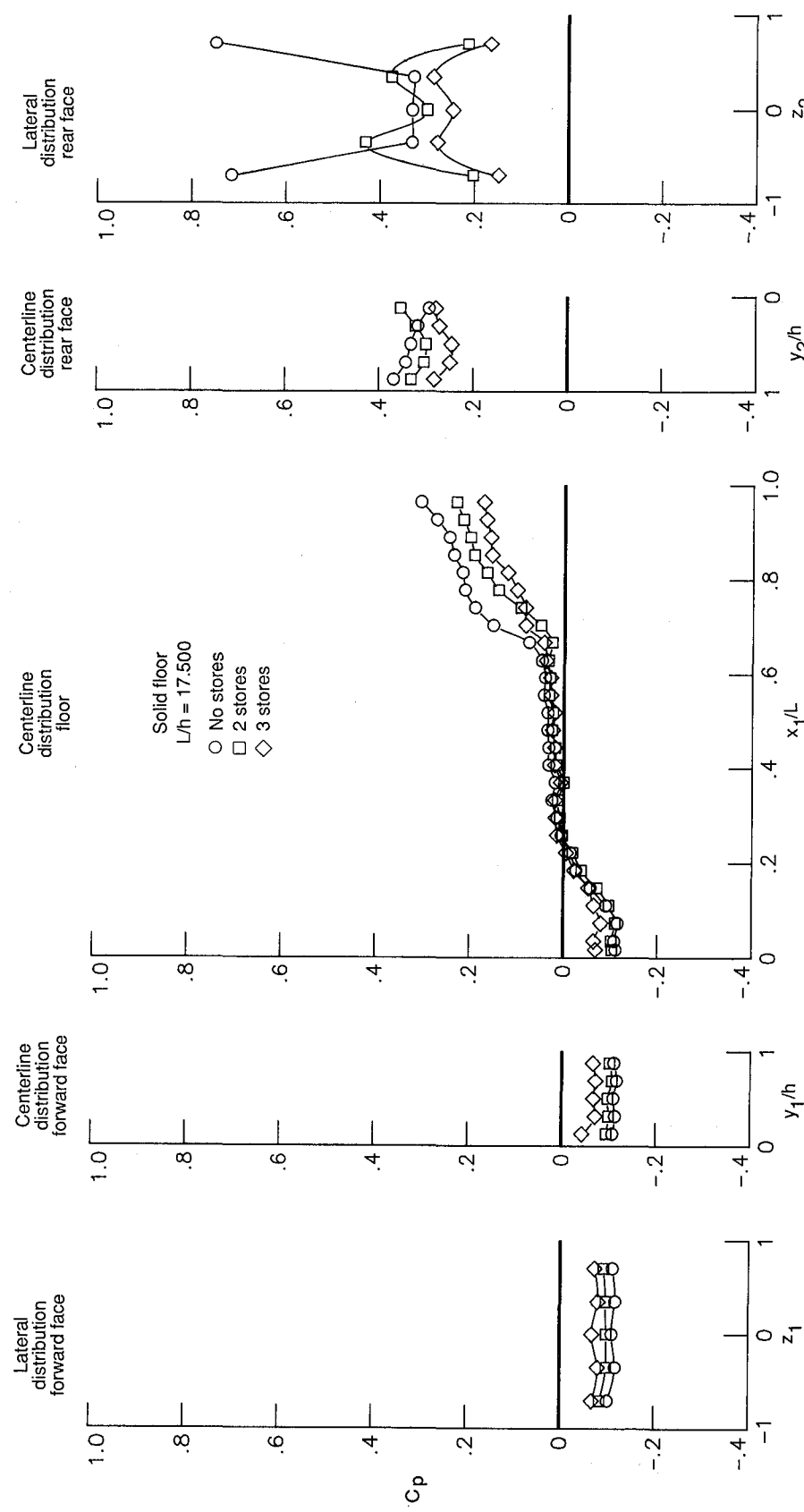
(b)  $M_\infty = 1.90$ .

Figure 37. Continued.



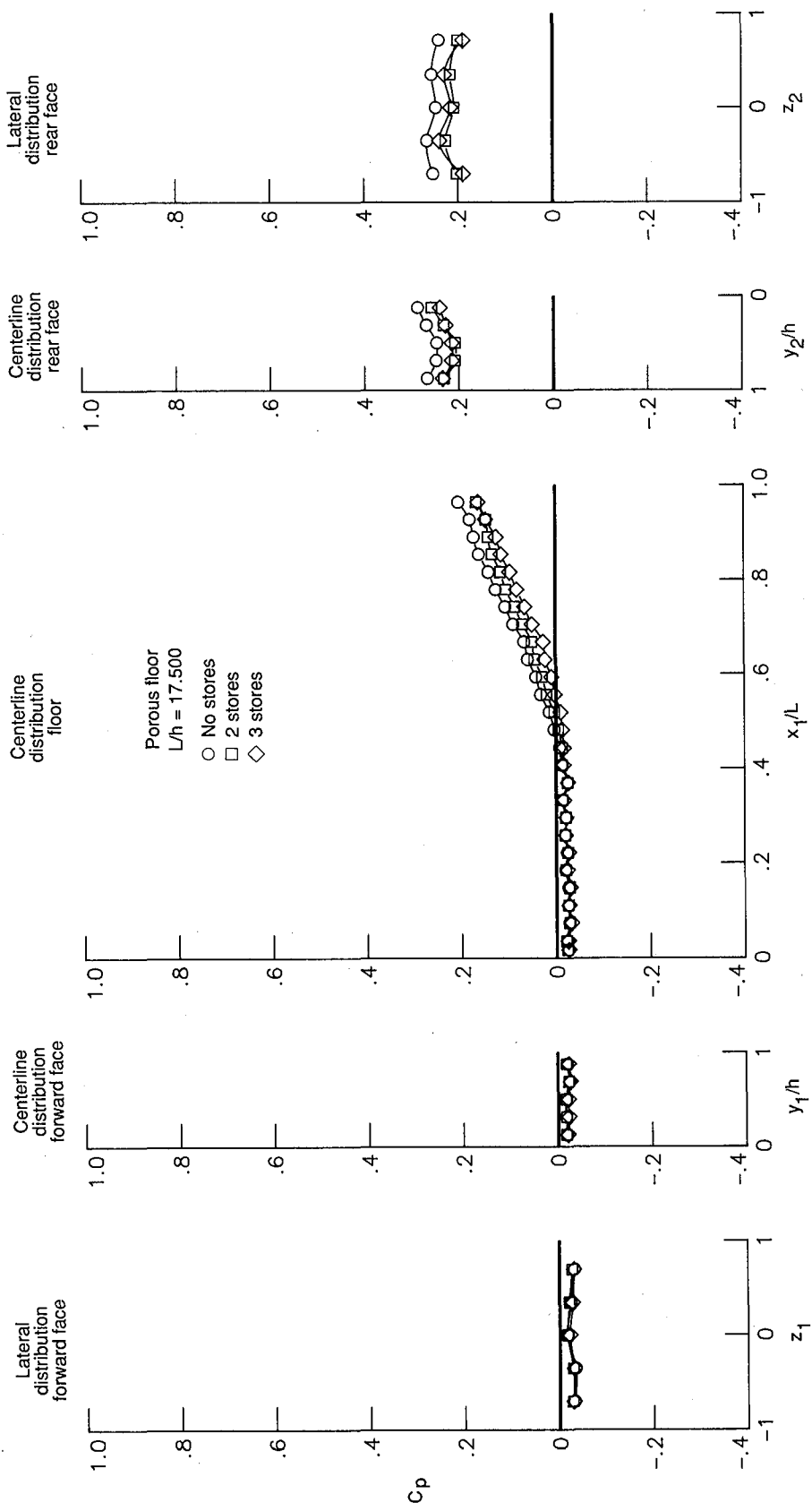
(c)  $M_\infty = 2.16$ .

Figure 37. Continued.



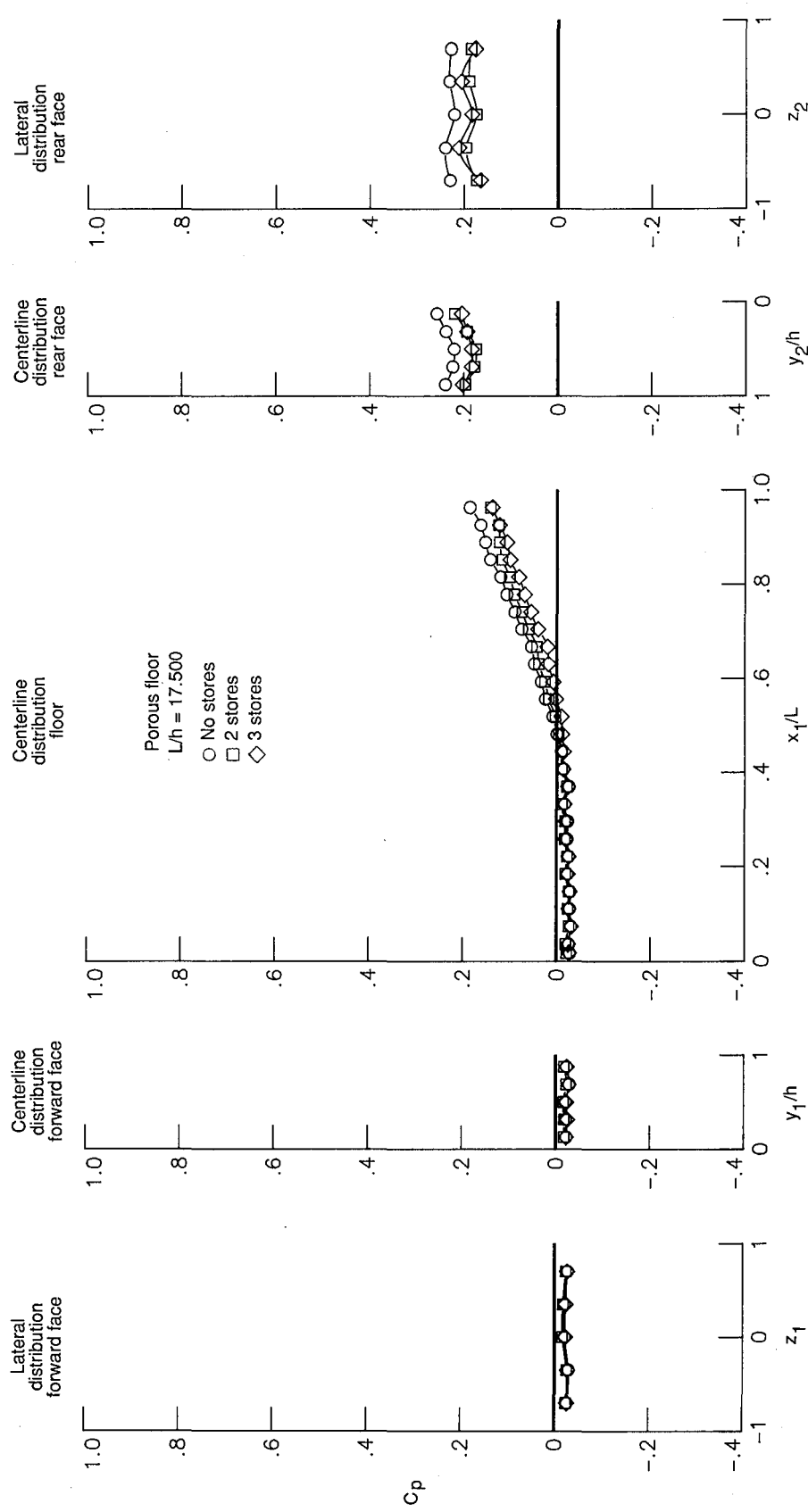
(d)  $M_\infty = 2.86$ .

Figure 37. Concluded.



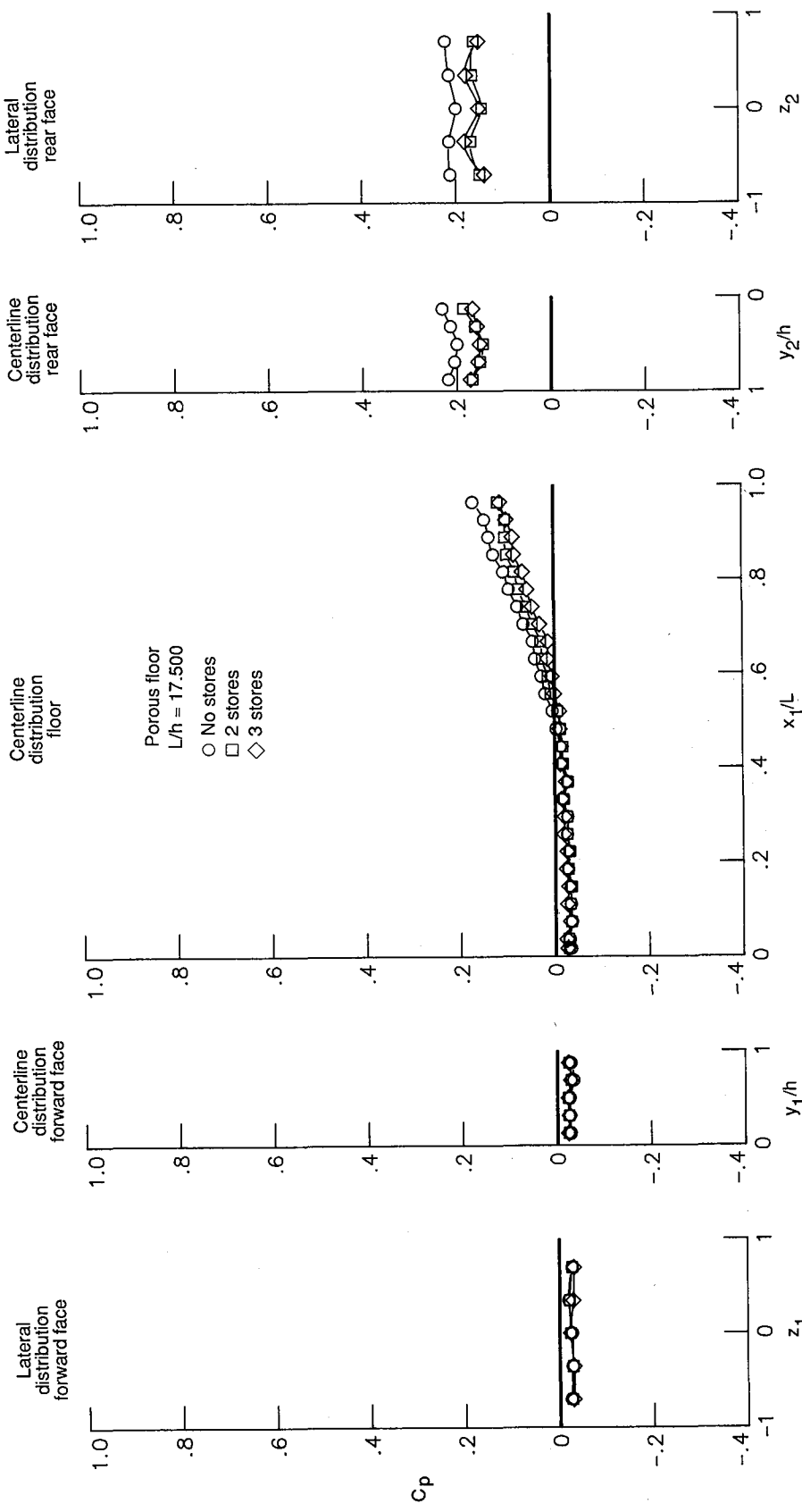
(a)  $M_\infty = 1.60$ .

Figure 38. Effect of stores on the porous-floor cavity pressure distributions.



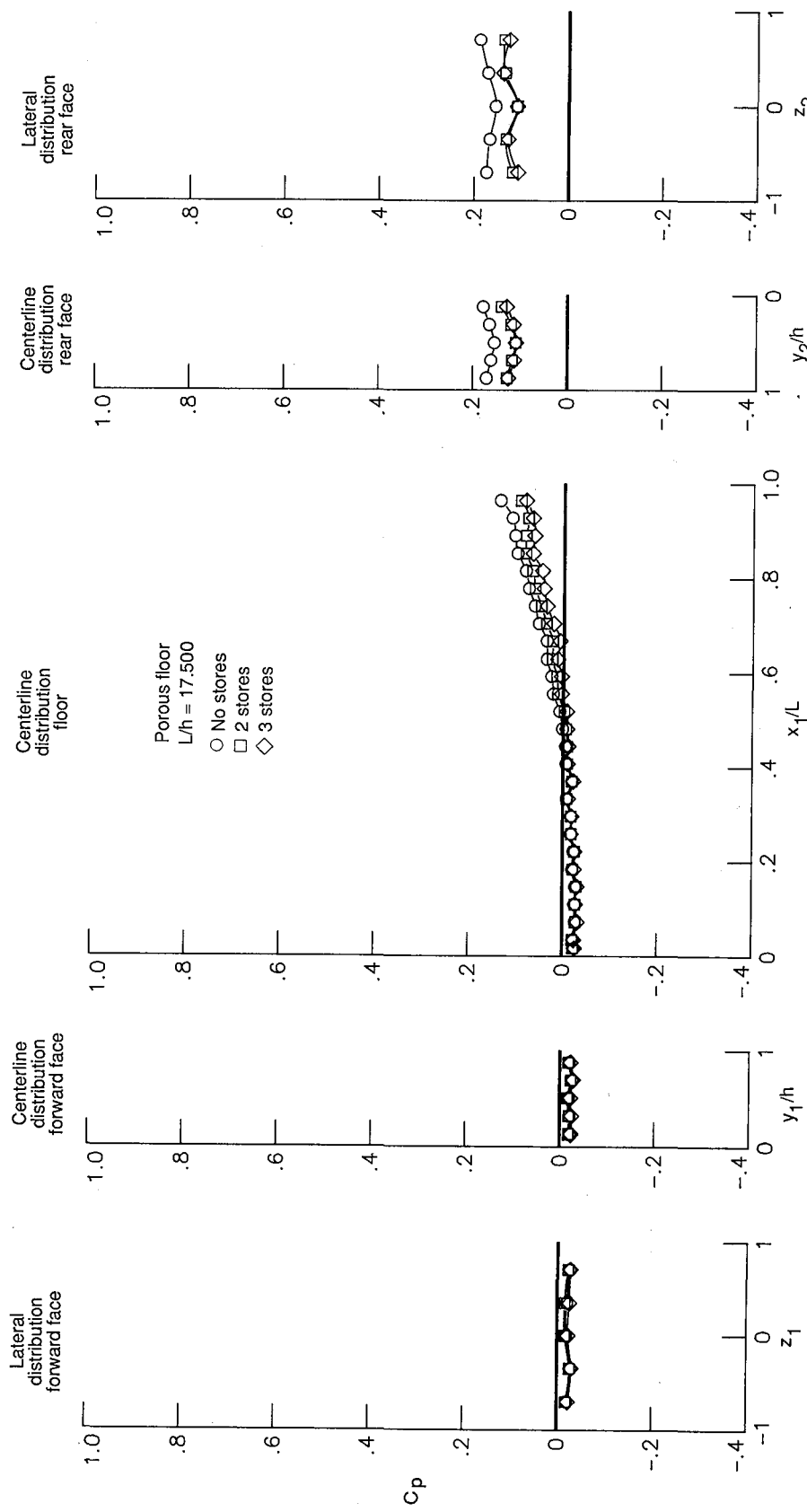
(b)  $M_\infty = 1.90$ .

Figure 38. Continued.



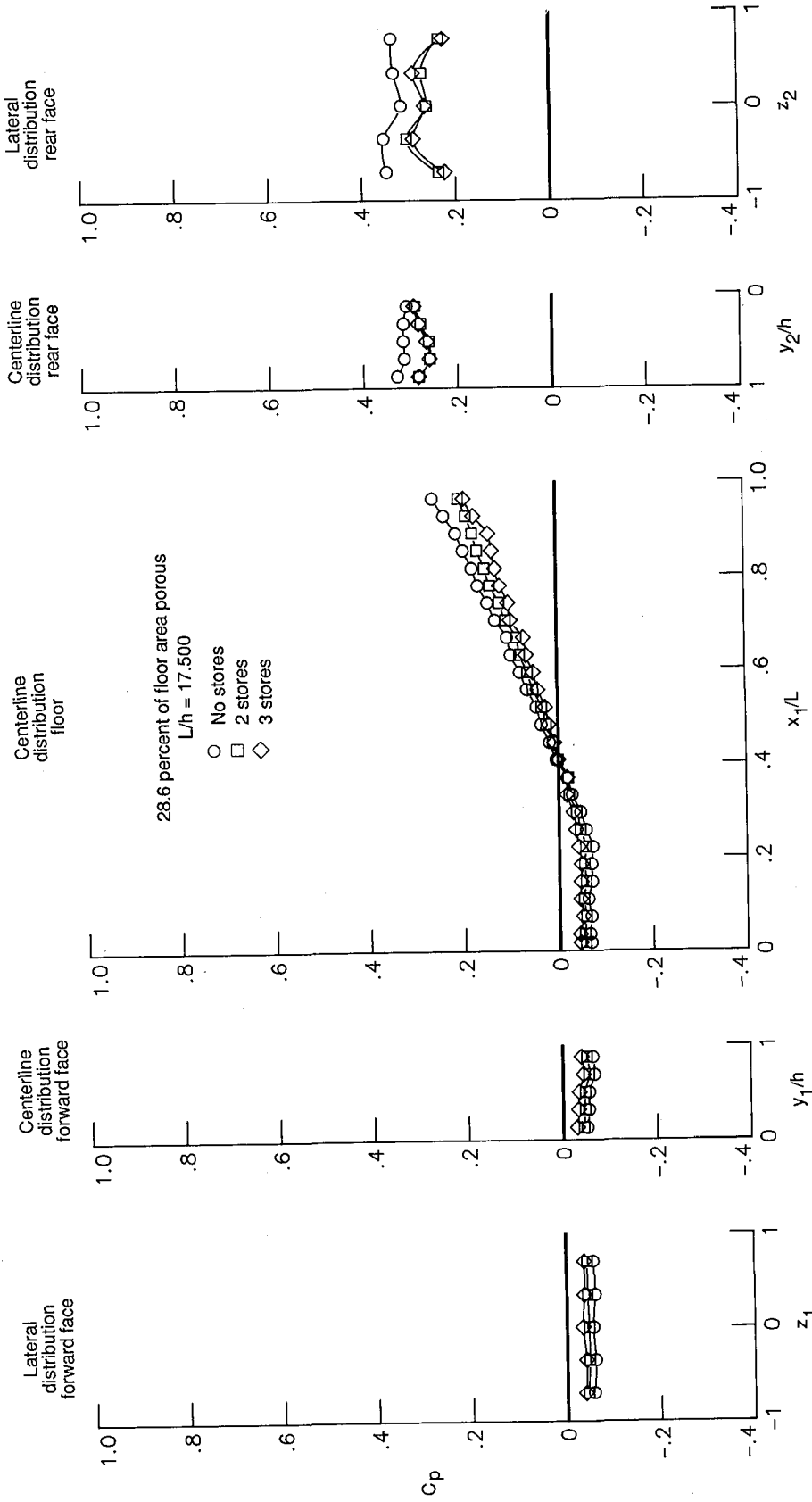
(c)  $M_\infty = 2.16$ .

Figure 38. Continued.



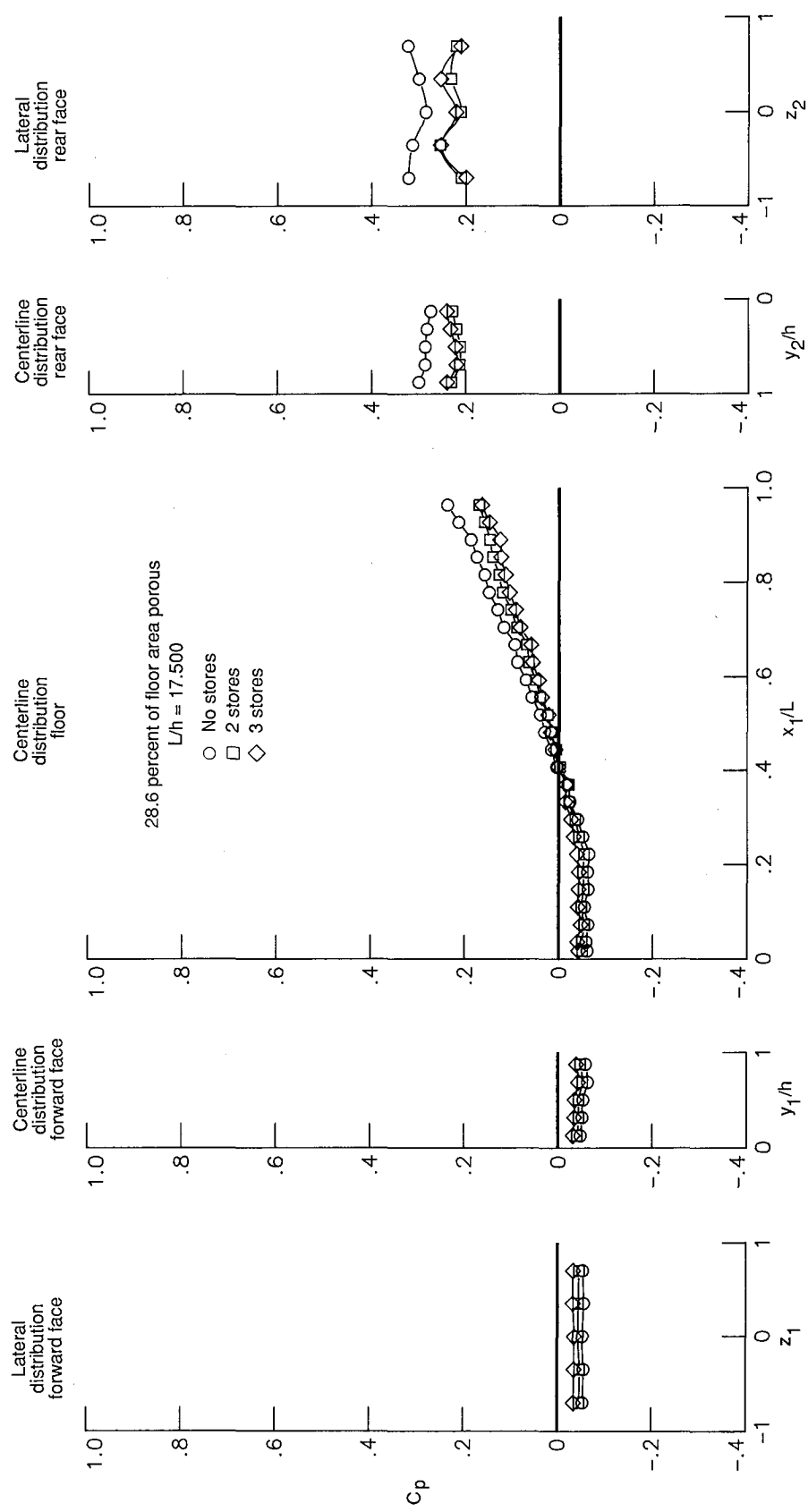
(d)  $M_\infty = 2.86$ .

Figure 38. Concluded.



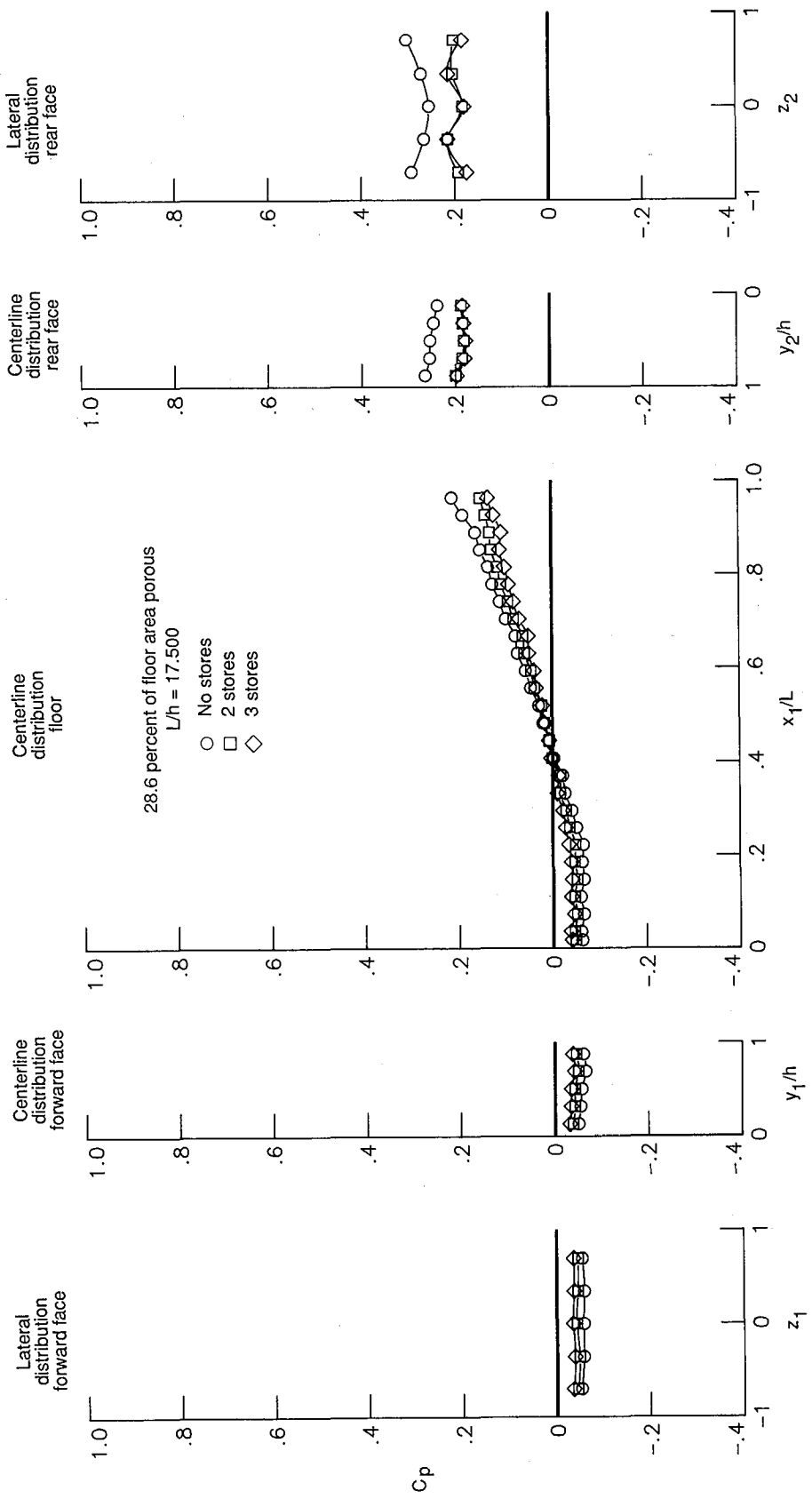
(a)  $M_\infty = 1.60$ .

Figure 39. Effect of stores on the partial-porous-floor (28.6 percent of floor area porous) cavity pressure distributions.



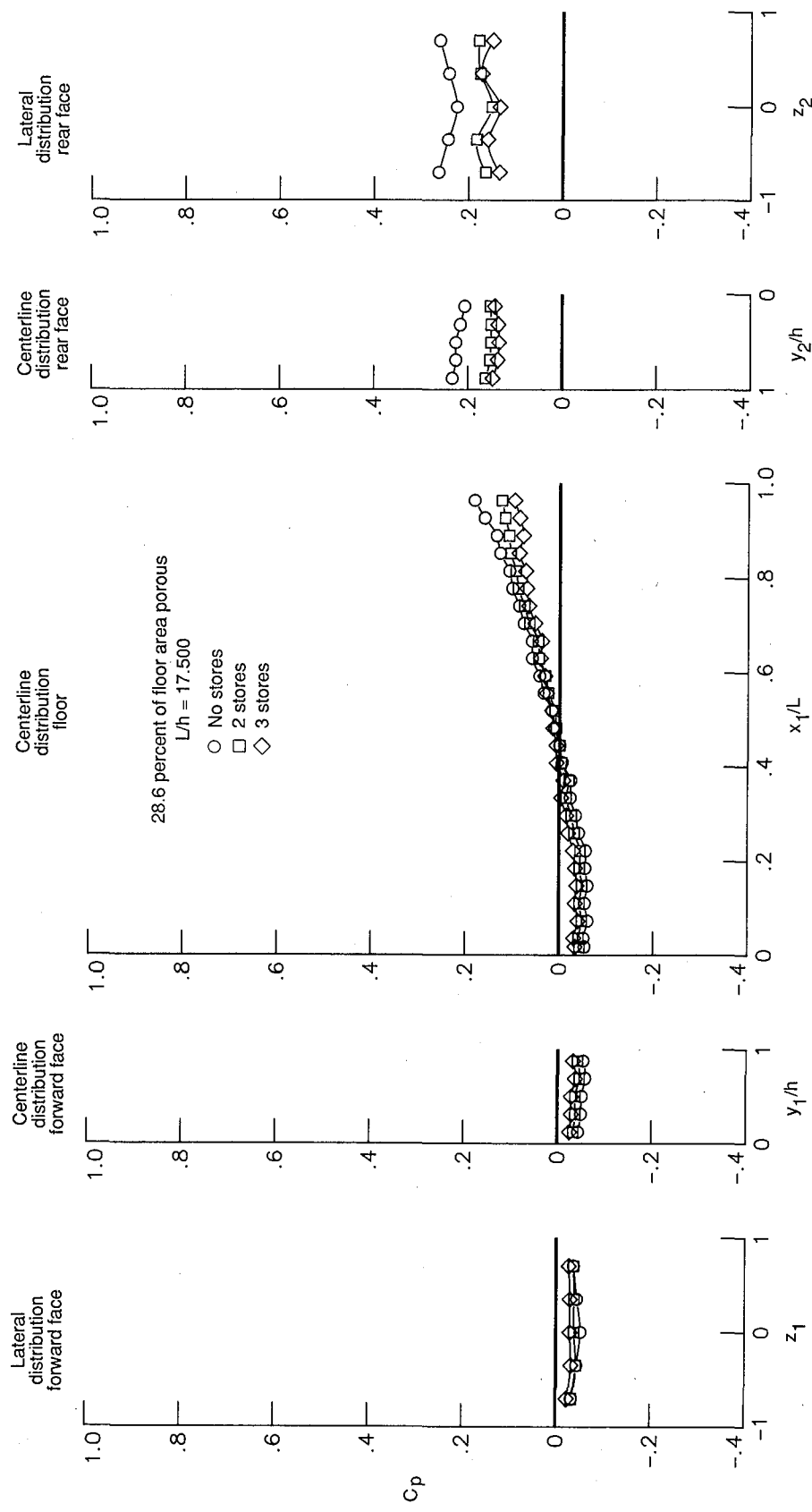
(b)  $M_\infty = 1.90$ .

Figure 39. Continued.



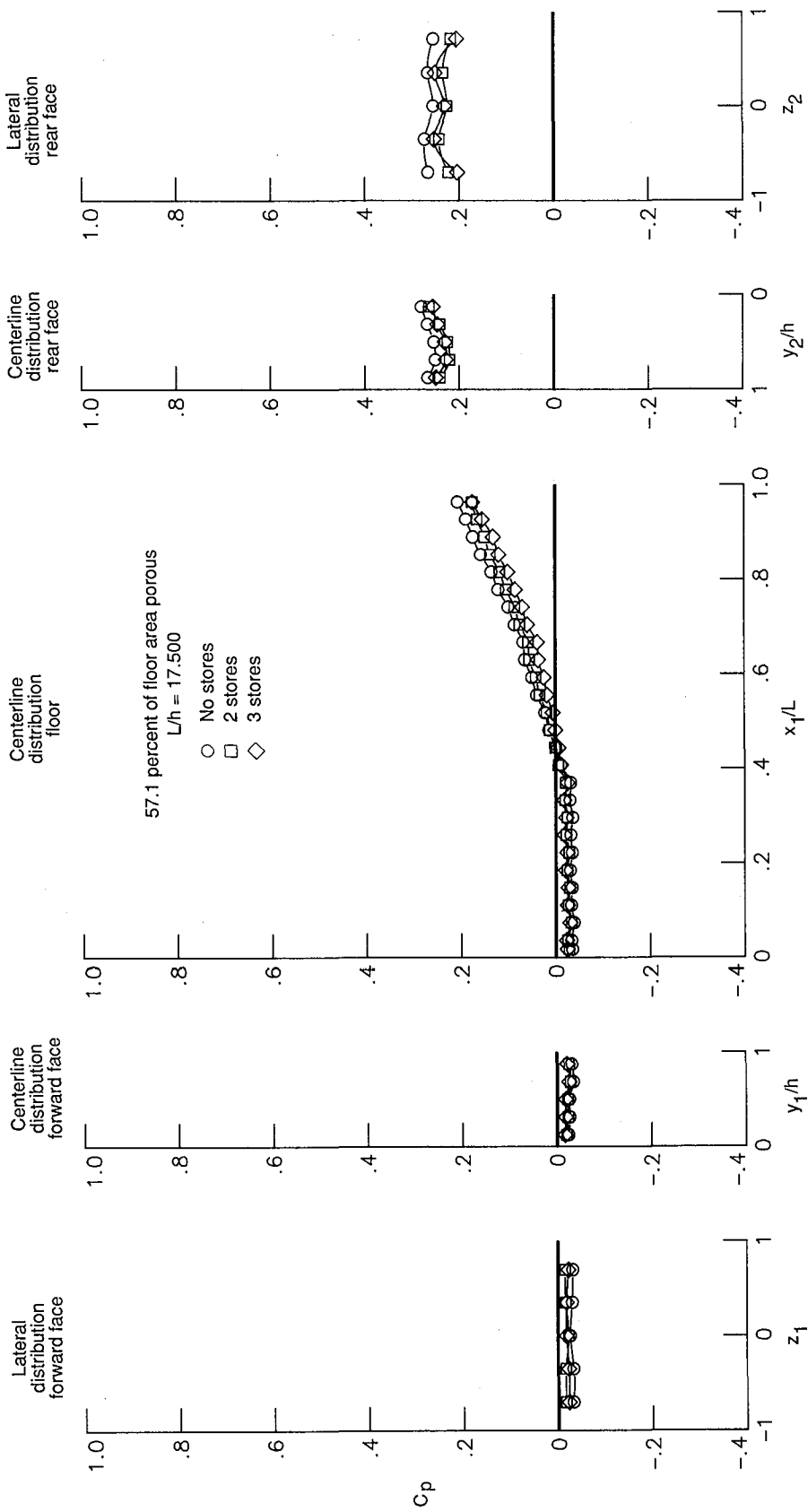
(c)  $M_\infty = 2.16$ .

Figure 39. Continued.



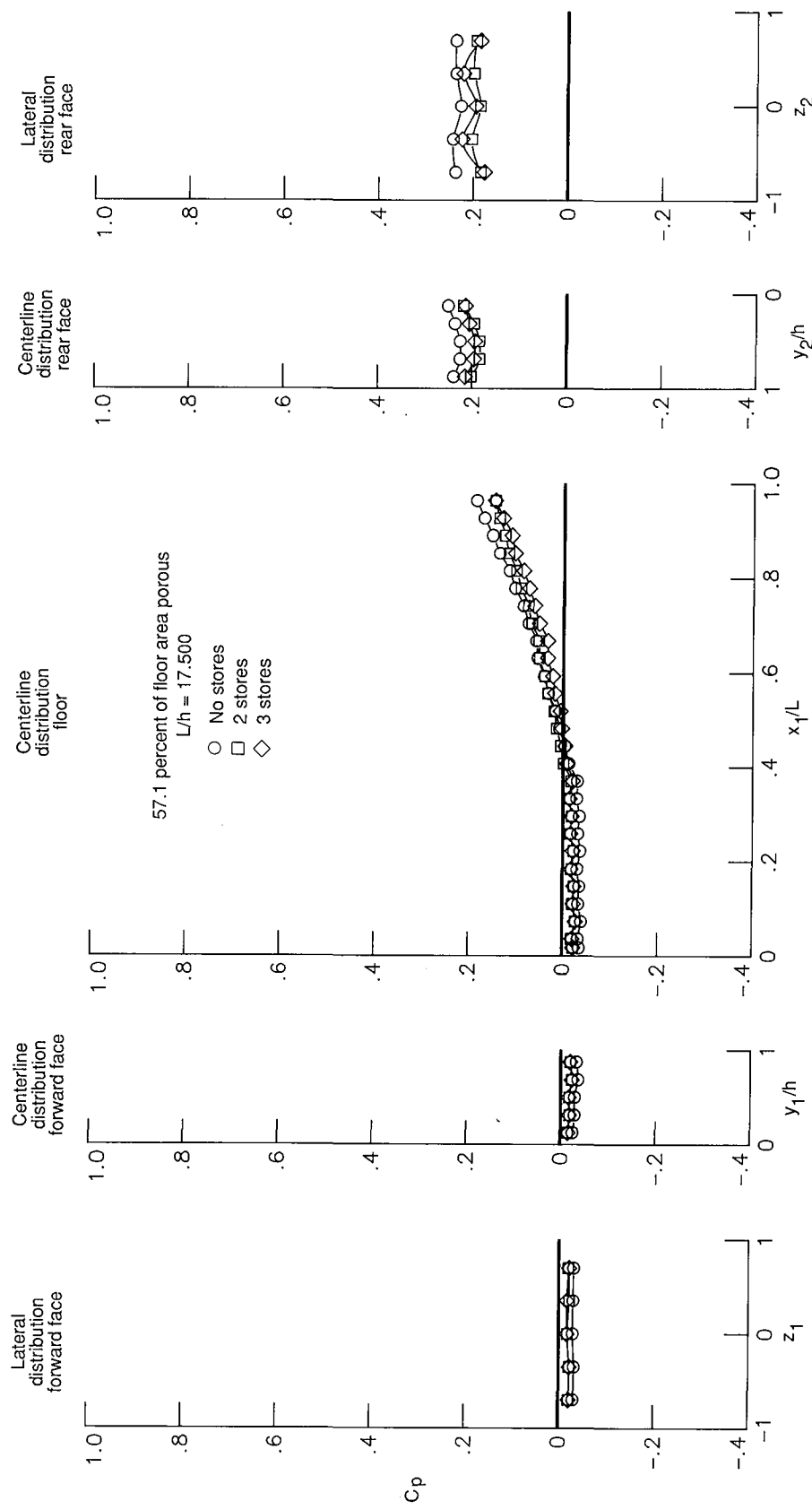
(d)  $M_\infty = 2.86$ .

Figure 39. Concluded.



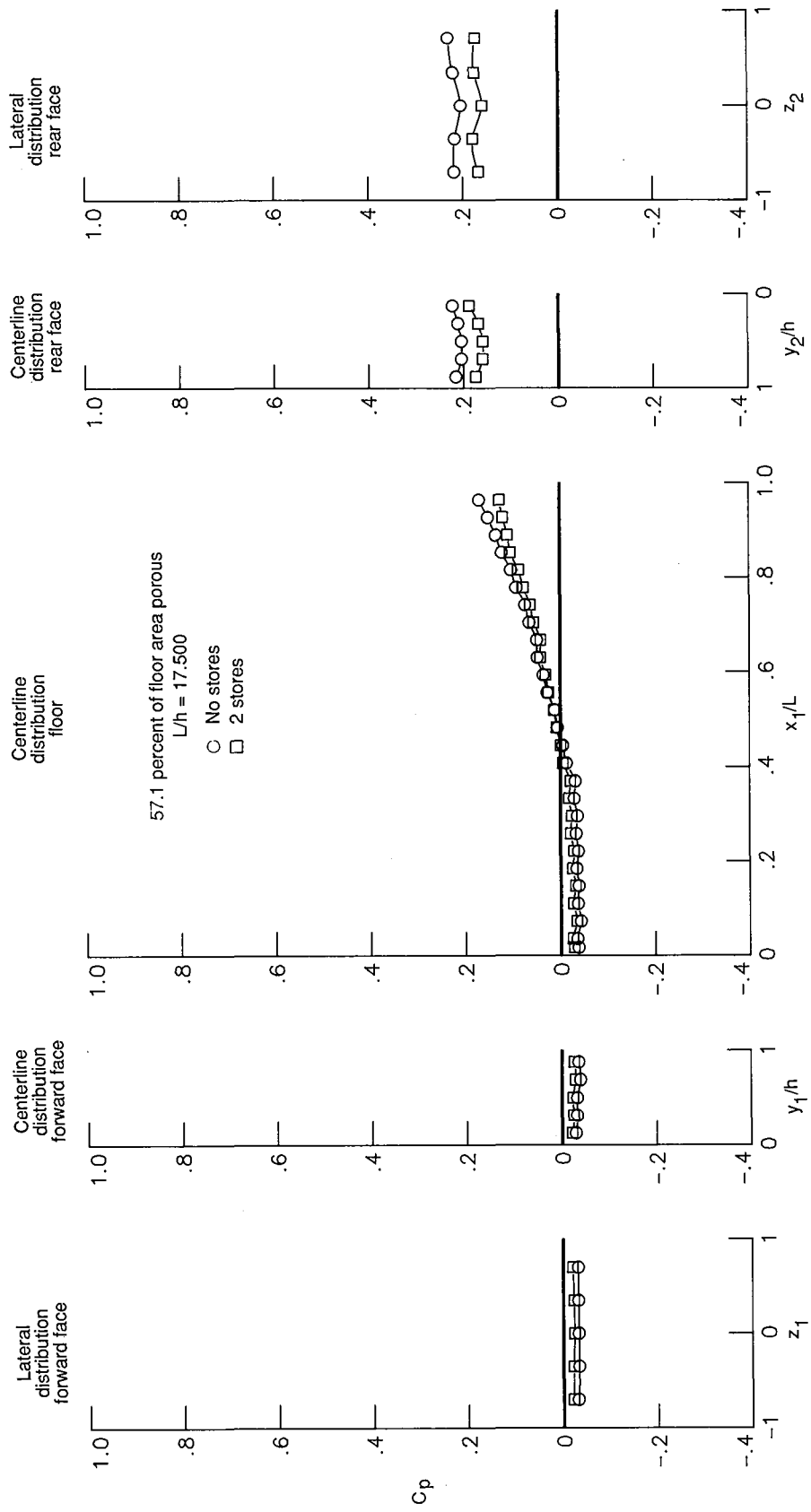
(a)  $M_\infty = 1.60$ .

Figure 40. Effect of stores on the partial-porous-floor (57.1 percent of floor area porous) cavity pressure distributions.



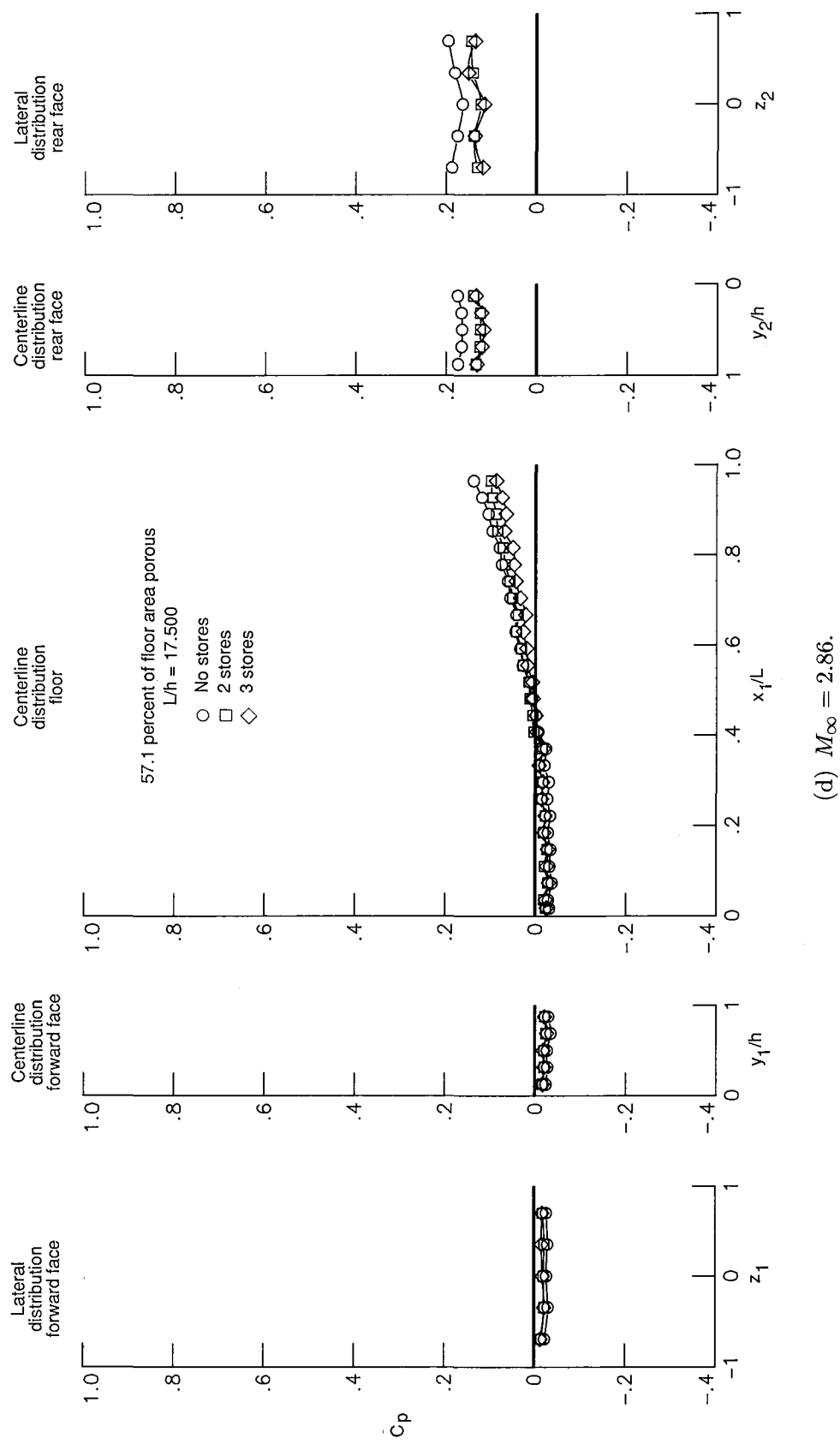
(b)  $M_\infty = 1.90$ .

Figure 40. Continued.



(c)  $M_\infty = 2.16$ .

Figure 40. Continued.



(d)  $M_\infty = 2.86$ .

Figure 40. Concluded.



## Report Documentation Page

1. Report No. NASA TP-3032	2. Government Accession No.	3. Recipient's Catalog No.	
4. Title and Subtitle Experimental Investigation of Porous-Floor Effects on Cavity Flow Fields at Supersonic Speeds		5. Report Date November 1990	
7. Author(s) Floyd J. Wilcox, Jr.		6. Performing Organization Code	
9. Performing Organization Name and Address NASA Langley Research Center Hampton, VA 23665-5225		8. Performing Organization Report No. L-16711	
12. Sponsoring Agency Name and Address National Aeronautics and Space Administration Washington, DC 20546-0001		10. Work Unit No. 505-61-71-01	
15. Supplementary Notes		11. Contract or Grant No.	
16. Abstract <p>An experimental investigation was conducted to determine the effectiveness of a passive-venting system to modify the flow field characteristics of a rectangular-box cavity at supersonic speeds. The passive-venting system consisted of a porous floor with a vent chamber beneath the floor. For certain cavity length-to-height ratios, this configuration allowed high-pressure air at the rear of the cavity to vent to the forward part of the cavity, thereby modifying the cavity flow field. The wind-tunnel model consisted of a flat plate that housed a cavity mounted on a balance such that only the cavity drag was measured. The cavity height remained constant, and the length was varied with rectangular-block inserts. Both solid- and porous-floor cavities were tested for comparison at Mach numbers of 1.60, 1.90, 2.16, and 2.86. These results showed that the passive-venting system did modify the cavity flow field. In order to determine the type flow field which existed for the porous-floor configuration, pressures were measured inside the cavity at the same conditions and for the same configurations as those used in the drag tests. Pressure data were also obtained with stores mounted in the cavity. These results, along with schlieren photographs and the tabulated data, are presented to document the porous-floor cavity flow field.</p>		13. Type of Report and Period Covered Technical Paper	
17. Key Words (Suggested by Authors(s)) Passive venting Porous floor Cavity flow Supersonic speeds Weapons bay		18. Distribution Statement Unclassified—Unlimited	
Subject Category 02			
19. Security Classif. (of this report) Unclassified	20. Security Classif. (of this page) Unclassified	21. No. of Pages 104	22. Price A06

National Aeronautics and  
Space Administration  
Code NTT-4

Washington, D.C.  
20546-0001

BULK RATE  
POSTAGE & FEES PAID  
NASA  
Permit No. G-27

Official Business  
Penalty for Private Use, \$300



POSTMASTER: If Undeliverable (Section 158  
Postal Manual) Do Not Return

---